



UNIVERSITY OF
LEICESTER

Flow of Fine and Cohesive Powders under Controlled Air Pressure Conditions

By

Reza Baserinia

Department of Engineering, University of Leicester, UK

Submitted for the degree of

Doctor of Philosophy

at the University of Leicester

September 2016

In the name of God

To my parents Narges and Javad

and

To my beautiful wife Parisa

Acknowledgment

I would like to express my deepest gratitude to my supervisor Dr Csaba Sinka for his continuous encouragement, support and guidance through my PhD. He was always there for me like a close friend and gave me useful and constructive advice.

I would like to thank FMC BioPolymer and AstraZeneca for providing the powders used in this research. I would also like to thank Mr Ian Bromley, Mr Paul Williams, Mr Alan Wale, Mr Graham Clarke, Mr Rashmikant Patel and all the other supporting staff in the Department of Engineering who helped me with the lab work and building the systems required for my research. I would like to thank all my friends and colleagues who made my time as a PhD student enjoyable and memorable.

I would like to thank the Department of Engineering at the University of Leicester for providing the opportunity for me to work as a teaching assistant through my studies and support myself financially.

I would like to greatly thank my parents, Narges and Javad for their devotion and support both emotionally and financially through all these years. Without them, I would not have been able to study at this University. Special thanks to my gorgeous wife, Parisa. She came to my life at the beginning of my PhD and gave me everything she could and supported me all the time with no hesitation. Without her, none of this would have been possible.

Abstract

Powder flow appears in many industrial processes, including pharmaceuticals, food, detergents etc. Understanding the parameters affecting powder flow is necessary for rational product and process design.

This research examines powder-air interactions for three powder handling systems: bin discharge, linear shoe-die system and rotary paddle feeder.

As a starting point the flow behaviour of powders was characterised using established procedures to provide basic set of properties for assessing flowability. Powder permeability and the influence of small levels of compaction on permeability were determined.

The influence of differential pressure on flow initiation from arching state was examined for powders discharging from bins. A dimensional model was developed to predict the differential pressure required to initiate powder flow as a function of orifice diameter and height of the powder above the exit. The mass flow rate of the powders were measured under a range of differential pressures. A dimensional model was developed to predict the mass flow rate as a function of differential pressure and exit diameter.

The effect of processing parameters on the mass of the powder delivered into the die in linear shoe-die systems under the gravity and suction fill mechanism were investigated. The system was accommodated with differential pressure transducers and the evolution of the pressure inside during the process was monitored. Dimensional models were developed to predict the mass delivered into the die as a function of powder differential pressure developed during gravity and suction fill, shoe velocity and the velocity of the punch in the die.

The influence of paddle rotational speed, exit diameter and differential pressure on the mass flow rate of powders in rotary feeding system was examined.

This research identified the dimensionless groups relevant for the understanding of the flow of fine and cohesive powders under differential air pressure conditions. The dimensional models developed account for air pressure effects for 1) flow initiation and 2) flow rate during bin discharge, 3) gravity and 4) suction fill mechanisms in linear shoe-

die filling systems. These models can be used to aid the design of powder flow processes where air pressure effects are influential.

List of Publications

Journal and conference papers

BASERINIA, R., SINKA, I. C. & RAJNIK, P. 2016. Vacuum assisted flow initiation in arching powders. *Powder Technology*, 301, 493-502.

BASERINIA, R., SINKA, I. C. 2016. Mass flow rate of fine and cohesive powders under differential air pressure. *Submitted to European Journal of Pharmaceutics and Biopharmaceutics*.

BASERINIA, R., SINKA, I. C. 2016. Influence of material and processing parameters on gravity/suction fill of shoe-die system. In preparation.

BASERINIA, R., SINKA, I. C. 2016. Permeability of powders under small levels of compaction. In preparation.

R. BASERINIA, I. C. SINKA, P. RAJNIK. 2015. Air pressure effects on powder flow rate for hopper discharge. *AIChE Annual Meeting, Salt Lake City, USA*.

I. C. SINKA, R. BASERINIA, H. ELMSAHLI. 2015. Experiments and modelling of air pressure effects on powder flow for die fill on rotary presses. *AIChE Annual Meeting, Salt Lake City, USA*.

R. BASERINIA, A. B. WOLDU, M. KHEIRIPOUR, P. RAJNIK, I. C. SINKA. 2013. Effect of particle size and density on flow of powders through feed frames on rotary tablet presses. *AIChE Annual Meeting, San Francisco, USA*.

Posters

R. BASERINIA, I. C. SINKA. 2016. Powder flow in air and vacuum. *Joint IFPRI Robert Pfeffer Symposium & UK Particle Technology Forum Conference, University of Surrey, UK*.

R. BASERINIA, I. C. SINKA, P. RAJNIK. 2015. Air pressure effects on flow initiation and flow rate for hopper discharge. *AIChE Annual Meeting, Salt Lake City, USA*.

H. ELMSAHLI, R. BASERINIA, I. C. SINKA. 2015. Discrete element modelling of flow rate during hopper discharge. *AIChE Annual Meeting, Salt Lake City, USA*.

List of Publications

H. ELMSAHLI, R. BASERINIA, I. C. SINKA. 2015. Modelling of particle-air interactions during flow into closed cavities. *Granulation Conference, Sheffield, UK.*

R. BASERINIA. 2015. Air and vacuum break down arching. *Festival of Postgraduate Research, University of Leicester, UK.*

R. BASERINIA, I.C. SINKA, P. RAJNIAK. 2015. Powder discharge into a low pressure environment. *Powder Flow 2015: Fundamentals to Applications, University of Leeds, U*

Table of Contents

Acknowledgment	I
Abstract.....	II
List of Publications	IV
Table of Contents.....	VI
List of Figures	IX
List of Tables	XIV
Notation	XV
Chapter 1. Introduction	1
1.1. Introduction to powder flow.....	1
1.2. Overall research aims.....	2
1.3. Research objectives.....	3
1.4. Structure of thesis	3
Chapter 2. Literature review.....	5
2.1. Parameters affecting powder flow	5
2.2. Powder flowability characterisation techniques	5
2.2.1. Bulk and tap density measurement	5
2.2.2. Hausner ratio and Carr index	6
2.2.3. Angle of repose.....	7
2.2.4. Critical orifice diameter	8
2.2.5. Flow rate through an orifice	9
2.2.6. Jenike’s flow function	9
2.3. Powder flow in industrial processes	14
2.3.1. Powder permeability	15
2.3.2. Arching of powders in bins and hoppers.....	16
2.3.3. Powder flow rate in bins and hoppers	19
2.3.4. Linear shoe-die systems	22
2.3.5. Rotary feeding systems	26
2.4. Summary of gaps in literature.....	28
2.5. Methodology.....	29
Chapter 3. Powder flow characterisation using standard techniques	31
3.1. Materials	31
3.1.1. Microcrystalline Cellulose (MCC)	31

3.1.2. Calcium Phosphate (ATAB)	32
3.1.3. Mannitol	33
3.2. Powder conditioning device.....	36
3.3. Bulk density measurement	37
3.3.1. Procedure	37
3.3.2. Results	38
3.4. Angle of Repose.....	38
3.4.1. Procedure	38
3.4.2. Results and discussions	40
3.5. Critical orifice diameter.....	41
3.5.1. Procedure	41
3.5.2. Results and discussions	42
3.6. Observations on flow behaviour of powders in rotary feeding systems.....	43
3.6.1. Description of the system.....	43
3.6.2. Procedure	45
3.6.3. Results and discussions	45
3.6.4. Conclusions.....	51
3.7. Comparison of the flowability measures and overall conclusions	52
Chapter 4. Measurement of powder permeability	54
4.1. System development.....	54
4.2. Procedure	55
4.3. Results and discussions	56
4.3.1. Powder permeability measurement	56
4.3.2. Influence of compaction on powder permeability.....	60
4.4. Conclusion	64
Chapter 5. Vacuum assisted flow initiation from arching state	67
5.1. System development.....	67
5.2. Procedure	68
5.3. Transducer calibration	69
5.4. Results and discussions	69
5.4.1. Effect of air pressure at discharge on flow initiation	69
5.4.2. Dimensional model development	72
5.5. Conclusions	78

Chapter 6. Mass flow rate of fine and cohesive powders under differential air pressure	80
6.1. System development.....	80
6.2. Procedure	81
6.3. Transducer calibration validation	82
6.4. Results and discussions	83
6.4.1. Flow rate under differential pressure	83
6.4.2. Analysis of the data using existing models.....	87
6.4.3. Dimensional model development	91
6.4.4. Discussion	95
6.1. Conclusions	97
Chapter 7. Linear shoe-die system under gravity fill mechanism	99
7.1. Description of the system	99
7.2. Procedure	101
7.3. Results and discussions	101
7.3.1. Mass of the powder delivered into the die	101
7.3.2. Measurement of differential pressure in the die.....	108
7.3.3. Existing model on prediction of the mass delivered	114
7.3.4. Modification of the model developed by Schneider.....	117
7.4. Conclusion	122
Chapter 8. Linear shoe-die system under suction fill mechanism.....	124
8.1. Procedure	124
8.2. Results and discussions	125
8.2.1. Measurement of the mass delivered into the die.....	125
8.2.1. Remarks on suction fill	126
8.2.2. Differential pressure measurement in the die	129
8.2.3. Dimensional model development	136
8.3. Conclusions	139
Chapter 9. Conclusions and future work	141
9.1. Conclusions	141
9.2. Future Work	145
References	146
Appendix.....	155

List of Figures

Figure 2-1. Flow function and lines of constant flowability	10
Figure 2-2. Uniaxial compression test to determine the flow function of a powder	11
Figure 2-3. The shear cell test used to determine the yield locus (Schulze, 2006).....	12
Figure 2-4. The shear cell of the Jenike shear tester (Jenike, 1964, Schulze, 2006, Party, 1989).	12
Figure 2-5. Shear cell of Schulze ring shear tester type RST-01 (Schulze, 1994a, Schulze, 2008, ASTM Standard).	13
Figure 2-6. Different types of powder flow into a die; a) nose flow, b) bulk flow, and c) intermittent flow (Schneider et al., 2007).	23
Figure 3-1. SEM images of a) PH101, b) PH102, c) PH200 and d) PH302 (Baserinia et al., 2016)	32
Figure 3-2. SEM image of Calcium Phosphate (ATAB) (Baserinia and Sinka, 2016)	33
Figure 3-3. SEM image of Mannitol (Baserinia and Sinka, 2016)	34
Figure 3-4. Particle size vs. volume percentage of the six materials.....	35
Figure 3-5. Particle size vs. cumulative volume percentage of the six materials.....	35
Figure 3-6. Powder conditioning device	36
Figure 3-7. Bulk density measurement apparatus.....	37
Figure 3-8. Angle of repose measurement apparatus.....	39
Figure 3-9. Critical orifice diameter measurement apparatus	42
Figure 3-10. The rotary feeding system illustrated in three pictures: a) the powder container connected to the feeder b) paddles and the exit orifice of the feeding system c) complete setup of the apparatus	44
Figure 3-11. The differential pressure between the feeder and ambient atmosphere measured for PH102 flowing through the feeder under the rotational velocity of 100 rpm.....	46
Figure 3-12. Time measured for 200 grams of powder to discharge from the feeder vs. the angular velocity of the paddles for four grades of MCC.	47
Figure 3-13. Average mass flow rate vs. paddle's angular velocity for four grades of MCC flowing under no differential pressure.....	48

Figure 3-14. Average volumetric flow rate vs. paddle's angular velocity for four grades of MCC flowing under no differential pressure.	50
Figure 3-15. The mass flow rates measured for PH102 in air and under differential pressure vs. paddle's angular velocity.	51
Figure 4-1. Powder permeability measurement apparatus	54
Figure 4-2. Permeability measurement apparatus.....	56
Figure 4-3. Differential pressure vs. air flow rate for a) PH101, b) PH102, c) PH200, d) PH302, e) ATAB and f) Mannitol (markers represent different repeat tests).	57
Figure 4-4. $A\Delta P/\mu L$ against air flow rate for a) PH101, b) PH102, c) PH200, d) PH302, e) ATAB and f) Mannitol (markers represent different repeat tests).....	58
Figure 4-5. Powder permeability measured for the six materials.....	59
Figure 4-6. Differential pressure vs the length of the powder sample for a) PH101, b) PH102, c) PH200, d) PH302, e) ATAB and f) Mannitol (markers represent different repeat tests)	62
Figure 4-7. Powder permeability vs bulk density for a) PH101, b) PH102, c) PH200, d) PH302, e) ATAB and f) Mannitol (markers represent different repeat tests)	65
Figure 4-8. Powder permeability vs. void fraction for six materials.....	66
Figure 4-9. Normalised permeability vs. normalised void fraction for six powders	66
Figure 5-1. Apparatus used to measure the differential pressure required to initiate powder flow from arching state	68
Figure 5-2. Schematic diagram of pressure transducer calibration setup	69
Figure 5-3. Orifice diameter vs. average differential pressure required to break the arch and initiate flow	70
Figure 5-4. Power law relationship between the two dimensionless groups H/D vs. ΔP	74
Figure 5-5. Plot of $ci(H/D)ni$ vs. ΔP based on the values of ci and ni obtained from fitting the relation on the results.....	75
Figure 5-6. Plot of $ci(H/D)ni$ vs. ΔP based on the values of ci obtained for a fixed ni	77
Figure 5-7. Schematic diagram of flow patterns; a) initial state (arching), b) mechanisms for good flowing powder and large orifice diameters, c) transition regime, d) mechanism	

for poor flowing powders and small exit diameters after discharge under differential pressure	78
Figure 6-1. Flow rate measurement device.....	81
Figure 6-2. Schematic diagram of the transducer calibration setup	83
Figure 6-3. Experimental mass flow rate vs. differential pressure for four grades of MCC	85
Figure 6-4. Experimental mass flow rate vs. differential pressure measured for all powders	86
Figure 6-5. Volumetric flow rate vs differential pressure.....	87
Figure 6-6. Mass flow rates calculated using Crewdson model with $cB = 0.58$ vs. mass flow rates measured experimentally for exit diameters of 5, 7 and 10 mm.....	88
Figure 6-7. Experimental mass flow rate vs. differential pressure for PH200 using exit diameter of 15 mm	89
Figure 6-8. Mass flow rate vs. differential pressure for ATAB through orifice diameters of a) 5 mm, b) 7 mm and c) 10 mm (measurement and prediction using the Crewdson model with $cB = 0.58$ and $cB = 0.48$) and for Mannitol through orifice diameters of d) 5 mm, e) 7 mm and f) 10 mm (measurement and prediction using the Crewdson model with $cB = 0.58$ and $cB = 0.42$).....	90
Figure 6-9. Mass flow rate vs. differential pressure for PH200 through orifice diameters of a) 5 mm, b) 7 mm, c) 10 mm and d) 15 mm (measurement and prediction using the Crewdson model with $cB = 0.58$ and $cB = 0.42$)	91
Figure 6-10. Theoretical mass flow rates calculated from the dimensional model vs experimental mass flow rates for all powders using exit diameters 5, 7 and 10 mm ...	98
Figure 7-1. Linear shoe-die system	100
Figure 7-2. Velocity profile of the motion of each axis in the linear shoe-die system.	101
Figure 7-3. Mass of the powder introduced into the die for vs. shoe velocity for PH101 and PH102 using different processing conditions. In the legends, the first number is the powder height in the shoe and the second value is the height of the die.....	104
Figure 7-4. Mass of the powder introduced into the die for vs. shoe velocity for PH200 and PH302 using different processing conditions. In the legends, the first number is the powder height in the shoe and the second value is the height of the die.....	105

Figure 7-5. Fill ratio of the powder in the die vs. shoe velocity for PH101 and PH102 using different processing conditions. In the legends, the first number is the powder height in the shoe and the second value is the height of the die.	106
Figure 7-6. Fill ratio of the powder in the die vs. shoe velocity for PH200 and PH302 using different processing conditions. In the legends, the first number is the powder height in the shoe and the second value is the height of the die.	107
Figure 7-7. Differential pressure profile measured during the delivery period for PH101 and PH200 under shoe velocities of 50 and 200 mm/s.....	109
Figure 7-8. Differential pressure profile measured during the delivery period for PH102 under shoe velocities of 30 and 50 mm/s	110
Figure 7-9. Differential pressure between the die and ambient atmosphere vs. shoe velocity for PH101 and PH102 under different processing conditions.	112
Figure 7-10. Differential pressure between the die and ambient atmosphere vs. shoe velocity for PH200 and PH302 under different processing conditions.	113
Figure 7-11. Mass flow rate of PH302 with powder height of 40 mm and die height of 20 mm measured and the theoretical flow rates calculated from the power law using the coefficients from fitting the experimental data to Equation (2-20).	115
Figure 7-12. Mass flow rate of PH102 with powder height of 30 mm and die height of 20 mm measured and the theoretical flow rates calculated from the power law using the coefficients from fitting the experimental data to Equation (2-20).	116
Figure 7-13. Experimental mass delivered into the die vs. the theoretical values calculated from Equation (2-21) for four grades of MCC.	120
Figure 7-14. Experimental mass delivered into the die vs. the theoretical values calculated from Equation (2-21) with $cg = 0.042$ for four grades of MCC.	122
Figure 8-1. Mass of the powder delivered into the die in suction fill using different shoe velocities vs. suction velocity for PH101 and PH102.	127
Figure 8-2. Mass of the powder delivered into the die in suction fill using different shoe velocities vs. suction velocity for PH200 and PH302.	128
Figure 8-3. Schematic diagram of differential pressure changes between the die and ambient atmosphere during suction fill and gravity fill mechanisms.	129
Figure 8-4. Differential pressure measured for PH101 using a) shoe velocity 100 mm/s and suction velocity 100 mm/s, b) shoe velocity 100 mm/s and suction velocity 200	

mm/s, c) shoe velocity 100 mm/s and suction velocity 300 mm/s, d) shoe velocity 300 mm/s and suction velocity 100 mm/s, e) shoe velocity 300 mm/s and suction velocity 200 mm/s and shoe velocity 300 mm/s and suction velocity 300 mm/s..... 132

Figure 8-5. Differential pressures between the die and ambient atmosphere measured for PH101 and PH102 during suction fill and gravity fill mechanisms for the experiments carried out using different shoe and suction velocities. 134

Figure 8-6. Differential pressures between the die and ambient atmosphere measured for PH200 and PH302 during suction fill and gravity fill mechanisms for the experiments carried out using different shoe and suction velocities. 135

Figure 8-7. The theoretical mass delivered in suction mechanism calculated from Equation (2-21) vs. the experimental values for four grades of MCC. 139

List of Tables

Table 2-1. Carr's classification of powder flowability based on the angle of repose.....	7
Table 2-2. Jenike's classification of powder flowability based on the flow function	9
Table 3-1. Specifications of the powders.....	34
Table 3-2. Bulk density of the materials	38
Table 3-3. The average angle of repose measured for three base diameters of 50, 75 and 100 mm	40
Table 3-4. Critical orifice diameters of the materials	43
Table 3-5. Summary of the bulk density, critical orifice diameter and angle of repose results.....	52
Table 4-1. Void fraction and permeability for uncompressed materials	60
Table 5-1. Values of ci and ni for the powders tested	75
Table 5-2. Values of ci calculated from fitting the expression to the data for a fixed $ni = 0.58$	77
Table 6-1. Flow parameters for the free flowing materials.....	94
Table 6-2. The values of the coefficients used to predict the mass flow rate.....	95
Table 7-1. The values of $1 + n$ and vc calculated from fitting the experimental data to Equation (7-1).	108
Table 7-2. The differential pressures between the die and ambient atmosphere measured for four grades of MCC under different processing parameters.....	111
Table 7-3. The values of c and $1 + n$ calculated from fitting the experimental data to Schneider model.	114
Table 7-4. The values of the coefficients cg , ag and ng calculated from fitting the experimental data to Equation (2-21).	119
Table 7-5. The values of coefficients calculated from fitting experimental data to Equation (2-21) with $cg = 0.042$	121
Table 8-1. Differential pressures measured for four grades of MCC in suction and gravity fill mechanisms under different shoe and suction velocities.	133
Table 8-2. The values of the constant cs , as , bs and ns calculated from fitting the experimental results to Equation (8-8)......	138

Notation

\dot{m}_B	Mass flow rate predicted by Beverloo relation
ΔP_g	Differential pressure in gravity fill
ΔP_s	Differential pressure in suction fill
L_g	Length of the shoe at which gravity fill is happening
L_s	Length of the shoe at which suction fill is happening
V_t	Volume of tapped powder
a_g	Empirical constant
a_r	Empirical constant
a_s	Empirical constant
b_s	Empirical constant
c_B	Beverloo coefficient
c_g	Empirical constant
c_i	Empirical constant
c_s	Empirical constant
ff_c	Critical hopper flow factor at which arching occurs
k_B	Constant depending on the particle shape
\dot{m}	Mass flow rate
m_g	Mass delivered in gravity fill
m_s	Mass delivered in suction fill
n_i	Empirical constant
n_r	Empirical constant
n_s	Empirical constant
r_0	Radius of free fall arch

v_c	Critical velocity
v_d	Velocity of the punch in the die
v_s	Velocity of shoe
μ_p	Coefficient of friction between particles
μ_{pw}	Coefficient of friction between particles and wall
ρ_b	Bulk density
ρ_f	Fluid density
ρ_s	Particle density
ρ_t	Tapped density
$\bar{\sigma}$	Mean compressive stress
σ_1	Consolidation stress
σ_c	Unconfined yield strength
ΔP	Differential pressure
Φ	Ratio between particle and air density
Ψ	Carr index
A	Cross-sectional area
Ar	Archimedes number
D	Exit diameter
FF	Powder flow function
H	Powder height
$H(\alpha)$	Function of half angle of the hopper
Hr	Hausner ratio
L	Length
Q	Volumetric flow rate

U	Superficial velocity
V	Volume of powder
Z	Correction factor
b	Width of the die
c	Empirical constant
d	Particle diameter
ff	Flow factor
g	Acceleration due to gravity
k	Permeability
l	Length of the die
m	Mass
n	Empirical constant
α	Half angle of the hopper
ε	Void fraction
λ	Function of powder compressibility
μ	viscosity

Chapter 1. Introduction

1.1. Introduction to powder flow

The flow of powder materials is a common phenomenon which is observed in everyday life, for example using flour, coffee, sugar and salt in domestic kitchen, detergents in the laundry etc., as well as in nature, e.g. avalanches, mudslides, pyroclastic flows. Powder and particulate flow also appears in a range of industries and processes where powders are handled in large volumes as well as small quantities. In the mining industry, the minerals and ores flow into the furnaces, calciners, roasters and smelters. In the manufacturing of pharmaceutical tablets, ceramic products and powder metallurgy components, small quantities of powder are fed into a die to be compressed into dense compacts. In agriculture and chemical industries, pneumatic conveying systems are used to transfer the grains into ships and large silos.

Powder processing operations, however, can experience flow related problems, ranging from arching of powders in hoppers (no flow) to flooding (uncontrolled flow). In the production of powder compacts the productivity of the process and the final properties of the product are directly influenced by powder flow behaviour. In tablet compaction, weight uniformity and properties such as tablet strength and disintegration rate are affected by the amount of powder introduced in the die. Segregation can lead to content uniformity problems. Understanding the parameters affecting the flow of powders is therefore necessary to enable the design and control of products and processes.

The parameters affecting the flow of powders can be categorised into three main groups:

1. Powder properties (particle size, shape, density, morphology, size distribution and etc.)
2. Processing operating conditions applied by the production equipment, including air-powder interactions
3. Environment (humidity, temperature, storage conditions, etc.)

Understanding these parameters and how they affect powder flow have been subject of theoretical and experimental studies in the past hundred years. Various techniques

have been developed to characterise the flowability of the materials and predict their flow behaviour. These techniques include bulk and tap density measurement, particle shape and size distribution measurement, angle of repose, critical orifice diameter and shear cell testing. Sampling, storage conditions, variability of the raw materials, etc. create repeatability issues in flow characterisation. Although these techniques can provide some understanding related to the flow behaviour of the powders, the results cannot be readily used for process design. For example the angle of repose may or may not be useful for the design of a fluid bed system. Scaling a process from lab to production remains a challenging issue.

The numerical and theoretical studies of powder flow behaviour are based on significant assumptions. In simulations, it is mostly assumed that the particles are mono-sized and spherical; and material properties such as cohesion energy density and friction between the particles are normally assumed to reproduce the experimental data available while there might not be an accurate explanation of the values taken. These assumptions can lead to the inaccurate prediction of the flow behaviour under different conditions. Also, some of the models available are developed for coarse powders and fail to predict the behaviour of fine and cohesive materials accurately. Powder flowability is also influenced by the environment. The interactions between the particles and air can alter the flow behaviour of the materials significantly. The importance of this interaction is obvious in pneumatic conveying applications, however, as this research will reveal it, it is significant also in small dosing of fine powders.

1.2. Overall research aims

The aim of this research is to develop an understanding of the relationships between powder characteristics and process parameters which influence the flow behaviour of powders and to predict powder flowability in different processing conditions. The focus is on the influence of air pressure on the flowability of fine and cohesive powders in a range of handling and dosing processes like hopper discharge, linear shoe-die system and rotary tablet press feeders.

1.3. Research objectives

The tasks required to achieve the overall research aim described in Section 1.2 lead to the formulation of the following specific objectives:

- Characterise the flowability of powders using standard flow measurement techniques and relate the flow behaviour to particle size and bulk density.
- Study the effects of the angular velocity of the paddles and differential pressure across the powder bed on the mass flow rate of powders through rotary feeders.
- Compare different powder flow measures and identify appropriate flowability testing method for different processes.
- Develop a new powder permeability measurement system to study the influence of low levels of compaction on the permeability.
- Develop a system to study powder flow initiation from the arching state using differential pressure conditions and develop a dimensional model to predict the differential pressure required to break the arch.
- Study the influence of differential pressure on the mass flow rate of powders in bin discharge and develop a new model to predict the mass flow rate as a function of differential pressure.
- Study the influence of shoe velocity and powder height in the shoe on the mass of the powder delivered into the die under gravity fill mechanism in a linear shoe die system and extend the existing models by including the effect of differential pressure between the die and ambient atmosphere.
- Study the influence of suction fill mechanism on the mass of the powder delivered into the die in a linear shoe-die system and develop a model to predict the mass introduced during the suction fill process.

1.4. Structure of thesis

Chapter 2 presents a review of the literature on powder flowability, flow characterisation methods and permeability. The methods are discussed in the context of the flow processes investigated in this thesis which include bin discharge, linear shoe-die filling systems and rotary feeders.

The materials used in this research are described in Chapter 3. Standard flow characterisation methods (bulk density, angle of repose and critical orifice diameter) are described and the results obtained are compared for the powders tested. The effects of processing parameters and material properties on the flow rate of powders through a model rotary feeder are examined.

In Chapter 4 the permeability of the materials is measured using a system built for this purpose. Also, the influence of small levels of compaction on powder permeability is discussed.

In Chapter 5 focusses on the influence of differential pressure on powder flow initiation from the arching state in bin discharge. A purpose built testing rig is designed and manufactured and the powders are characterised. A dimensional model is developed to predict the differential pressure required to break the arch and initiate flow.

In Chapter 6 the mass flow rate of the materials under a range of differential pressures is measured. A model is developed to predict the mass flow rate under differential pressure for different exit diameters.

The influence of processing parameters and material properties on the mass of the powder introduced into the die in a linear shoe-die system are investigated for gravity fill in Chapter 7 and for suction fill in Chapter 8. Dimensional models are developed for both gravity and suction fill mechanisms.

Chapter 9 presents the main conclusions of this research.

Chapter 2. Literature review

In this chapter established experimental flow characterisation methods are reviewed. The existing literature on research into powder permeability, discharge from bins and hoppers as well as die filling using linear and rotary feeding systems is reviewed.

2.1. Parameters affecting powder flow

The parameters affecting the flow behaviour of the powders can be categorised into three main groups.

1. Material properties which can be divided into two main subgroups:
 - a. Particle properties such as particle size and shape, density, friction between the particles.
 - b. Bulk properties such as bulk and tap density, particle size distribution, voidage and porosity.
2. Processing parameters such as the geometry of the container, velocity of the shoe or paddles in feeders and height of the powder.
3. Environment such as storage conditions, temperature and humidity.

The techniques developed to measure powder flowability and identify effect of the parameters listed above on the flow behaviour of the powders are reviewed below.

2.2. Powder flowability characterisation techniques

The following flow characterisation methods are of particular importance in industrial product and process development: bulk and tapped density measurement (used in widely used flow measures such as Carr's index and Hausner ratio (Carr, 1965b, Hausner, 1967)) (USP29-NF24, 2006), angle of repose, flow rate through orifice, and flow functions (Jenike, 1964, USP29-NF24, 2006, Schulze, 2006). These techniques are based on different principles and are used for specific applications.

2.2.1. Bulk and tap density measurement

Bulk density (ρ_b) (also known as the apparent density) is the ratio between the mass of the powder and the volume it occupies including any void spaces:

$$\rho_b = \frac{m}{V} \quad (2-1)$$

The methods used to measure bulk density are known as Graduated Cylinder, Volumeter and Vessel methods as described in the United States Pharmacopeia (USP29-NF24, 2006).

Tap density (ρ_t) is the mass of the powder divided by the volume it occupies after tapping (V_t). Tapping involves shacking of a powder under controlled conditions to obtain a closer packing of particles. Similar to the bulk density measurement, different methods are developed to measure tap density (USP29-NF24, 2006).

$$\rho_t = \frac{m}{V_t} \quad (2-2)$$

2.2.2. Hausner ratio and Carr index

The change in the density of the powder bed subject to tapping can be used as a measure of powder flowability. The Hausner ratio (Hr) is defined as the ratio of the tap density to the bulk density of the material:

$$Hr = \frac{\rho_t}{\rho_b} \quad (2-3)$$

The Carr index (Ψ) is defined as the difference between the tap and bulk density divided by the tap density of the material.

$$\Psi = \frac{\rho_t - \rho_b}{\rho_t} \quad (2-4)$$

The Hausner ratio and Carr index are based on the ability of the powder particles to rearrange and can be used as an indication of compressibility. They are also interpreted as a measure of powder cohesiveness where higher values are obtained for more cohesive materials (Grey and Beddow, 1969, Dutta and Dullea, 1990). Typically a Hausner ratio smaller than 1.2 shows good powder flowability and for poor flowing powders Hausner ratio is above 1.5 (Wells, 1988). According to the Carr index the powders are ranked as excellent, good, fair and poor flowing materials; the corresponding values are 5–10, 12–16, 18–21, and 23–28, respectively (Carr, 1965a).

Abdullah and co-workers (Abdullah and Geldart, 1999) studied the influence of particle size on the flowability of the powders using Hausner ratio and observed that there exist a critical size above which the flowability is not improved significantly (typically increasing the particle size improves powder flow behaviour). Different scientists (Lindberg et al., 2004, Lavoie et al., 2002, Kumar et al., 2002) compared the flowability of different materials using Hausner ratio and Carr index.

2.2.3. Angle of repose

The angle of repose is one of the simplest measures of powder flowability and consists of discharging a powder from a hopper onto a flat surface and determining the angle between the heap and the horizontal base. A poor flowing powder forms a steep angle while a good flowing powder spreads more forming a smaller angle. However, the heap can be created in different ways, e.g. by fixing the height from which the powder is discharging onto the surface or the fixed base diameter as prescribed by USP (USP29-NF24, 2006) or ASTM (Standard, 2000). In a flowability classification proposed by Carr (Carr, 1965b) materials are categorised into seven groups based on their angle of repose. These groups are presented in Table 2-1.

Table 2-1. Carr's classification of powder flowability based on the angle of repose

Flowability	Angle of Repose, °
Excellent	25-30
Good	31-35
Fair – aid not needed	36-40
Passable – may hang up	41-45
Poor – must agitate, vibrate	46-55
Very poor	56-65
Very, very poor	>66

There are some variations from this classification but much of the pharmaceutical literature is consistent with Carr's classification (USP29-NF24, 2006). Other methods for measuring the angle of repose include: 1) the "drained" angle of repose, which is determined by measuring the angle of the slope of the powder remaining in the bin - this angle depends on the shape of container (Schulze, 2006, Carrigy, 1970); 2) the semi-cone angle formed between a base and a right angle wall (Geldart et al., 2006); 3) the

tilting table (Geldart et al., 2006); 4) the dynamic angle of repose (Carrigy, 1970) where the angle of the powder in a rotating cylinder is determined; 5) scoop deposition (Cornforth, 1973); 6) the cone lifting method (Pascale, 2014); and 7) measuring the angle of repose in liquid medium (Santamarina and Cho, 2001). There is no general agreement on the best design or size of the equipment or the amount of powder that should be used for testing (Geldart et al., 1990). The method used in this work to measure the angle of repose of the powders is described in Section 3.4.

2.2.4. Critical orifice diameter

The critical orifice diameter is the minimum diameter required for the powder to discharge freely under its own weight from a bin which has an opening in the base. For good flowing powders, the critical orifice diameters are larger than the relatively poor flowing powders.

When powders are flowing through the containers like bins or hoppers with exit diameters smaller than the critical orifice diameter, formation of a stagnant zone of material above the exit of the container known as arching inhibits the flow of powder. Further flow can only be achieved by breaking the arch formed. In industries which handle large volumes of powders the arch formed is typically broken by mechanical action (hammering the side of the container and damaged containers is a common sight). Arching is discussed in more detail in Section 2.3.2.

Many scientists like Walker, Vemavarapu and Jallo (Walker, 1966, Vemavarapu et al., 2009, Jallo et al., 2012) used critical orifice diameter as a measure of powder flowability while Podczek and co-workers (Podczek and Jones, 2004) used it as a measure of the ability of a powder to form an arch.

The critical orifice diameter can be measured using standard techniques (USP29-NF24, 2006). Lee and co-workers (Lee et al., 2000) compared the critical orifice diameter results with Carr's index and the dynamic angle of repose and observed that there are some similarities in the classification of powder flowability between these techniques.

The critical orifice diameter measurement rig used in the current research is described in Section 3.5.

2.2.5. Flow rate through an orifice

Measurement of the flow rate of powders through an orifice provide a practical method for assessing flowability where a good flowing powder has a larger mass flow rate. Standard flow rate measurement techniques e.g. Hall flowmeter (International Organization for Standardization (ISO), 2014, ASTM Standard) have been developed to characterise powder flowability. The models developed to predict the flow rate of powders through hoppers and bins are discussed in Section 2.3.3.

2.2.6. Jenike's flow function

The flowability of a powder can be characterised by the consolidation stress (σ_1), unconfined yield strength (σ_c) and the storage time of the powder material (Schulze, 2006). The ratio between the consolidation stress and the unconfined yield strength known as the flow function (FF) is used to measure powder flowability (Jenike, 1964). The unconfined yield strength is obtained from the Mohr's stress circle tangent to the material yield locus which passes through the origin i. e. the minor principal compressive stress is zero (Seville et al., 1997).

$$FF = \frac{\sigma_1}{\sigma_c} \quad (2-5)$$

A better flowing powder has higher values of the flow function. The Jenike flowability classification of bulk solids is defined in Table 2-2 (Jenike, 1964).

Table 2-2. Jenike's classification of powder flowability based on the flow function

Flow function	Flowability
$FF < 1$	Not flowing
$1 < FF < 2$	Very cohesive
$2 < FF < 4$	Cohesive
$4 < FF < 10$	Easy flowing
$10 < FF$	Free flowing

The flowability of a given material might change based on the consolidation stress applied (powder P, at $t=0$ in Figure 2-1). The strength of some of the bulk solids increase by storing them for a longer time at rest under a compressive stress (for example powder storage in silos). This is called time consolidation or caking (Schulze, 2006). The

influence of caking on the flow function of powder P, is illustrated by the dashed line (time= t_1) in Figure 2-1.

Different methods have been developed to determine the flow function for powders and measure the flowability at different consolidation stresses. These methods are reviewed here.

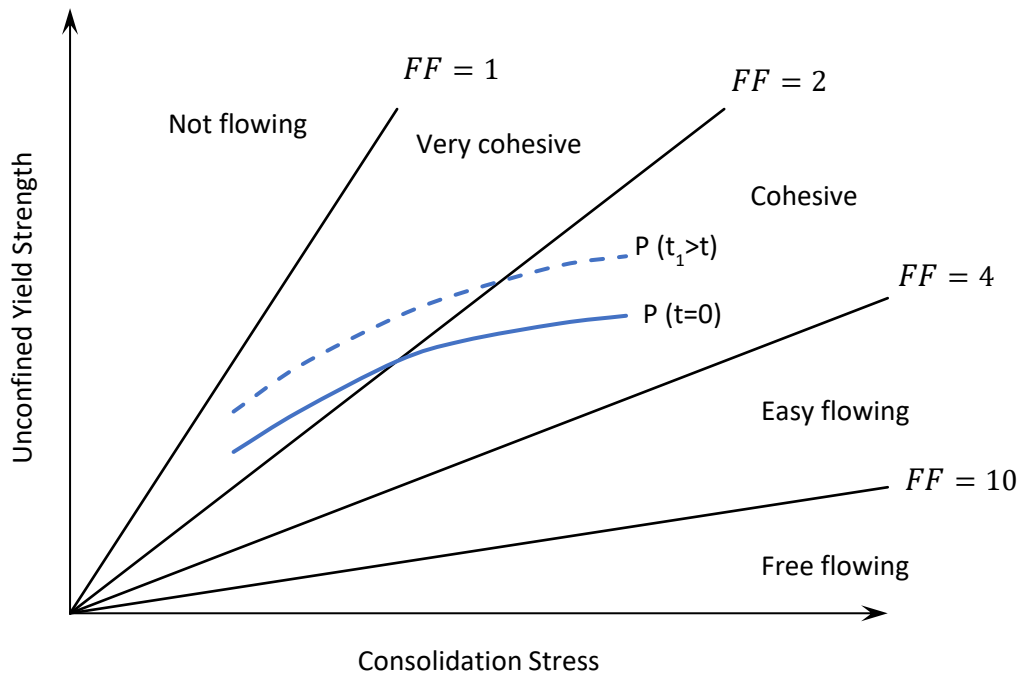


Figure 2-1. Flow function and lines of constant flowability

2.2.6.1. Uniaxial compression test

In the uniaxial compression test, a hollow cylinder is filled with powder material and the specimen is compressed under uniaxial compression stress of σ_1 . The sample is unloaded and the cylinder is removed. The compacted powder is then subject to increasing compressive stress. The stress at which the specimen fails is recorded as the unconfined yield strength (σ_c). The schematic diagram of this procedure is demonstrated in Figure 2-2. The flow function of the powder is usually plotted using the unconfined yield strengths measured for different consolidation stresses.

The uniaxial compression test has some limitations: 1) Preparing a cylinder with frictionless walls is problematic; 2) The values of the unconfined yield strength

calculated can be too low (Schwedes and Schulze, 1990); and 3) the important parameters such as internal friction angle and wall friction angle cannot be determined using this method.

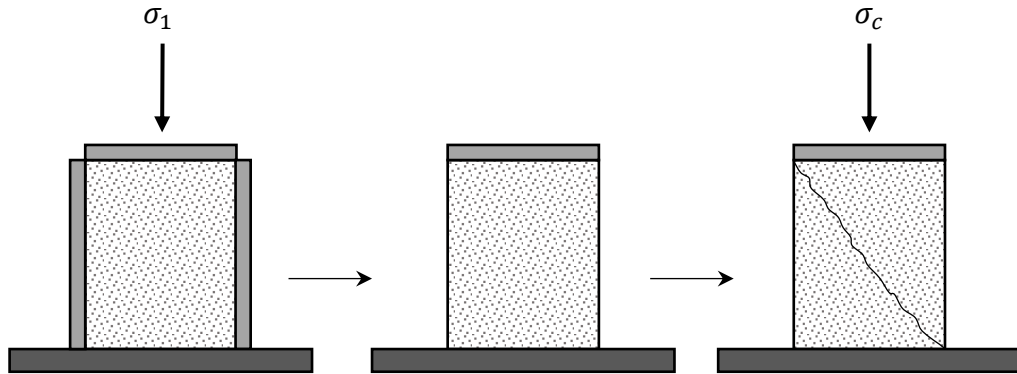


Figure 2-2. Uniaxial compression test to determine the flow function of a powder

2.2.6.2. Shear testing

Shear cells are used to determine the yield locus (yield limit) of a powder. The powder sample is initially loaded under a normal stress of σ_{pre} (referred to as pre-shear stress) and is sheared until the shear stress reaches the steady state (τ_{pre}). The shear deformation is reversed until the shear stress returns to zero. The point (σ_{pre}, τ_{pre}) is the first point on the normal stress – shear stress diagram (pre-shear point). The bulk solid is then consolidated under a reduced normal stress (σ_{sh}) and the sample is sheared again. When the shear stress is sufficiently large (τ_{sh}) the flow starts (incipient flow) and the particles move against each other resulting in dilation of the material and reduction in the shear stress. The shear point (σ_{sh}, τ_{sh}) is added to the normal stress – shear stress diagram and the test is repeated with a smaller σ_{sh} . The yield locus for the applied σ_{pre} is plotted by drawing a curve through the shear points obtained (The procedure used to plot the yield locus is illustrated in Figure 2-3). The unconfined yield locus is then determined by drawing the Mohr's stress circle tangent to the yield locus and crossing the origin.

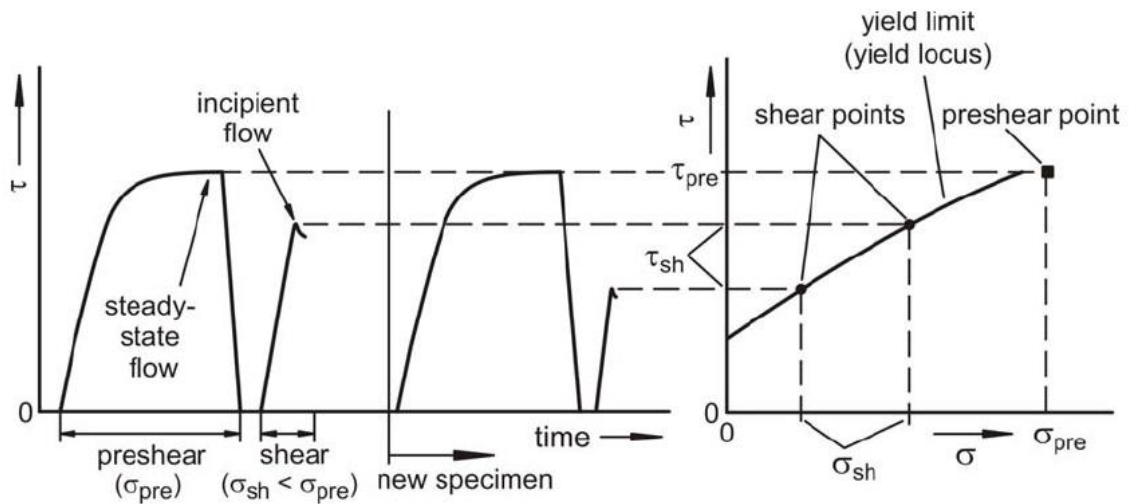


Figure 2-3. The shear cell test used to determine the yield locus (Schulze, 2006).

Different types of shear cells have been developed to obtain the yield locus of bulk solids. The Jenike shear tester (Jenike, 1964) is a translational tester consisted of a mould ring, an upper ring and a lid which is presented in Figure 2-4. In order to measure the yield locus, the shear cell is filled with the bulk powder and is manually pre-consolidated (Party, 1989). The powder sample is then pre-sheared and sheared following the procedure described earlier. For the second point of the yield locus, a fresh specimen is prepared and tested.

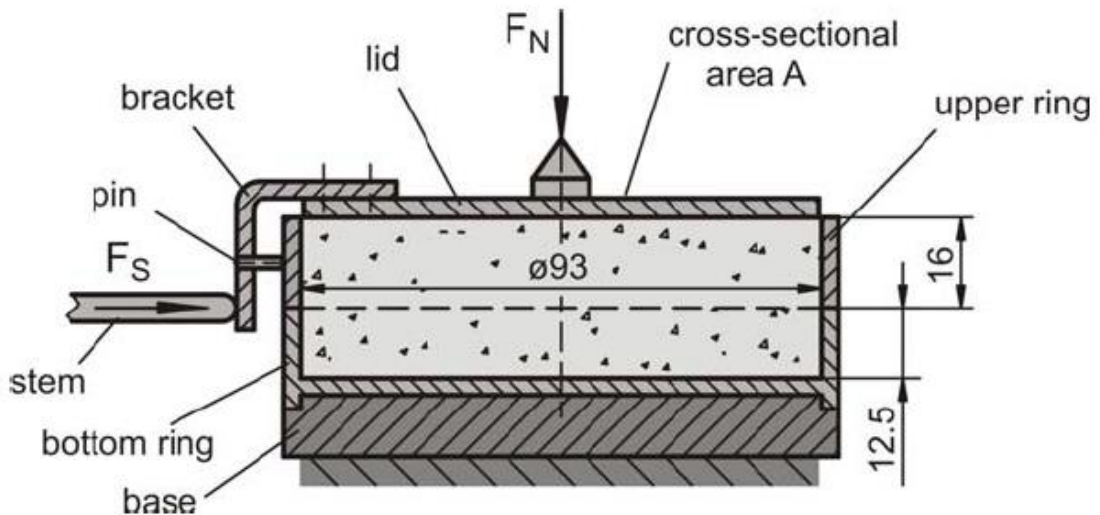


Figure 2-4. The shear cell of the Jenike shear tester (Jenike, 1964, Schulze, 2006, Party, 1989).

The disadvantages of the Jenike shear tester are: 1) a long time is required to obtain the yield locus and the operator should be present; 2) manual pre-consolidation of the specimen is a source of error in measurement; and 3) it is difficult to measure the yield locus of the materials which require large deformation to reach steady state flow due to limited shear displacement (Schulze, 2006).

The second type of the shear testers is the ring shear tester (annular shear tester) which is similar to the Walker shear tester (Carr and Walker, 1968), Schulze shear testers (Figure 2-5) (Gebhard, 1982, Schulze, 1994a, Schulze, 1994b), FT4 powder rheometer (Freeman, 2007) and Brookfield powder flow tester (PFT) (Ding et al., 2012, Berry et al., 2015).

The ring shear testers consist of a base cell which is filled with the powder and a lid placed on top of the powder bed. A normal force is applied to consolidate the powder in the cell. The powder is then sheared by rotation of the lid (both the lid and the cell rotate in opposite directions in Schulze shear tester). The force required for shear deformation (proportional to shear stress) under different normal forces is measured and the yield locus is determined similarly to the principles described.

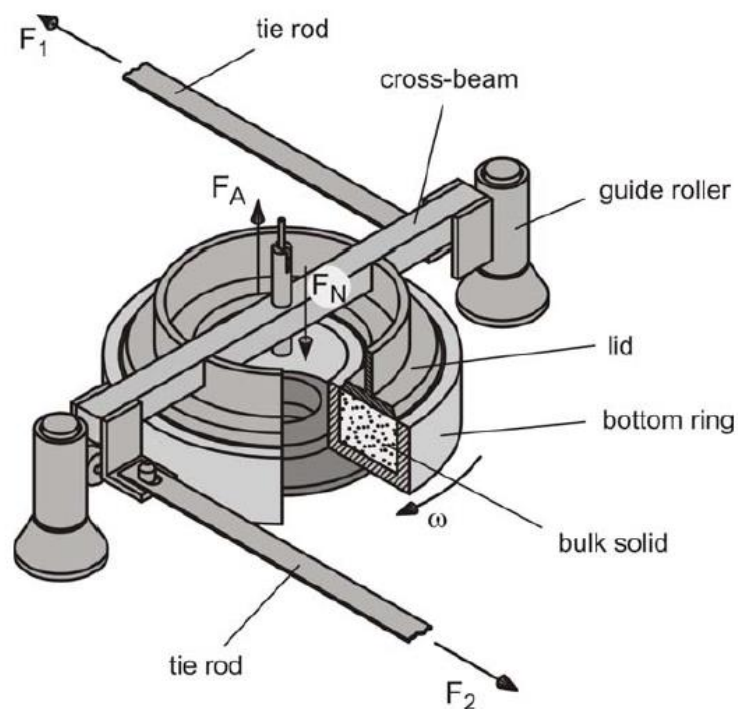


Figure 2-5. Shear cell of Schulze ring shear tester type RST-01 (Schulze, 1994a, Schulze, 2008, ASTM Standard).

2.2.6.3. Ball indentation method

In the ball indentation method developed by Hassanpour and co-workers (Hassanpour and Ghadiri, 2007) the cohesive powder sample is compacted under a small compressive stress. The yield stress of the compacted material is then determined by measuring the hardness using a ball indenter. The yield stress and the consolidation stress are then used to obtain the Jenike's flow function (Jenike, 1961) and classify powder flowability.

The ball indentation method can be used to characterise the flowability of the powders using small quantities of the material (Wang et al., 2008). The ball indentation method has been compared with other powder flow characterisation techniques (Zafar et al., 2015) such as the Schulze Shear Cell (Schulze, 2008), Raining Bed Method (Manuel Valverde et al., 2000) and Sevilla Powder Tester (Formisani et al., 2002). These methods provided similar powder flow ranking for the range of powders considered. It was shown that the stress history and testing methods are influencing the results obtained from different tests. Numerical studies have been carried out to evaluate the hardness of cohesive powders in the ball indentation method (Pasha et al., 2013, Pasha et al., 2015).

2.3. Powder flow in industrial processes

Powder flow appears in many industrial processes such as discharge from silos and hoppers, die filling in linear shoe-die systems and pharmaceutical tableting using rotary press feeders. Uniformity of the operation and the properties of the product in these processes is directly influenced by powder flow (and the parameters affecting it) and the amount of powder involved. For example, in hopper discharge, if the exit diameter of the hopper is below a given size, the powder will form an arch above the orifice which inhibits powder flow. In pharmaceutical tableting, the properties of the tablet such as weight uniformity, density, mechanical strength and disintegration rate are directly affected by the amount of powder introduced into the die before compaction.

The parameters affecting the flow behaviour of the powders have been the subject of intense research. The ability to predict the flow behaviour of the powders is necessary to eliminate the challenges in different processes and designing products with desired

properties. Powder flowability is significantly influenced by air pressure conditions and the extent of these effects is directly proportional to the permeability of the powders.

2.3.1. Powder permeability

Permeability is defined as the ability of a fluid (usually air) to migrate through the powder. Permeability was first studied by Darcy (Darcy, 1856) who proposed an empirical relation between the rate at which an interstitial fluid (e.g. air) migrates through the powder and the pressure gradient.

$$U = k \frac{dP}{dx} \quad (2-6)$$

In Equation (2-6), U is the superficial velocity, $\frac{dP}{dx}$ is the pressure gradient and k is permeability. For a cylindrical container with cross-sectional area, A , and length, L , this relation becomes

$$Q = \frac{kA \Delta P}{\mu L} \quad (2-7)$$

where Q is the flow rate through the powder, ΔP is the pressure difference across the powder bed and μ is the viscosity of the fluid.

Darcy's law was placed on a firmer theoretical basis for spherical particles by Kozeny (Kozeny, 1927) and Carman (Carman, 1937)

$$\frac{dP}{dx} = 180 \frac{\mu U (1 - \varepsilon)^2}{d^2 \varepsilon^3} \quad (2-8)$$

where d is particle diameter and ε is the void fraction. The relation between the pressure gradient, $\frac{dP}{dx}$ and $\frac{\mu U}{d^2}$ has been derived using dimensional analysis. The numerical factor, 180, is an empirical constant.

At high flow rates the interstitial effects of the fluid and so its density (ρ_f) become important and a correlation was obtained by Ergun (Ergun, 1952).

$$\frac{dP}{dx} = 150 \frac{\mu U (1 - \varepsilon)^2}{d^2 \varepsilon^3} + 1.75 \frac{\rho_f U^2 (1 - \varepsilon)}{d \varepsilon^3} \quad (2-9)$$

For low fluid velocities, the second term in Ergun's equation is negligible and the relation becomes similar to Kozeny and Carman relation (Equation (2-8)).

Equations (2-6) and (2-8) were combined by Nedderman (Nedderman, 1992) to calculate the permeability based on the particle diameter and void fraction.

$$k = \frac{d^2 \varepsilon^3}{180\mu(1 - \varepsilon)^2} \quad (2-10)$$

The particle diameter in the relations developed can be modified to account for the effect of shape factor for non-spherical particles and particle size distribution (Nedderman, 1992). However, the permeability of powders is often measured directly due to difficulty in determining the shape factor and considering the effect of particle size distribution.

In the relation developed by Kozeny and Carman as well as Ergun equation the influence of particle packing on the permeability of the powder is not included and for non-random packing arrangement they should be used with caution (Nedderman, 1992).

Different systems have been developed to measure powder permeability (Kaye, 1967) and permeametry has been used to characterise powders (Wasan et al., 1976a, Le et al., 2010) and measure the specific surface area of the particles (Kamack, 1954, Allen and Haigh, 1954, Wasan et al., 1976b). However, as permeability is highly influenced by the technique used (e.g. packing of powder in the device), measurements cannot always be compared with each other.

2.3.2. Arching of powders in bins and hoppers

Filling and discharge from silos, hoppers and bunkers are important for high volume process industries such as mining and mineral processing, construction, energy, agriculture, food and for high value-added processing industries such as

pharmaceuticals and fertilisers. A common challenge appearing in the flow of particulate materials from bins and hoppers is “arching”. Arching occurs when particles interlock above the exit of the container and form a stable arch. This phenomenon presents significant technical challenges for handling and dosing of both free flowing and cohesive powders. Typically arching occurs when the exit diameter is smaller than a “critical orifice diameter”, which can be measured using standard equipment (USP29-NF24, 2006).

The stress conditions leading to arching in hoppers have been studied extensively since the 1960s. Jenike’s investigation (Jenike, 1961, Jenike, 1964, Jenike, 1967) lead to development of the hopper flow factor defined by

$$ff = \frac{\sigma_1}{\bar{\sigma}} \quad (2-11)$$

where σ_1 is the major consolidating stress in flow and $\bar{\sigma}$ is the mean compressive stress on the arch which is a function of half angle of the hopper, internal friction angle and wall friction angle. The critical orifice diameter of the hopper to avoid arching appearing was determined by comparing the values of hopper flow factor with the flow function of the powder (Equation (2-5)). When the material flow function lies below the hopper flow factor, powder flow occurs. The critical orifice diameter (CoD) can be determined from the intersection of the hopper flow factor (ff) and flow function (FF).

$$CoD = \frac{\bar{\sigma}H(\alpha)}{\rho_b g} \quad (2-12)$$

where $H(\alpha)$ is an empirical function depending on the shape of the hopper, ρ_b is the bulk density and g is acceleration due to gravity (Seville et al., 1997). Although this method is effective for large-scale applications, the minimum orifice diameter determined is of the order of a meter for cohesive materials and have limited use for chemical, food and pharmaceutical applications where small flow rates are required (Seville et al., 1997).

Walker's theoretical studies (Walker, 1966) determined the approximate stresses within the powder flowing through a hopper and the results were compared with the findings of Jenike (Jenike, 1961). Drescher and co-workers (Drescher et al., 1995a, Drescher et al., 1995b) compared the experimental critical orifice sizes with the values obtained from theoretical analysis and demonstrated that the theories overestimate the critical orifice size as a result of neglecting self-weight of powder above the exit.

The theoretical studies carried out on arching are focusing on designing the geometry of the hopper to avoid arching. For fine and cohesive powders, theoretical models give large values for the outlet size required to eliminate arching while in fine-dosing applications such as pharmaceutical tableting where the powders should flow into small cavities the systems cannot be designed based on the sizes obtained from the models and often other mechanisms are used to improve the efficiency of these processes.

The flow of powder from hoppers is usually assumed to take place in open atmosphere. However, in powder pressing industries (e.g. pharmaceutical tablets, detergents, ceramics, powder metallurgy etc.) the powders are filled into closed cavities; this is followed by compaction using rigid punches and finally, the product is ejected from the die. During die fill the air pressure is increased as the powder is introduced into the die. The interplay between powder and air during die fill has been studied using model shoe-die systems (Sinka et al., 2004, Wu et al., 2003). Models for mass flow rate have been developed (Schneider et al., 2007) prompting further research on air pressure effects in die fill (Jackson et al., 2007, Mills and Sinka, 2013), and on understanding suction fill mechanisms. These mechanisms are essential for practical manufacturing processes. For example, a typical pharmaceutical tablet has a diameter smaller than 10 mm. A typical pharmaceutical formulation has a critical orifice diameter larger than 10 mm. This poses a simple question: how is die fill possible? Jackson et al. (Jackson et al., 2007) identified qualitatively the effect of differential pressure on this process.

The importance of air pressure conditions has been documented since the 1960s. Bulsara (Bulsara et al., 1964) developed a model that considered the air pressure above and below the powder bed as well as the pore pressure in the powder just above the orifice. Shinohara (Shinohara et al., 1973) constructed a theoretical model validated by

experiments which show that the flow rate of cohesive powders is facilitated by positive air pressure above the hopper as well as negative pressure at the outlet.

In applications where the powder discharges into a closed cavity, using air pressure conditions in the vicinity of the outlet introduces a potential method for eliminating arching.

2.3.3. Powder flow rate in bins and hoppers

In industries such as mineral extraction, agriculture, etc., the flow of powders from bins or hoppers appears in many processes. Understanding the parameters affecting the flow has been subject to considerable experimental and theoretical research and the key models are reviewed below. In addition, handling and dosing of fine powders in food and pharmaceuticals involve air pressure effects that make such processing operations possible. For example, on rotary tablet presses, the powder is fed into dies only because of the “suction fill” effect (Sinka and Cocks, 2009, Jackson et al., 2007, Mills and Sinka, 2013). The models developed to date that incorporates the influence of air on powder flow are also reviewed in this section.

Nedderman et al. (Nedderman et al., 1982) describe studies of mass flow rate of granular materials carried out by Hagen (Hagen, 1852) as early as 1852. Deming and co-workers (Deming and Mehring, 1929) investigated the effects of half angle of the hopper, orifice size, particle size and bulk density on the flow rate of powders. In 1952, Weighardt (Weighardt, 1952) proposed that the mass flow rate is a function of $(D - Z)^{2.5}$ where D is the exit diameter. This is similar to the well-known model introduced by Beverloo et al. (Beverloo et al., 1961) in 1961:

$$\dot{m}_B = c_B \rho_b g^{0.5} (D - k_B d)^{2.5} \quad (2-13)$$

where ρ_b is the bulk density, g is acceleration due to gravity, D is the orifice diameter and d is the particle diameter. The value of the Beverloo constant, c , was found to be close to 0.58 and the term $k_B d$ (Z in Weighardt’s relation) is a correction factor used to fit the experimental data to the model which is compatible with the concept of “empty annulus” proposed by Brown and Richards (Brown and Richards, 1960, Brown and

Richards, 1970). In Beverloo's study, the mass flow rate was found to be independent of the height of the powder above the orifice.

The Beverloo model (Equation (2-13)) is only applicable to cylindrical bunkers and core flowing hoppers. A pre-Beverloo correlation was developed for mass flow hoppers by Rose and Tanaka (Rose and Tanaka, 1959) where the mass flow rate was a function of the half angle of the hopper.

Using the "Minimum Energy Theorem", Brown and Richards (Brown, 1961, Brown and Richards, 1970) developed a theoretical model to describe the flow rate of coarse and incompressible powders from bins and hoppers (Equation (2-14)). This model was in good agreement with the experimental data obtained for coarse particles (α is the half angle of the hopper).

$$\dot{m} = \frac{\pi}{6} \rho_b g^{0.5} (D - Z)^{2.5} \left(\frac{1 - \cos^{1.5} \alpha}{\sin^{2.5} \alpha} \right) \quad (2-14)$$

Davidson and co-workers (Davidson and Nedderman, 1973) used the approach known as "the Hour-Glass Theory" to determine the mass flow rate of incompressible coarse powders. The predicted flow rates using this model was found to be double the experimental values. They concluded that this inconsistency was due to the effect of wall friction.

The models proposed for predicting the mass flow rate of bulk solids are often developed for non-cohesive materials. Johanson (Johanson, 1965) proposed a theoretical correlation for cohesive materials by including the effects of inertia in the equilibrium of a cohesive arch of uniform thickness:

$$\dot{m} = \dot{m}_B \sqrt{\left(1 - \frac{ff}{ff_c} \right)} \quad (2-15)$$

In Equation (2-15), \dot{m}_B is the mass flow rate of a non-cohesive material of the same density predicted using the Beverloo correlation, ff is the hopper flow factor and ff_c is the critical flow factor at which arching occurs. This relation showed a good agreement

for coarse materials. However, larger experimental discrepancies were observed for fine powders.

The first major study of the effect of air pressure on the flow rate of bulk solids was carried out by Bulsara et al. (Bulsara et al., 1964). They applied additional air pressure on the top of the powder bed in the hopper and found that the mass flow rate is related to the differential pressure (ΔP) by

$$\dot{m} \propto \Delta P^{0.5} \quad (2-16)$$

McDougal and Knowles (McDougal and Knowles, 1969) modified this relation to the form of Equation (2-17) where ΔP_0 is the adverse pressure gradient required to prevent flow. Resnick and co-workers (Resnick et al., 1966) mentioned that in the absence of additional air pressure McDougal's relation should reduce to the expression for gravity flow and the mass flow rates should be closely related to the values predicted by the Beverloo correlation.

$$\dot{m} \propto (\Delta P + \Delta P_0)^{0.5} \quad (2-17)$$

The first theoretical work on air effects was carried out by Crewdson et al. (Crewdson et al., 1977) by including a modification to the acceleration of particles. In gravity flow, the particles accelerate because of their weight ($\rho_b g$) while in the presence of an interstitial pressure gradient an additional body force will be applied. Based on this analogy the Beverloo correlation was modified for hoppers to:

$$\dot{m} = \dot{m}_B \left(1 + \frac{\Delta P}{\rho_b g r_0} \right)^{0.5} \quad (2-18)$$

where r_0 is the radius of the free fall arch. This relation is similar to the model proposed by Bulsara (Bulsara et al., 1964). Two modified versions of this model are presented elsewhere for intermediate and high Reynolds numbers (Nedderman, 1992). By assuming that there is no air percolation through the stagnant zone, Equation 6 can be

used for flat-bottomed bins by treating it as a hopper of angle equal to that of a flowing core which can be assumed to be 45° and $r_0 = D/\sqrt{2}$ (Nedderman, 1992).

The mass flow rate predicted by the Beverloo correlation is significantly larger than the experimental values recorded for fine powders (with an average particle size smaller than $400\ \mu\text{m}$) and it was suggested that the value of the coefficient should be modified. This effect was explained by Nedderman (Nedderman, 1992) to be as a result of voidage change and pressure gradient in the powder bed. For coarse powders, the pressure gradient effects due to dilation are negligible but become significant for fine powders. The effects of negative pressure gradient were investigated experimentally by Verghese (Verghese, 1991). It was observed that the magnitude of pressure gradient at the vicinity of the orifice increased by decreasing particle size and a model for predicting mass flow rate was proposed

$$\dot{m} = \dot{m}_B \left(1 - \frac{\lambda}{\rho_b g d^2} \right)^{0.5} \quad (2-19)$$

where λ is a function of compressibility of the material and gas properties. They found that for a series of sands with small size distribution the mass flow rate can be predicted using $\lambda/\rho_b g = 1.48 \times 10^{-8}\ \text{m}^2$. However, there is no reason why this value should be the same for other powders.

Donsi and co-workers (Donsi et al., 2004) proposed a model to predict the mass flow rate of cohesive powders in aerated systems by modifying the relation developed by De Jang and co-workers (De Jong and Hoelen, 1975). However, this model failed to capture the behaviour of poor flowing and cohesive powders. Barletta et al. (Barletta et al., 2007) modified Donsi's relation assuming that cohesive powders flow in form of aggregates. They included the aggregate size and density in Donsi's relation which gave a better prediction, however, it still overestimated the mass flow rate.

2.3.4. Linear shoe-die systems

In different industries such as pharmaceuticals, metals, food and chemicals the powder products are in the form of compacts. In compaction processes, the powder is introduced into a die using linear or rotary feeding systems before being compressed

into the compact form using rigid punches. The final properties of the compact are directly influenced by the mass of the powder delivered into the die. Therefore, predicting the flow behaviour of the powder can lead to designing a process and production of a compact with desired properties. Linear feeding systems consist of a shoe filled with powder passing over a die with specific opening geometry and depositing powder into the cavity. In this process, the powder is delivered into the die under three different mechanisms: 1) nose flow, 2) bulk flow, and 3) intermittent flow.

As the motion of the shoe in die filling process initiates, the acceleration of the shoe and the friction between the powder particles inside the shoe and the base plate result in the formation of a nose shaped heap inside the shoe. As the tip of the nose passes over the die, the powder can flow into the die which is referred to as nose flow (Figure 2-6-a). At high shoe velocities or for small die openings, the nose of the heap passes over the die and particles discharge continuously from the bottom of the powder bed into the die. This mechanism is known as bulk flow (Figure 2-6-b). For cohesive powders, powder discharge from the bottom of the heap is not continuous and occurs in a series of discrete clusters of particles. This mechanism is referred to as intermittent flow (Figure 2-6-c). The three types of powder flow into the die was documented using high-speed videos by Schneider and co-workers (Schneider et al., 2007).

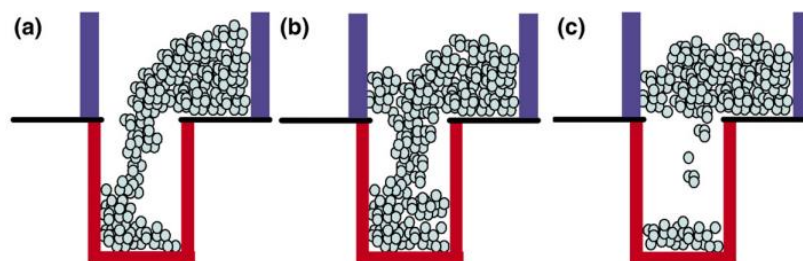


Figure 2-6. Different types of powder flow into a die; a) nose flow, b) bulk flow, and c) intermittent flow (Schneider et al., 2007).

In the studies carried out by Wu and co-workers (Wu et al., 2003) a model shoe-die system was used to study the mass delivered into different die geometries. They introduced the term of critical velocity defined as the maximum shoe velocity below which the die is completely filled. Wu proposed the critical velocity as a measure of

powder flowability whereby a powder with higher critical velocity is ranked as a better flowing powder. However, the critical velocity is specific to the geometry of the system, the height of the powder in the shoe and parameters related the state of the powder inside the shoe (Sinka and Cocks, 2009).

The influence of particle shape on the flowability of powders in linear shoe-die systems was investigated numerically by Wu and Cocks (Wu and Cocks, 2006). Based on this study, the particle shapes are classified in terms of flowability in two main groups of 1) particle shapes that can tessellate (rectangular and hexagonal) and 2) non-tessellating particle shapes.

In die filling, the introduction of powder mass into the die result in a reduction in the volume of air and development of a pressure gradient opposite to the direction of the flow. This pressure gradient grows in magnitude as more powder enters the die and inhibits the further flow of powder. These effects were captured using high-speed videos (Wu et al., 2003, Wu and Cocks, 2004, Schneider et al., 2007). The flow behaviour of pharmaceutical powders in the linear shoe-die system was studied by Schneider and co-workers (Schneider et al., 2007) with experiments carried out both in air and vacuum. A dimensional model was developed to predict the mass of the powder delivered into the die as a function of shoe velocity.

$$\frac{m_g}{\rho_b D^2 L} = c \left(\frac{v_s}{\sqrt{gD}} \right)^{-(1+n)} \quad (2-20)$$

In this relation, m_g is the mass of the powder delivered into the die (in gravity), ρ_b is the bulk density of the powder, D is the opening size of the die, L is the length of the shoe, g is the acceleration due to gravity and v_s is the velocity of the shoe. In this relation, c and n are empirical parameters depending on material properties and processing parameters.

Based on the high-speed videos captured, it is observed that most of the powder mass is introduced at early stages of delivery (Schneider et al., 2007). However, without any accurate measurement of the mass flow rate, it should be assumed that the mass flow rate is consistent during the mass delivery period.

Fitting the experimental results to the model developed (Equation (2-20)) showed that the relation can predict the mass of the powder delivered into the die in vacuum. However, large scatter in the data was observed for the experiments carried out in air. This is due to the fact that this model cannot capture the air pressure effects on the mass of the powder delivered into the die.

The effects of particle size and density on die filling in air and vacuum from a stationary shoe was investigated by Guo and co-workers (Guo et al., 2009). They observed that the mass flow rate of monodisperse and polydisperse powders into the die in vacuum is constant. For powders with smaller particle size and smaller density, the impact of air is more significant and if the particle size and density are large enough the presence of air does not have any effect on the mass flow rate. They proposed a power law relation between the dimensionless mass flow rate (Equation (2-21)) and $Ar \cdot \Phi$ (Equation (2-22)) where Ar is the Archimedes number defined by Equation (2-21) and Φ is the ratio between the particle and air density.

$$\bar{M} = \frac{m}{\rho_b g^{0.5} l b^{1.5} \left(1 - k_B \frac{d}{b}\right)^{1.5}} \quad (2-21)$$

$$\bar{M} = B(Ar \cdot \Phi)^{0.2} \quad (2-22)$$

$$Ar = \frac{\rho_a (\rho_s - \rho_a) g d^3}{\mu^2} \quad (2-23)$$

In equations above, l is the length of the die, b is the width of the die, ρ_a is the air density, ρ_s is particle density and μ is the viscosity of air. The constant B is a function of void fraction.

Schneider and co-workers (Schneider et al., 2007) used the experimental results obtained to predict the flowability of powders in rotary tablet presses (described in Section 2.3.5) and calculate the maximum rotational speed at which the die is filled completely (using the values c and n obtained from experiments). The velocity calculated was half of the maximum speeds used in industry. This is due to the effect of

suction fill created by the downward motion of the lower punch in rotary tablet presses. Suction fill mechanism is not limited to high-speed rotary tablet presses. Many of the powder metallurgy parts with complex shapes are produced using suction fill mechanism particularly for dies with small cross-sectional area (Sinka and Cocks, 2009). The effect of suction fill on the fill ratio was investigated by Jackson and co-workers (Jackson et al., 2007). They observed that using suction fill, the critical velocity of the material used was increased by a factor of approximately 2.5.

Wu and Guo (Wu and Guo, 2012) carried out a numerical study of suction fill effects in die filling using a 2D CFD/DEM model and found similar results to the observations made by Jackson et al. (Jackson et al., 2007). They observed that the mass flow rate under gravity in vacuum is equivalent to the mass flow rate of powders under suction in air.

More experiments on the influence of suction fill mechanism on the mass of powder delivered in linear shoe-die systems was carried out by Mills and Sinka (Mills and Sinka, 2013) using different grades of MCC. They observed that in gravity fill the critical velocity of powders with larger particle size was one order of magnitude above the critical velocities obtained for fine powders. Also, they observed that powders with fine particle size are influenced more by suction fill mechanism such that the critical velocity of the materials determined for suction fill was similar to each other. Mills and Sinka used the model developed by Schneider (Equation (2-21)) to calculate the empirical constants c and n for the materials used and showed that the constant change for different processing parameters.

2.3.5. Rotary feeding systems

Pharmaceutical tablets are produced using high-speed rotary tablet presses. In these systems, the powder flows through a hopper into the feed frame and then into the moving dies. The bottom punch inside the die is initially covering the die opening. As the die enters the feeding cam, the downward motion of the bottom punch inside the die creates a suction effect which facilitates the flow of powder. The mass of the powder inside the die is adjusted using the metering wheel before compaction using the two punches and ejection of the tablet from the die. The mechanisms that can be employed to assist the filling process can be listed as:

- Paddle wheels (force feed)
- Downward motion of the lower punch(suction fill)
- Weight adjustment mechanism (the powder is partially ejected)
- Metering wheel (to increase weight uniformity)
- Centrifugal forces and vibrations of the system

The kinematics of compression and the compaction parameters are discussed in detail in a study carried out by Sinka and co-workers (Sinka et al., 2009). The effects of feed frame on powder flow properties and weight uniformity of the powder introduced into the die were investigated by Mendez and co-workers (Mendez et al., 2010). They demonstrated that the residence time of powder inside the feed frame decreased by increasing the feed frame speed and die disc speed. The die filling weight was observed to increase with feed frame speed while it reduced for larger die disc velocity. In a study by Mendez and co-workers (Mendez et al., 2012), the effects of feed frame on particle transformation were investigated. It was observed that the particle size distribution of the powders changes as the powder flows through the feeder. Also, the bulk and tap density of the powders increased with the feed frame speed. Similar investigations were carried out by Peeters and co-workers (Peeters et al., 2015) to find an optimum combination of processing parameters to minimise tablet weight variability. Ketterhagen (Ketterhagen, 2015) carried out a numerical study to investigate how the paddle wheel shape, rotation speed and direction affect the tablet quality attributes such as weight, weight uniformity and attrition. He concluded that using a paddle wheel with large hub generally improve the tablet attributes relative to the other two paddle wheels used in his study. The rotational speed of the paddles has conflicting effects. Increasing the speed, result in a better-mixing performance and reduced tablet mass variation while it potentially increases the attrition and over-lubrication.

The influence of die table speed, die opening size and a series of material dependent parameters on the die filling processes was examined numerically by Gopireddy and co-workers (Gopireddy et al., 2016). In this study, the influence of air on powder flow is not considered and the particles are flowing in vacuum. Similar to the observations made by Mendez and co-workers (Mendez et al., 2012) they observed that the mass of the powder delivered into the die reduced for larger die disc speeds.

2.4. Summary of gaps in literature

There are a range of powder flow characterisations methods developed. However, the results obtained from these techniques are not always consistent with each other (Lee et al., 2000). A powder that is characterised as a good flowing material in one flow testing method can show reduced flow behaviour in another flow characterisation technique or under different processing parameters. Therefore, the powder flow characterisation technique should be selected based on the process under investigation. The studies carried out on powder arching in hoppers and bins are mostly theoretical and the solutions proposed to eliminate arching are based on the critical orifice diameter. Fine and cohesive powders have large critical orifice diameters and the hopper design calculations suggest that the opening size of the containers to avoid arching should be larger than the critical orifice diameter. However, in many applications (such as tableting), these materials are required to flow into cavities with openings sizes that are significantly smaller, which poses challenges. The effects of air pressure conditions on the flow behaviour of the powders have been observed previously (Wu and Cocks, 2004, Sinka et al., 2004, Schneider et al., 2007, Jackson et al., 2007, Mills and Sinka, 2013) and proposes a new potential method to avoid arching and facilitate powder flow into closed cavities.

For powder discharge into open atmosphere, the model available (Beverloo correlation) cannot predict the mass flow rate correctly for fine and cohesive powders and in order to obtain a correct flow rate the Beverloo coefficient should be adjusted for the specific material in use (Nedderman, 1992). However, the value of the Beverloo constant for commonly used pharmaceutical excipients is not reported in the literature. Also, the models available to calculate the mass flow rate under differential pressure (Crewdson model presented in Equation (2-18)) cannot predict the flow rates of fine and cohesive powders accurately (this is discussed in detail in Chapter 6) and there is still a need to develop a new model to capture the behaviour of fine and cohesive materials under differential pressure.

The Schneider model (Schneider et al., 2007) to predict the mass of powder delivered into the die in linear shoe-die systems (Equation (2-20)) was developed for gravity fill.

It was noted that for powder discharge in air this model does not give a good prediction of the mass delivered (Schneider et al., 2007). The empirical constants present in this model was found to change for different processing conditions (Mills and Sinka, 2013) and in order to use this model, the coefficients should be calibrated for each set of parameters. The relation proposed by Guo et al. (Guo et al., 2009) regarding the mass flow rate cannot easily be validated experimentally due to the particle size distribution of the powders. The influence of suction fill and air pressure conditions on the flow behaviour of the powders should be studied in more detail and a new model is required to predict the mass delivered into the die under suction fill mechanism.

A limited number of studies have been carried out regarding the effects of processing and material dependent parameters on powder flow behaviour in rotary feeding systems. Majority of these studies are numerical simulations and the experimental data are not available for validation. This is due to the large number of variables involved in this process including the paddle wheel shape, paddle cross-sectional shape, size of the paddles, rotational speed, size of the opening of the feeder, exit diameter and shape of the feeder and etc. which makes experimentation really challenging.

2.5. Methodology

The methodology used in this research consist of a series of experiments designed to identify key features of the flow behaviour of powders under the influence of different atmospheric pressure and differential pressure conditions. The design of the experiments was guided by dimensional analysis. In order to describe the features observed in the experiments the results were analysed using the framework of dimensional analysis and Buckingham Π theorem and new models were developed to identify and quantify air pressure effects.

Six commonly used pharmaceutical excipients were selected based on their average particle size, bulk density and flow behaviour. A powder conditioning device was built to ensure consistent and repeatable initial condition of the material prior to testing. The powders were characterised using secondary electron microscopy (SEM), bulk density, angle of repose and critical orifice diameter measurement techniques.

The testing equipment and experimental procedures required were developed in order to 1) measure powder permeability and study the influence of small levels of compaction on permeability, 2) study the effect of differential pressure on powder flow from arching state, 3) measure the mass flow rate of powders under the influence of differential pressure, 4) study the parameters affecting the mass of powder delivered into a die under gravity and suction fill mechanisms in linear shoe-die system, and 5) study the effect of processing parameters on the mass flow rate of powders in rotary feeding systems.

Chapter 3. Powder flow characterisation using standard techniques

The materials used in the experimental studies presented in this thesis are described in this chapter. In order to obtain a consistent and repeatable initial condition of the powders in the experiments, a powder conditioning device was designed (Section 3.2). The bulk density of the powders is measured using the procedure described in Section 3.3. The flowability of the materials is categorised using the angle of repose and critical orifice diameter in Sections 3.4 and 3.5, respectively and the influence of average particle size and bulk density on powder flow behaviour is discussed. The results obtained from the two measurements are compared in Section 3.7.

The observations on the flow behaviour of powders in rotary feeding powders are presented in Section to highlight the complex interplay of material properties and processing parameters influencing powder flowability.

3.1. Materials

Three groups of commonly used pharmaceutical excipients were selected for use in the experimental investigations. These materials were chosen based on their average particle size, bulk density and flow behaviour in order to examine the influence of these parameters in different processes. The SEM images of the materials were taken using a Philips XL30 ESEM with the spot size set to 5 under the voltage of 20kV. The particles were gold-plated before imaging to stop particles from charging under high beam voltages.

3.1.1. Microcrystalline Cellulose (MCC)

Four grades of microcrystalline cellulose ($C_6H_{10}O_5$), Avicel PH101, PH102, PH200 and PH302 (manufactured by FMC BioPolymer, Belgium) are used. Microcrystalline cellulose is a white odourless powder commonly used in pharmaceutical formulations as an excipient due to its high compressibility and excellent binding capacity in solid dosage forms such as tablets. The particle density of microcrystalline cellulose (MCC) is 1.512-1.668 g/cm³ (Rowe et al., 2009). Average particle size (d_{50}) of PH101 and PH102 are 50 and 100 μ m respectively (data provided by the manufacturer). Two different batches of

PH200 were used in this study. For the experiments carried out in Chapter 5, the average particle size of the batch of PH200 used was 200 μm . For the rest of the experiments presented, the second batch with average particle size of 180 μm were used. The similar bulk density of PH101, PH102 and PH200 allows identifying the influence of average particle size on flow.

PH302 with the same average particle size as PH102 (100 μm) is designed to have a higher bulk density. Comparison of the results obtained for PH102 and PH302 highlights the influence of bulk density. The SEM (Scanning Electron Microscopy) images of four grades of MCC are presented in Figure 3-1.

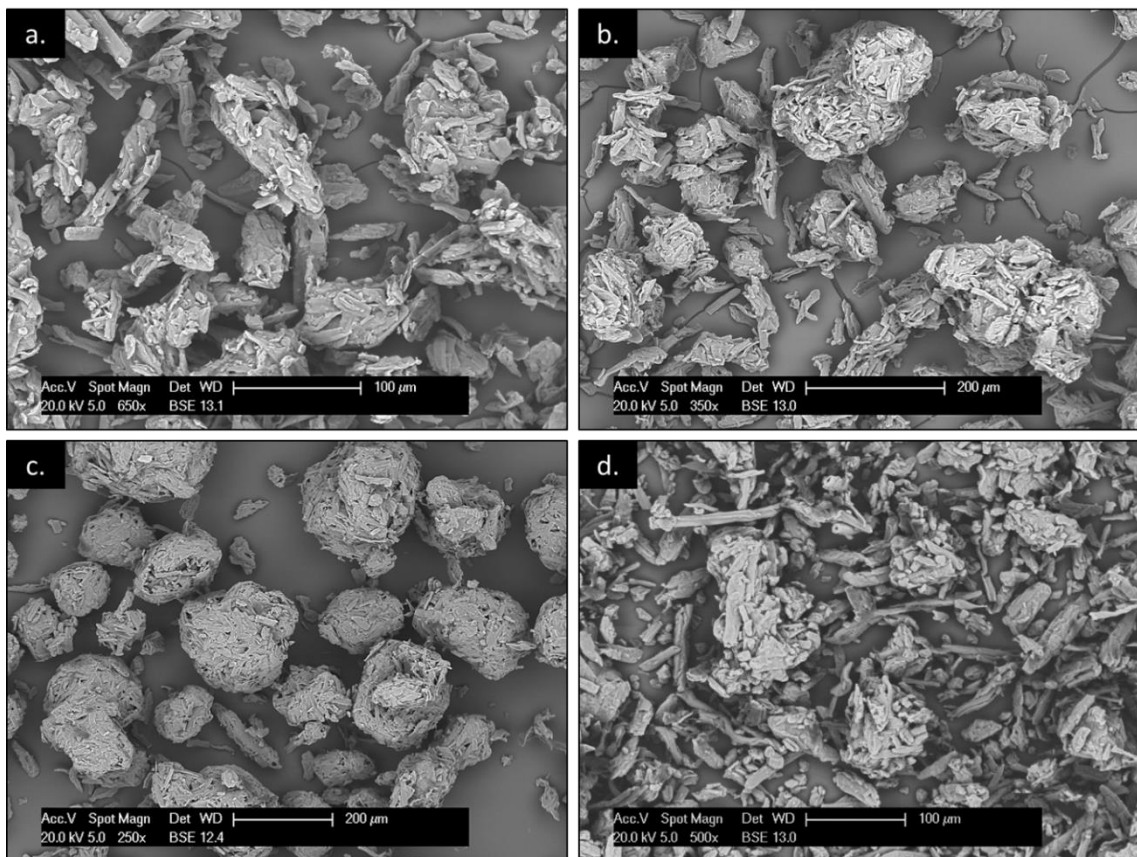


Figure 3-1. SEM images of a) PH101, b) PH102, c) PH200 and d) PH302 (Baserinia et al., 2016)

3.1.2. Calcium Phosphate (ATAB)

Calcium Phosphate anhydrous grade (ATAB) with chemical formula of CaHPO_4 is a white and odourless powder used as a pharmaceutical excipient because of its good compaction properties and powder flow behaviour. The powder used in this thesis is

manufactured by Innophos. ATAB is typically used in the nutritional/health and food sectors as a source of calcium. The particle density of ATAB is 2.89 g/cm^3 and the average particle size is $180 \text{ }\mu\text{m}$ (Rowe et al., 2009). The SEM image of ATAB particles is presented in Figure 3-2.

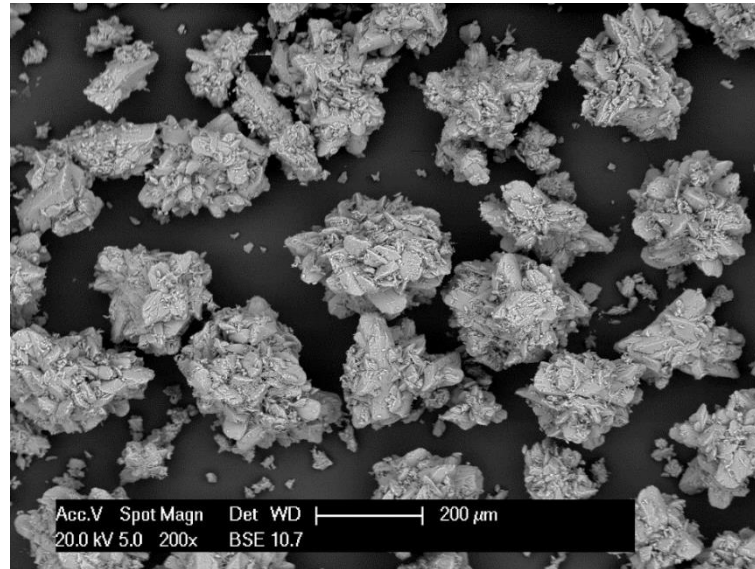


Figure 3-2. SEM image of Calcium Phosphate (ATAB) (Baserinia and Sinka, 2016)

3.1.3. Mannitol

Mannitol ($\text{C}_6\text{H}_{14}\text{O}_6$) (grade Pearlitol 200SD) is a white and odourless pharmaceutical excipient used as diluent in tablet formulation. The batch of Mannitol (grade Pearlitol 200SD) used was manufactured by Roquette. It is also used in direct compression tablet applications and the manufacture of chewable tablet formulations (Rowe et al., 2009). The particle density of Mannitol is 1.514 g/cm^3 (Rowe et al., 2009) and the average particle size is $180 \text{ }\mu\text{m}$ (data provided by the manufacturer). The SEM image of Mannitol is presented in Figure 3-3.

The specifications of the powders used in this thesis are summarised in Table 3-1. The particle size distribution of the six powders measured using a Malvern Mastersizer 2000 are presented in Figure 3-4 representing the percent volume of each particle size and in Figure 3-5.

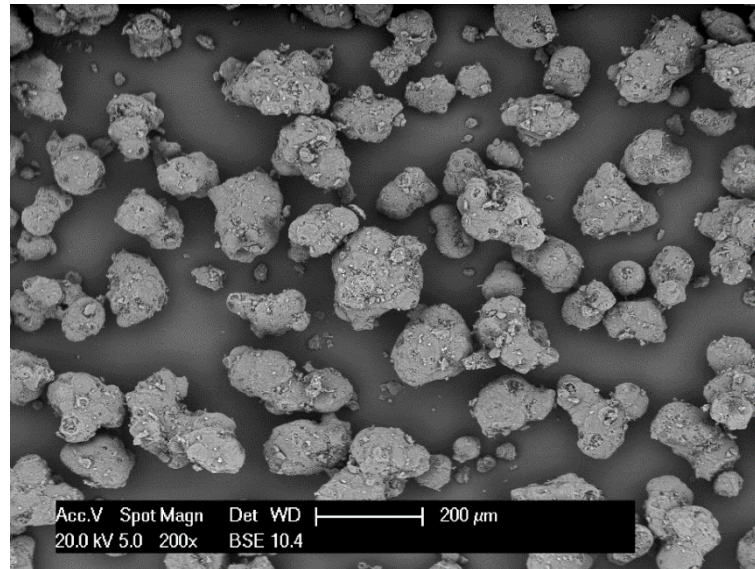


Figure 3-3. SEM image of Mannitol (Baserinia and Sinka, 2016)

Table 3-1. Specifications of the powders

Material	Chemical Formulation	Manufacturer	Reference Name	Average particle size (d_{50}), μm
Microcrystalline Cellulose	$\text{C}_6\text{H}_{10}\text{O}_5$	FMC BioPolymer	Avicel PH101	50
Microcrystalline Cellulose	$\text{C}_6\text{H}_{10}\text{O}_5$	FMC BioPolymer	Avicel PH102	100
Microcrystalline Cellulose	$\text{C}_6\text{H}_{10}\text{O}_5$	FMC BioPolymer	Avicel PH200	180/200
Microcrystalline Cellulose	$\text{C}_6\text{H}_{10}\text{O}_5$	FMC BioPolymer	Avicel PH302	100
Calcium Phosphate	CaHPO_4	Innophos	ATAB	180
Mannitol	$\text{C}_6\text{H}_{14}\text{O}_6$	Roquette	Mannitol	180

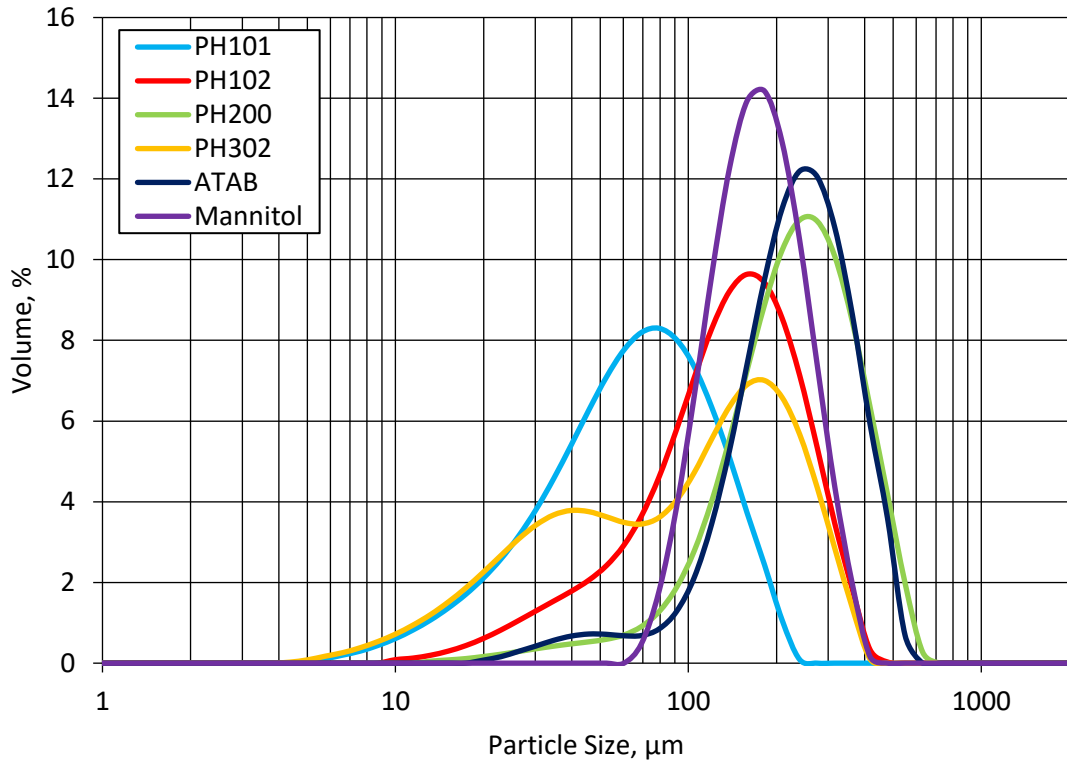


Figure 3-4. Particle size vs. volume percentage of the six materials

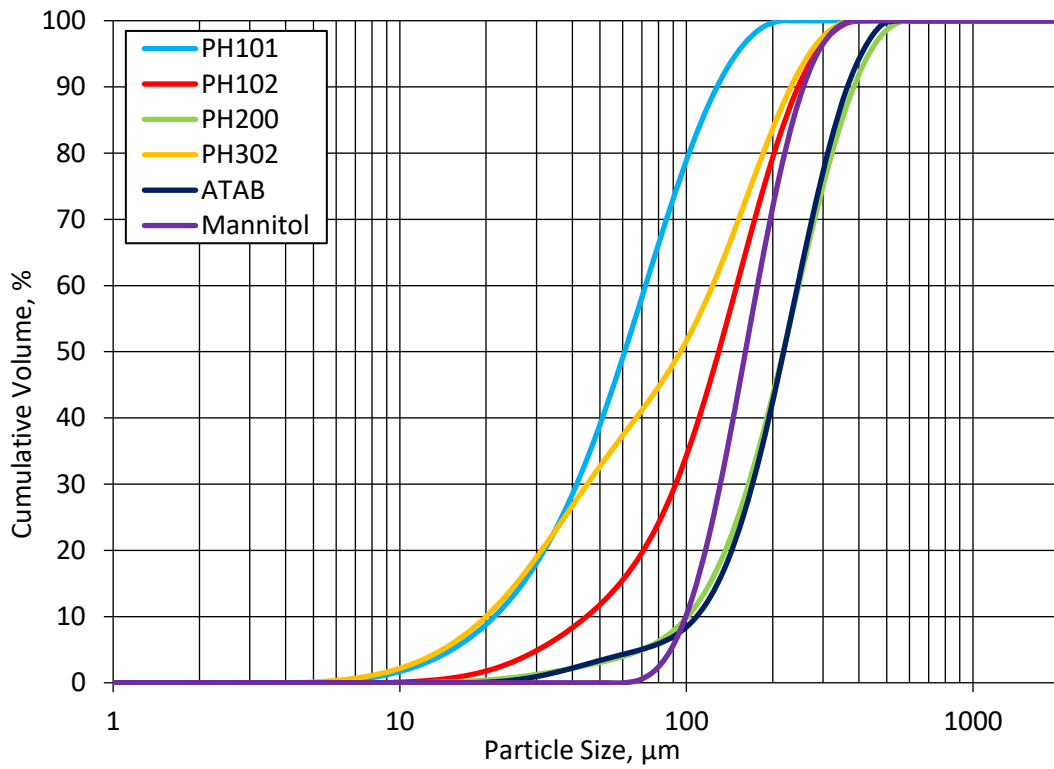


Figure 3-5. Particle size vs. cumulative volume percentage of the six materials

3.2. Powder conditioning device

In the experiments presented in this thesis, a powder conditioning device was used to introduce the powders into the containers in order to ensure consistent and repeatable initial condition of powder before the experiment. As the powders go through the conditioning device they slide on the sloped surfaces and the possible agglomerates formed during handling and storage of the powders break. The conditioning device was designed based on the Scott Volumeter used in a standard bulk density measurement procedure (USP29-NF24, 2006).

The device was made of Acrylic. The plates were 5 mm thick forming an angle with the vertical walls of 35° . A plastic funnel with the opening of 30 mm was attached to the top of the device. The device is secured in position using a stand as illustrated in Figure 3-6.

As the powder is introduced from the top, the particles slide on the surface of the angled plates and discharge into a container below. Using this device the repeatability of the experiments was improved considerably. All the experiments presented in this thesis use this device.

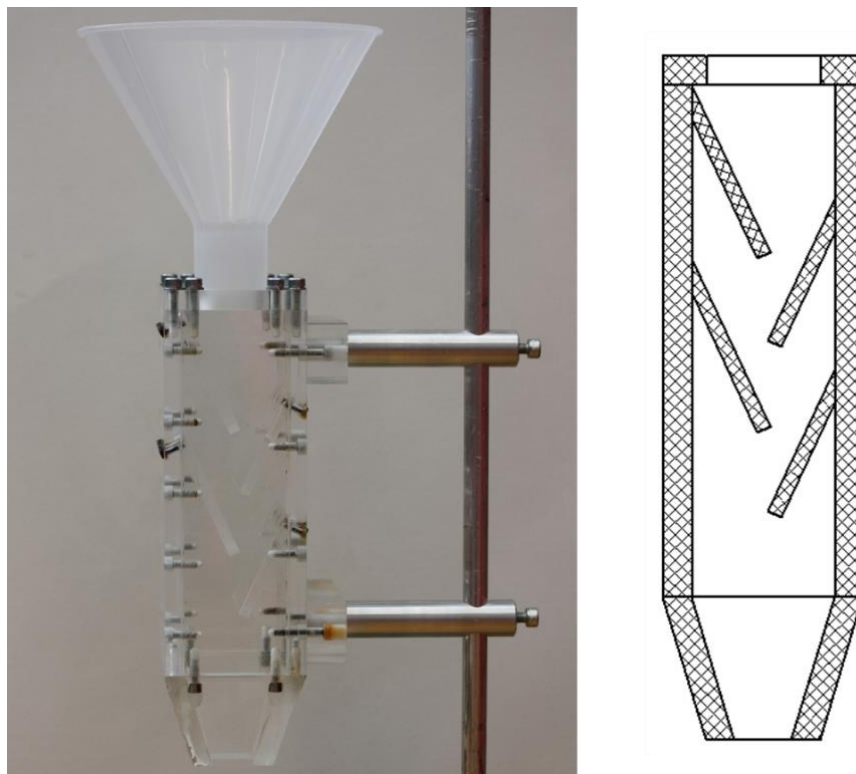


Figure 3-6. Powder conditioning device

3.3. Bulk density measurement

The bulk density is defined as the mass of powder in a loose state divided by the volume it occupies. Therefore, the bulk density of a material is smaller than the particle density (true density). The bulk density of the materials is measured using the procedure explained in the following section.

3.3.1. Procedure

The powder conditioning device was placed above an aluminium cup with an internal diameter of 57.4 mm and height of 76 mm (Figure 3-7) so that the distance between the exit of the conditioning device and top of the cup was approximately 25 mm. The powder was introduced into the cup using the conditioning device. Once the container was full, the hip formed on the top was removed using a horizontal blade and the full cup was weighed. The mass of the powder in the cylinder was measured by subtracting the total mass by the mass of the empty cup. Using the volume of the cup, the bulk density was determined. This procedure was repeated ten times for each material using a fresh sample for each test.

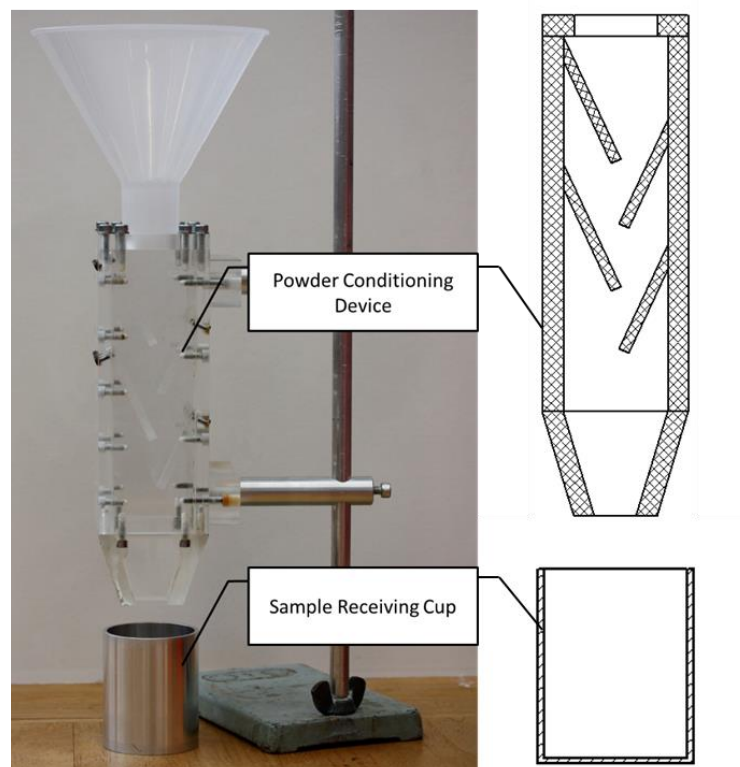


Figure 3-7. Bulk density measurement apparatus

3.3.2. Results

The bulk densities measured for the six materials are presented in Table 3-2. It is evident that the PH101, PH102 and PH302 have similar bulk density. The bulk density of PH302 with similar average particle size as PH102 is nearly 1.5 times higher. ATAB and Mannitol with similar average particle size as PH200 have significantly larger bulk densities. The particle density of ATAB (2.89 g/cm³) is nearly 2 times higher than the particle density of the four grades of MCC and Mannitol (with particle densities of 1.512-1.668 g/cm³ and 1.514 g/cm³ respectively). Also, as illustrated in Figure 3-2 and Figure 3-3, the particles of ATAB and Mannitol are more spherical compared with the four grades of MCC and the number of fines are lower. These result in lower void fraction in the powder bed and larger bulk density.

Table 3-2. Bulk density of the materials

Material	PH101	PH102	PH200	PH302	ATAB	Mannitol
Bulk Density, kg/m ³	309	318	363	428	725	498
Standard Deviation	2.27	2.79	2.79	4.25	2.89	2.68

3.4. Angle of Repose

In this section, the flowability of the materials described in Section 3.1 is characterised using the angle of repose experiment. The fixed base diameter method was used to measure the angle of repose. The results obtained are compared with regard to the average particle size and bulk density.

3.4.1. Procedure

The system used to measure the angle of repose (AoR) is illustrated in Figure 3-8 and consists of a cylindrical base, a funnel and the powder conditioning device. The base and the funnel are both made from aluminium. The base allows creating heaps with precise

diameters of 50, 75 or 100 mm. The funnel conforms to the geometry of the Hall flowmeter (International Organization for Standardization (ISO), 2014).

The funnel was lowered to cover the exit with the base. The powder conditioning device was positioned above the funnel while the distance between the exit of the device and top of the funnel was approximately 25 mm. 75 grammes of powder was introduced into the funnel using the powder conditioning device. The conditioning device was removed to allow the funnel to move upward. The funnel was raised gradually as the powder was discharged forming a heap. The height of the heap formed was measured using a height gauge. A rectangular gauge with a precise thickness of 5 mm was attached to the tip of the height gauge to increase its length. The angle of repose was calculated using the tangent rule. This procedure was repeated five times (using a fresh sample of powder for each repeat experiment) for each of the six materials for the three different base diameters.

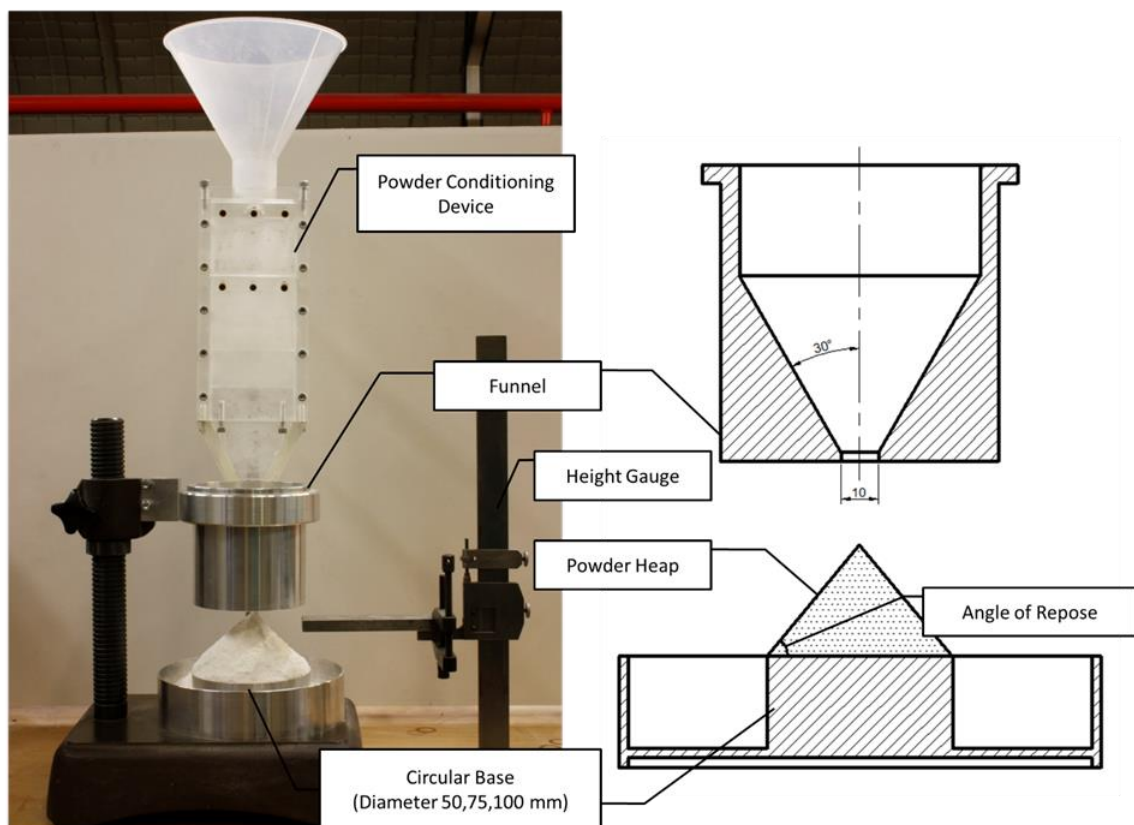


Figure 3-8. Angle of repose measurement apparatus

3.4.2. Results and discussions

The average values of the angle of repose of the six powder materials and the standard deviations (STDEV) are presented in Table 3-3. There is a small variation in the values of angle of repose calculated for different base diameters which highlight the sensitivity of angle of repose to the measurement technique used. The results obtained are used to rank the flow behaviour of the materials. The smaller angle of repose is indicative of better powder flowability.

Flowability of Avicel PH200, Mannitol and ATAB are classified as “Good” based on the Carr’s angle of repose ranking (Carr, 1965b). Avicel PH102 is categorised as the “Fair – aid not needed” while PH101 and PH302 are classified as “Passable – may hang up”. This ranking is consistent with the observation made while carrying out the experiment. It was observed that PH101 and PH302 occasionally formed an arch above the exit of the funnel and tapping of the system was required to initiate the flow of the powder. The angle of repose measured for PH101 and PH302 are at the higher boundary of the range associated with the “Passable – may hang up” group which suggest that these powders may perform similar to powders ranked as “Poor – must agitate, vibrate”.

Table 3-3. The average angle of repose measured for three base diameters of 50, 75 and 100 mm

Material	Base Diameter					
	50 mm		75 mm		100 mm	
	AoR, °	STDEV	AoR, °	STDEV	AoR, °	STDEV
PH101	45	0.96	45	0.43	44	0.56
PH102	39	0.89	40	1.39	39	0.66
PH200	33	1.03	34	0.29	33	0.74
PH302	46	0.87	45	0.59	43	0.39
Mannitol	32	0.33	33	0.35	33	0.10
ATAB	35	0.77	36	0.29	35	0.36

Generally, powder flowability improves for powders with larger average particle size. Comparing the results obtained for PH101, PH102 and PH200 with similar morphology (Katdare and Chaubal, 2006) show that PH200 with average particle size of 180 μm is ranked as a better-flowing powder and flowability reduces for PH102 and PH101 with average particle sizes of 100 μm and 50 μm respectively.

Comparing the results obtained for PH102 and PH302 (which have similar average particle size) shows that PH302 with higher bulk is ranked as poor flowing. This is not consistent with the observations made by Hou and Sun (Hou and Sun, 2008) using a ring shear cell tester stating that flowability improves for powders with higher bulk density. This contrast highlights the fact that different testing methods give a different ranking of powder flowability and other factors, e.g. particle shape, morphology etc. should be considered.

Podczek (Podczek and Mia, 1996) and Fu (Fu et al., 2012) showed that powder flowability increased from needle shape, cubic, angular to round shape particles. Based on the SEM images presented in Figure 3-1, Figure 3-2 and Figure 3-3 the number of fine and elongated particles are larger for PH101, PH102 and PH302 suggesting that these materials might show poor flow behaviour. This is consistent with the angle of repose results. For ATAB, Mannitol and PH200 where the particles are mostly spherical smaller values of angle of repose are recorded.

3.5. Critical orifice diameter

The flow behaviour of the six materials described in Section 3.1 was characterised by the critical orifice diameter (COD) measurement. The critical orifice diameter measurement is based on the tendency of a powder to discharge through a hole. When the orifice diameter is above the critical value, the powder will flow freely out of the container while for exit diameters smaller than the critical orifice diameter, the powder forms an arch above the exit. The powder with larger critical orifice diameter is ranked as poor flowing powder as a larger exit size is required to enable consistent discharge of the material. A set of disks with orifice diameters of 1-16, 18, 20, 22, 24, 25, 26, 28 and 30 mm with a thickness of 1.5 mm made from aluminium were used. The results are compared in terms of the average particle size and bulk density.

3.5.1. Procedure

The cylindrical container with an internal diameter of 57.4 mm and height of 76 mm was closed using a shutter as indicated in Figure 3-9. The disk with the orifice diameter of 30 mm was placed at the bottom of the container.

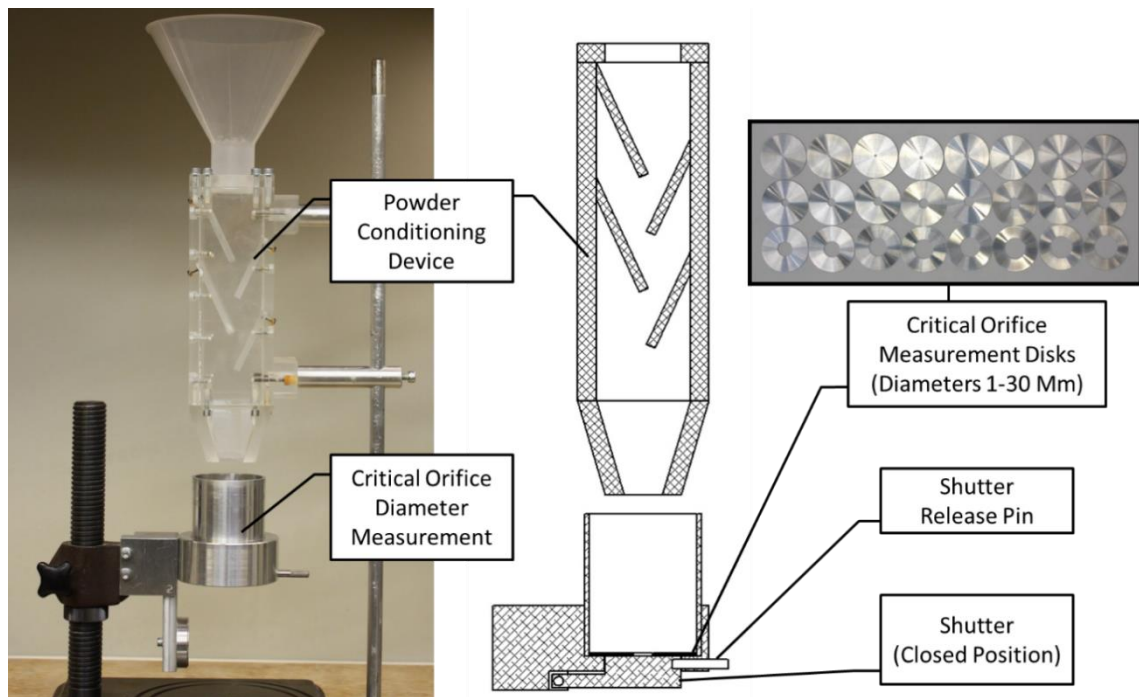


Figure 3-9. Critical orifice diameter measurement apparatus

The powder was introduced into the container using the powder conditioning device described in Section 3.2. The heap formed on top of the filled container was removed using a horizontal blade. The shutter was opened using the associated pin. If the powder was discharged, the test was repeated using a disk with smaller orifice diameter. The smallest orifice diameter from which the powder discharged was recorded as the critical orifice diameter. The procedure was repeated five times to confirm the critical orifice diameter.

3.5.2. Results and discussions

The critical orifice diameters measured for the materials are presented in Table 3-4. The results can be used to categorise the materials in terms of powder flowability where a good flowing powder has smaller critical orifice diameter. Based on the results the flowability of the powders can be ranked as follows starting with poor flow

PH101 => PH102 => PH302 => PH200 => Mannitol => ATAB

Comparing the critical orifice diameter of PH101, PH102 and PH200 with similar bulk densities suggest that flowability increases for larger particle size. For PH302 with similar

average particle size as PH102 but with higher bulk density, the critical orifice diameter measure is smaller suggesting that flowability improves for higher bulk density. Also, for ATAB and Mannitol which have higher bulk densities than the four grades of MCC, smaller critical orifice diameters are recorded.

For PH101, PH102 and PH302 with a higher number of elongated particles larger critical orifice diameters are recorded (30, 26 and 24 mm respectively) while for powders with mostly spherical particles (ATAB, Mannitol and PH200) the critical orifice diameters measured are smaller. This is consistent with the observations of Podczec (Podczec and Mia, 1996) and Fu (Fu et al., 2012) for particles of different shape.

Table 3-4. Critical orifice diameters of the materials

Material	PH101	PH102	PH200	PH302	ATAB	Mannitol
COD, mm	30	26	11	24	3	6

3.6. Observations on flow behaviour of powders in rotary feeding systems

In this section, a model rotary feeding system developed at University of Leicester is used to study the effects of material properties and processing parameters on the mass flow rate of four grades of microcrystalline cellulose. The mass flow rate of the powders is measured for a range of paddle rotational velocity (25-325 rpm) both in air and under differential pressure. The influence of exit diameter is also investigated.

3.6.1. Description of the system

The system consists of a powder container connected to a rotary feeder (Figure 3-10). The powder container is formed of a hopper with half angle of 15° attached to a cylindrical section. The container is extended with a large hopper and a cylinder to accommodate approximately 1 kg of powder. The powder inside the feeder is stirred with four sets of four interchangeable paddles with different cross-sectional shapes of square, circle, push down and push up. The paddles are driven using an electrical motor where the rotational velocity of the paddles is adjusted by changing the input voltage of

the motor. The power of the motor is transferred to the paddles using two spur gears with speed ratio of 1:1. A reflective plate is attached to one of the gears and a light tachometer is used to measure the angular velocity of the paddles in rpm. Three different exit diameters of 5, 10 and 15 mm can be used (in the experiments carried out only the exit diameter of 10 mm was used). The powder discharging from the container is collected using a beaker placed on a scale to measure the mass flow rate. The feeder is attached to a vacuum chamber to allow control of the pressure at the exit using a vacuum pump and a vacuum regulator (Airtrol V-900-10 W/K). The pressure difference between the vacuum chamber and the ambient atmosphere is measured using a differential pressure transducer (Sensirion SDP1000-L) connected to the side of the vacuum chamber. A connecting port is also placed on the feeder to allow pressure measurement inside the feeder as well. The pressures and flow time are logged using a data acquisition device (National Instruments NI USB-6221) and PC software (LabVIEW).

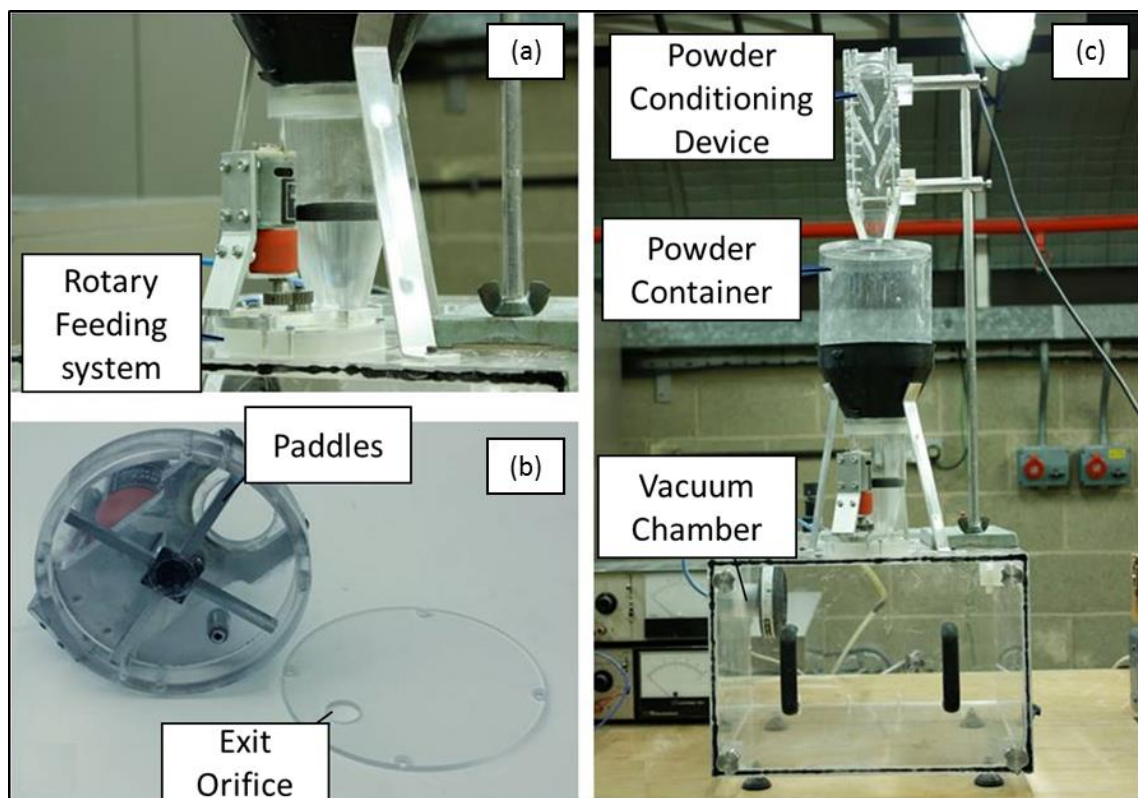


Figure 3-10. The rotary feeding system illustrated in three pictures: a) the powder container connected to the feeder b) paddles and the exit orifice of the feeding system c) complete setup of the apparatus

3.6.2. Procedure

The input voltage of the electrical motor described in the previous section was adjusted to set the angular velocity (25-325 rpm). The motor was turned off and 400 grams of powder was introduced into the container using the powder conditioning device (described in Section 3.2) to ensure consistent and repeatable initial conditions of the powder. The motor was turned on and the discharging of the powder from the exit orifice of the feeder started. In order to ensure measurements in steady state, time measurement was started after 100 grams of powder was discharged and the time required for 200 grams of powder to discharge was recorded. An extra set of experiments were carried out for PH102 by pre-setting the differential pressure below the exit of the feeder to 100 Pa using the vacuum regulator and the vacuum pump described before turning the motor on.

The experiments were repeated three times for each angular velocity using fresh samples for each set of velocities. The top layer of powder was agitated to prevent “rathole” forming in the bed. The experiments were carried out for square paddles only.

3.6.3. Results and discussions

3.6.3.1. Observation on air pressure build-up

For the experiments carried out under the influence of differential pressure (100 Pa), the changes in the pressure difference between the feeder and ambient atmosphere was recorded using the differential pressure transducer described. Analysing the pressure profile shows that every time a paddle covered the exit of the feeder, powder flow from the container into the feeder resulted in air pressure build-up inside the feeder. After the paddle passed the exit, powder discharge initiated again from the feeder. Powder flow results in dilation of the powder inside the feeder and development of a negative pressure gradient which opposes powder flow out of the feeder.

The air pressure build-up and the negative pressure gradient result in an oscillation in the mass flow rate of the powder discharging from the feeder; however, the overall mass flow rate remained constant during the measurement period. The pressure profile for PH102 using the paddle speed of 100 rpm is plotted in Figure 3-11 showing the

repeating development of the positive and negative pressure gradients in the feeder. It is observed that the sum of the time for air pressure build-up and the negative pressure gradient to develop is equal to the time interval between two consecutive paddles to cross the exit (0.15 s for rotational speed of 100 rpm).

3.6.3.1. Mass flow rate measurement

The time required for four grades of MCC to discharge from the feeder measured for different angular velocities are plotted in Figure 3-12. The error bars are generated using the standard deviation of the times measured. It is observed that the error in time measurement is relatively small and the procedure can produce repeatable results.

The mass flow rate of four grades of MCC was calculated by dividing the mass of the powder discharged from the feeder (200 g) by the time recorded. The average mass flow rate from the three repeat experiments is plotted against the paddle's angular velocity in Figure 3-13.

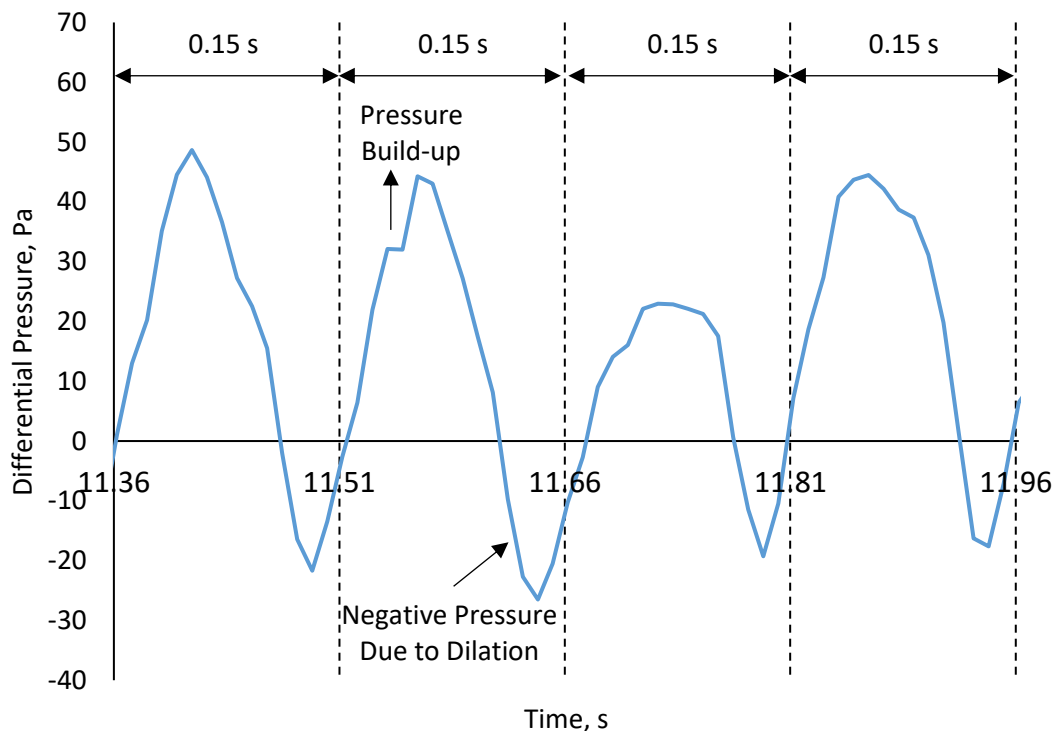


Figure 3-11. The differential pressure between the feeder and ambient atmosphere measured for PH102 flowing through the feeder under the rotational velocity of 100 rpm.

The results show that initially the mass flow rate of the powders increases with the angular velocity. By increasing the angular velocity above a specific value, which can be referred to as the critical angular velocity, the mass flow rate of the powder reduces. This effect is explained in detail below.

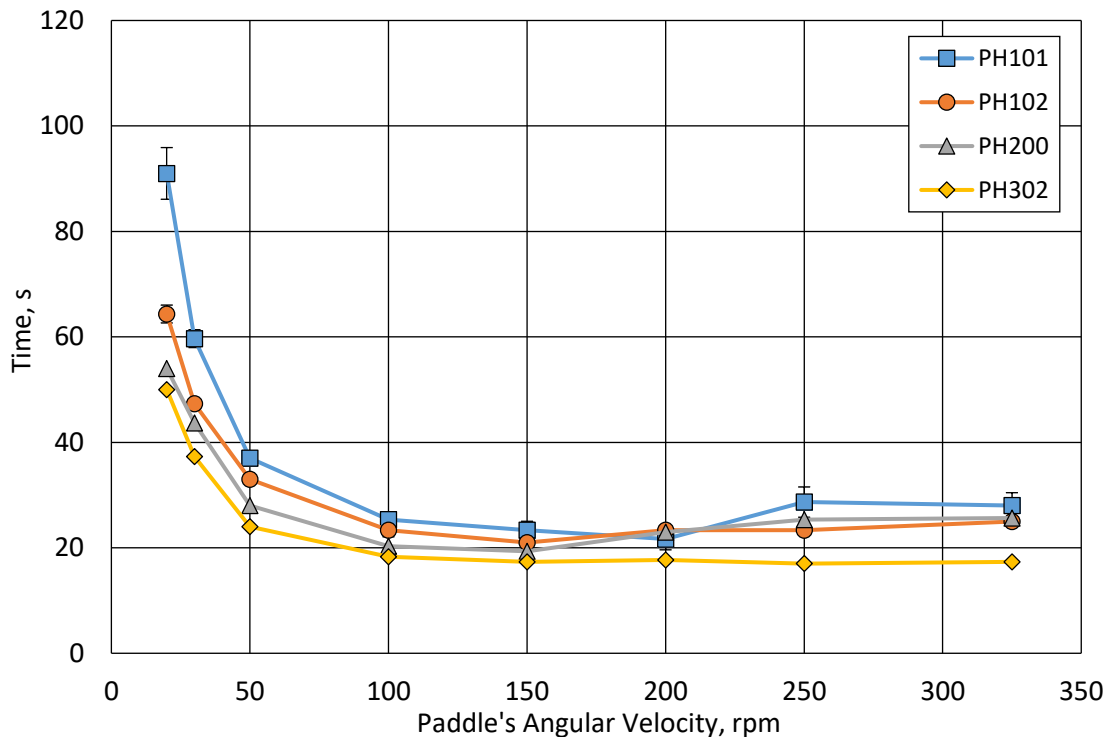


Figure 3-12. Time measured for 200 grams of powder to discharge from the feeder vs. the angular velocity of the paddles for four grades of MCC.

As a paddle passes below the opening of the feeder (exit of the powder container), there is a time frame in which the powder can discharge into the feeder before the opening is blocked by the adjacent paddle. At low angular velocities, this period is longer and the powder flowing into the feeder fills the empty area inside the feeder forming a heap. This heap eventually grows in size as more powder is discharged and blocks the exit of the feeder disrupting powder flow until the next paddle sweeps the heap in the feeder. Therefore, an oscillating flow of powder into the feeder occurs and only a limited amount of material is available inside the feeder. Increasing the rotational velocity of the paddles, reduces the time frame and a smaller heap is formed as a result. Smaller heaps cannot block the exit completely leading to a more continuous flow of the powder

into the feeder. Also, for higher angular velocities, the powder available inside the feeder is transferred quicker to the exit resulting in a higher flow rate.

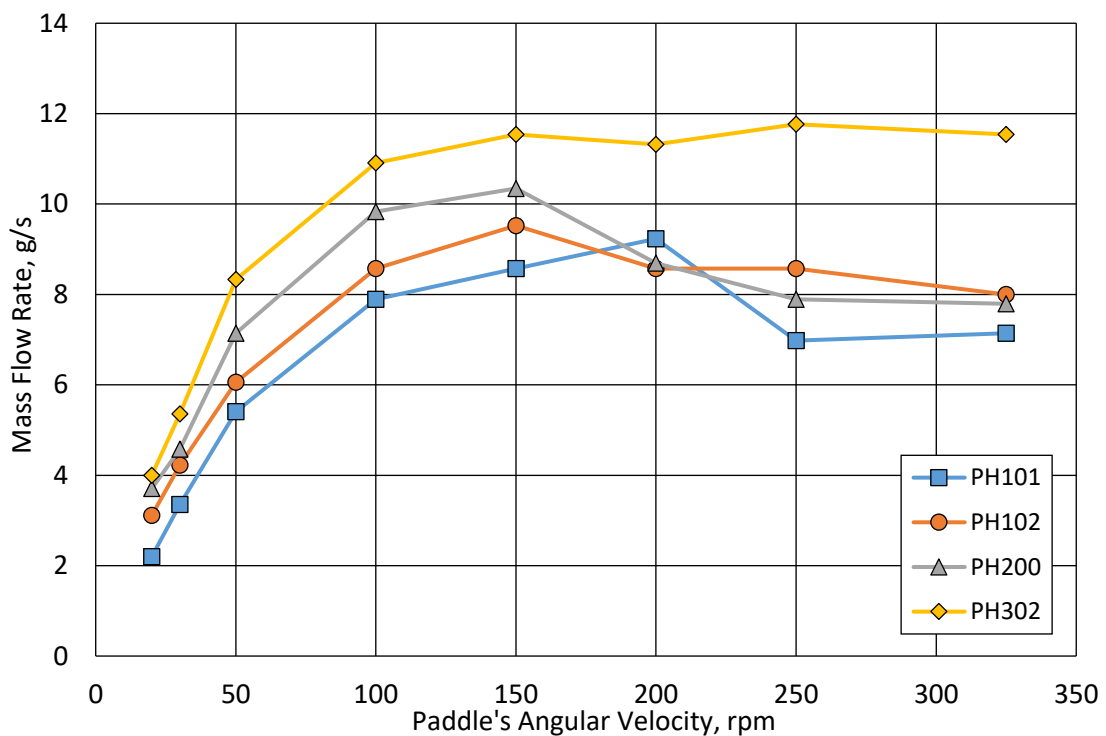


Figure 3-13. Average mass flow rate vs. paddle's angular velocity for four grades of MCC flowing under no differential pressure.

The mass flow rate of the powder discharging from the feeder increases with paddle velocity until the velocity reaches a critical value. Above the critical value, the mass flow rate reduces to some extent as the paddles start to shear through the powder in the feeder i.e. the particles that are in front of the paddles are swept and the particles that are between the paddles and the feeder walls are not transferred to the exit effectively. Increasing the velocity further results in higher inertial force and tendency of particles to stay inside the feeder which reduces the mass flow rate. For PH302 the reduction in the mass flow rate is not as significant as the other grades of MCC.

Mass flow rate can be used as a measure of powder flowability such that a good flowing powder has higher mass flow rate. Therefore, it is expected that the powders ranked as poor flowing based on the characterising techniques described in Chapter 3 to have smaller mass flow rate. However, it is observed that by changing the angular velocity of the paddles in the feeder the flow behaviour of the four grades of microcrystalline

cellulose changes significantly. The results presented in Figure 3-13 show that at low rotational velocities, poor flowing PH101 has smaller mass flow rate, and it increases with powder flowability for PH102 and PH200 (with similar bulk density as PH101). However, by increasing the rotational velocity of the paddles, the rank order changes such that at 200 rpm the mass flow rate recorded for PH101 exceeds the flow rate of PH102 and PH200. For PH101 the mass flow rate then reduces sharply by increasing the velocity further. For PH200, the mass flow rates measured are higher than PH101 and PH102. Above the critical velocity (~130 rpm) the flow rate started to reduce and it reached the mass flow rate of PH102 at 200 rpm. The reduction in mass flow rate by increasing the angular velocity continued for PH200 at higher velocities. It is observed that by changing the angular velocity of the paddles in the feeder the flow behaviour of the four grades of microcrystalline cellulose changes significantly. The flowability is influenced by the processing conditions and the materials that are ranked as poor flowing by standard flow measures can outperform the good flowing materials.

The mass flow rates measured for PH302 with similar powder flow behaviour as PH101 (based on the angle of repose results presented in Table 3-3) are higher than the other three grades of MCC due to higher bulk density of the material. The influence of bulk density is eliminated by plotting the volumetric flow rate of the materials (Figure 3-14).

In Figure 3-14, it is observed that at low rotational velocities, the volumetric flow rate of PH101 is the smallest and the flow rates measured for PH102, PH200 and PH302 are very similar to each other. Increasing the velocity, changes the flow behaviour of the materials. For PH302, the increase in volumetric flow rate is not as significant as the other materials and at 150 rpm the flow rate recorded is the smallest. The reduction in the flow rate as a result of increasing the velocity above the critical value is not discernible and the flow rates recorded become larger than the values measured for PH101, PH102 and PH200. For PH200, by increasing the rotational velocity, the volumetric flow rate reduces to the extent that the flow rates become smaller than the other materials. PH101 with poor flow behaviour (based on both critical orifice diameter measurement and the angle of repose techniques) is highly affected by changes in rotational velocity. At 200 rpm the volumetric flow rate measured for PH101 is larger

than the other materials. The maximum volumetric flow rate of PH101 and PH102 are similar but they are recorded for different angular velocities.

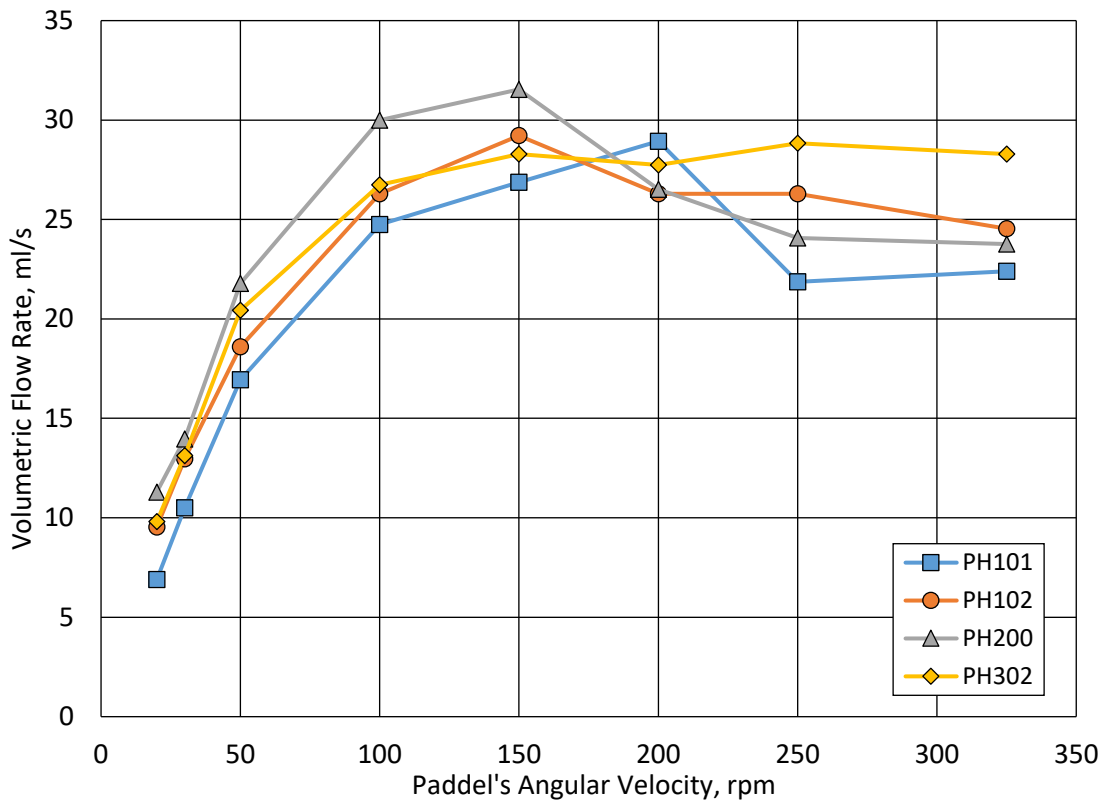


Figure 3-14. Average volumetric flow rate vs. paddle's angular velocity for four grades of MCC flowing under no differential pressure.

For PH102, a set of experiments were carried by setting the differential pressure to 100 Pa before flow initiation. The mass flow rates measured under differential pressure are compared with the values recorded in air are compared in Figure 3-15. After the flow initiated, the differential pressure between the chamber and ambient atmosphere was reduced to nearly 80 Pa as it was easier for air to enter the chamber through the powder bed.

In Figure 3-15, it is shown that by applying small levels of differential pressure, the mass flow rate is increased significantly. This effect is smaller at low angular velocities as the amount of powder available in the feeder is limited. By increasing the velocity, this influence becomes more significant. Similar to powder discharge in open atmosphere, the mass flow rate of the powder under differential pressure reduces after a critical value.

Based on the results available, it is not possible to develop a model to predict the flow rate of the powders in rotary feeders and more experiments are required to find how other processing parameters such as feeder's orifice size and shape, the shape of the paddles and size of the feeder.

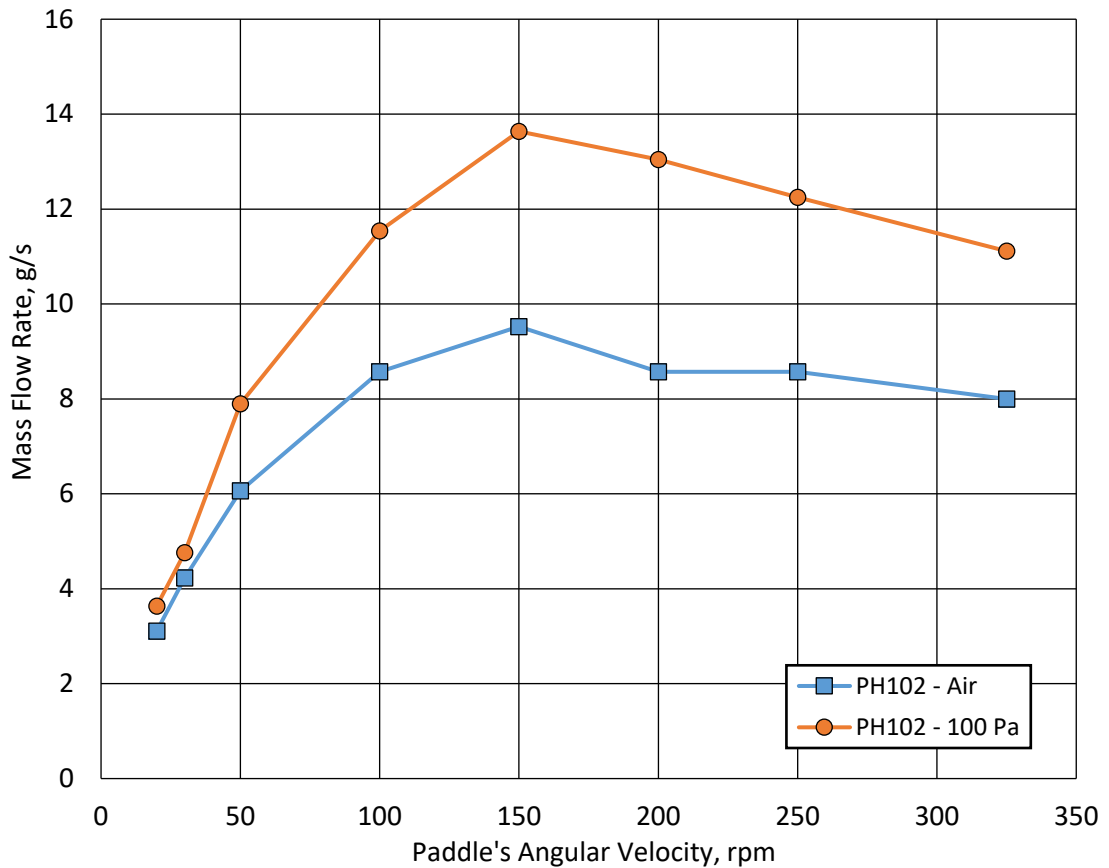


Figure 3-15. The mass flow rates measured for PH102 in air and under differential pressure vs. paddle's angular velocity.

3.6.4. Conclusions

When the paddles cover the exit of the feeder, powder discharge from the container into the feeder result in air pressure build-up and when the paddles pass the exit, a negative pressure gradient is developed in the feeder due to powder dilation. The pressure changes in the feeder result in oscillating mass flow rate. However, the overall mass flow rate remains constant during flow measurement period.

The mass flow rate of the powder in rotary feeders is highly influenced by the rotational velocity of the paddles inside the feeder. The maximum mass flow rate can be achieved

under a specific velocity known as the critical velocity. At velocities below the critical value, the mass flow rate of the powders increases with velocity. Increasing the velocity above the critical value results in the reduction of mass flow rate. This effect was observed for all materials considered in this study and highlights the importance of processing parameters on the flow behaviour of the powders. It was observed that under specific conditions a poor flowing powder ranked using standard characterising techniques can outperform a good flowing material in terms of the mass flow rate.

Applying a small level of differential pressure at the exit of the rotary feeder significantly increases the mass flow rates; especially at high angular velocities.

More experimentation is required to develop a model to predict the mass flow rate of powders in rotary feeders based on the material properties and the processing conditions involved.

3.7. Comparison of the flowability measures and overall conclusions

The results obtained from the angle of repose and critical orifice diameter measurements are summarised in Table 3-5. Comparison of the results obtain shows that in both techniques the powders with larger average particle size show improved flow behaviour. Also, the powders with higher number of elongated particles are consistently characterised as poor flowing in these techniques.

Table 3-5. Summary of the bulk density, critical orifice diameter and angle of repose results.

Material	Bulk Density, kg/m ³	Critical Orifice Diameter, mm (Cylinder Height 75 mm)	Angle of Repose, °		
			Base Diameter		
			50mm	75mm	100mm
PH101	309	30	45	45	44
PH102	318	26	39	40	39
PH200	363	11	33	34	33
PH302	428	24	46	45	43
ATAB	725	3	35	36	35
Mannitol	498	6	32	33	33

In terms of bulk density, the flowability ranking obtained from the angle of repose experiment is not consistent with the critical orifice diameter measurements. PH302 with higher bulk density but similar average particle size to PH102 is characterised as a better flowing powder based on the critical orifice diameter while the angle of repose measured for PH302 is larger than PH102 showing reduced flowability. The observed influence of average particle size and bulk density on flowability characterised using the critical orifice diameter technique is consistent with the observations of other scientists (Hou and Sun, 2008).

This inconsistency in flow ranking is due to the difference in processing parameters and mechanisms involved and emphasises on the fact the flow measurement techniques must be chosen based on the process under investigation.

In order to develop a model to predict the flow behaviour of powders in complex practical processes (e.g. rotary feeding systems), the influence of different material and processing parameters should be identified. In Section 3.6 the effects of paddle speed, exit diameter and differential pressure on the mass flow rate of powders were highlighted. In order to achieve this, it is required to gain a better understanding of the effect of material and processing parameters on the flow behaviour of powders in simpler processes such as hopper discharge and linear shoe-die systems where the number of parameters involved is smaller. This provided the motivations for the series of experimental studies from simple to complex systems presented in this thesis.

Chapter 4. Measurement of powder permeability

A system was designed to measure the pressure difference across the powder bed as a flow of air passes through. Darcy's law (Equation (2-7)) was used to calculate powder permeability. The results obtained are discussed in terms of the powder void fraction, particle size and bulk density. The system had the capability of applying small levels of compaction to the sample and studying this effect on powder permeability. The results were analysed with respect to the bulk density of the powder.

4.1. System development

Different parts of the system developed to measure powder permeability is presented in Figure 4-1 and the assembled system is presented in Figure 4-2. The apparatus was made of stainless steel and consists of a powder container with an internal diameter of 20 mm and height of 50 mm. The outside of the container was threaded with a pitch length of 1 mm to allow it to be attached to other parts of the system. Two glass filters with porosity of 20 μm were used to keep the powder inside the container. Two 5 mm tube connection ports were attached to the rotating top part and the fixed bottom.

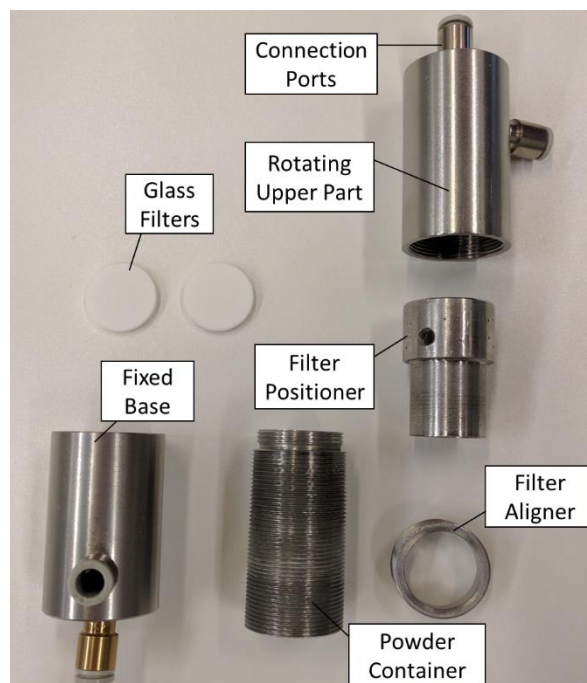


Figure 4-1. Powder permeability measurement apparatus

The rotating upper part and filter positioner were fixed together using the tube connection port on the side so that as the top part was rotated the filter positioner rotated with it. Rotation of the upper part allowed the powder sample in the container to be compacted. The system was held in position using an aluminium mount. An air flow meter with a capacity of 0-1 l/min was used to adjust the air flow rate. The pressure difference across the powder bed was monitored using a Freescale MPX5200DP differential pressure transducer and the data was logged using a data acquisition device (National Instruments NI USB-6221) and PC software (LabVIEW).

4.2. Procedure

The fixed bottom of the system was attached to the aluminium mount and the lower glass filter was placed in position (Figure 4-2). The first set of experiments were carried out for uncompacted samples with variable air flow rate. The powder container was connected to the bottom part. The powder conditioning device described in Section 3.2 was used to introduce the powder into the container and the heap formed on the top was removed using a horizontal blade. The filter aligner was attached to the top of the container and the second glass filter was inserted. The top part and the filter positioner were connected to the system and positioned so that the glass filter was placed on top of the powder bed without compacting it. The air flow rate was set to 0.2 l/min using the flow meter and the pressure difference was measured for 30 seconds. The air flow rate was increased to 1 l/min with increments of 0.1 l/min and the pressure difference was logged for each flow rate. The mass of the powder in the container was measured using a Mettler Toledo PL83-S scale. This experiment was repeated three times for each material using fresh samples.

In order to study the influence of powder compaction on permeability the experiments were carried out for a fixed flow rate. The powder container was filled using the procedure described earlier and the rotating part was positioned so the powder in the container was not compacted. The flow rate was set to 1 l/min and the pressure difference across the powder bed was measured for 30 seconds. By rotating the upper part of the system, the filter positioner displaced the filter downwards and compressed the powder sample. The pressure difference was logged after each complete rotation.

The compaction was continued until the further rotation of the upper part was not possible. The mass of the powder inside the container was measured using the scale described earlier. This experiment was repeated four times for each material using fresh samples.

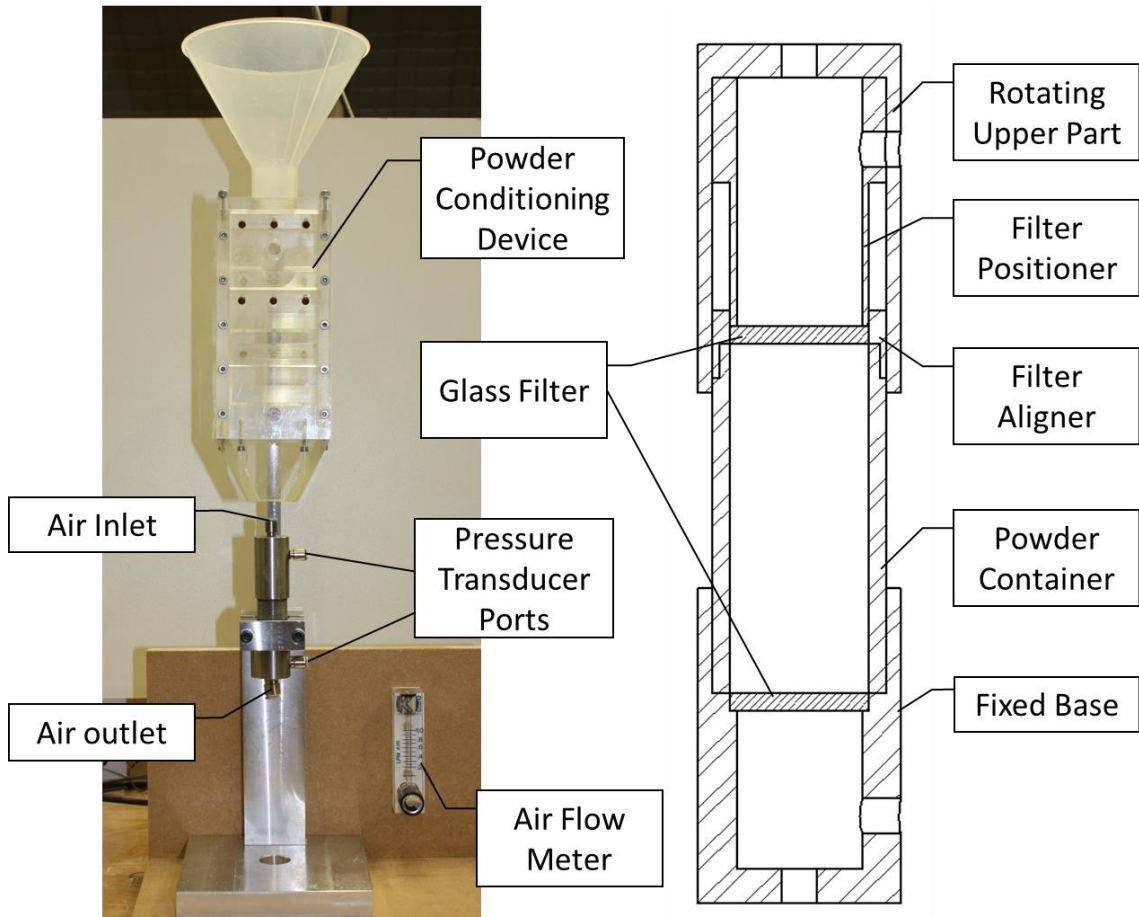


Figure 4-2. Permeability measurement apparatus

4.3. Results and discussions

4.3.1. Powder permeability measurement

The differential pressures (ΔP) measured for the range of air flow rates are presented in Figure 4-3. Each marker in the figures represent a different repeat experiment. It is observed that the pressure drop across the powder bed increases for higher air flow rates (consistent with Darcy's Law).

Comparing the results obtained for four grades of MCC shows that for PH101 with average particle size of 50 μm , the pressure drops recorded for different flow rates are

higher and the values reduce for materials with larger average particle size. Also, for PH302 with higher bulk density than the other grades of MCC the pressure drops measured are higher. Generally, for powders with smaller particle size and higher bulk density, tighter packing of particles results in narrower passage between the particles for air which will result in higher pressure drop across the powder bed.

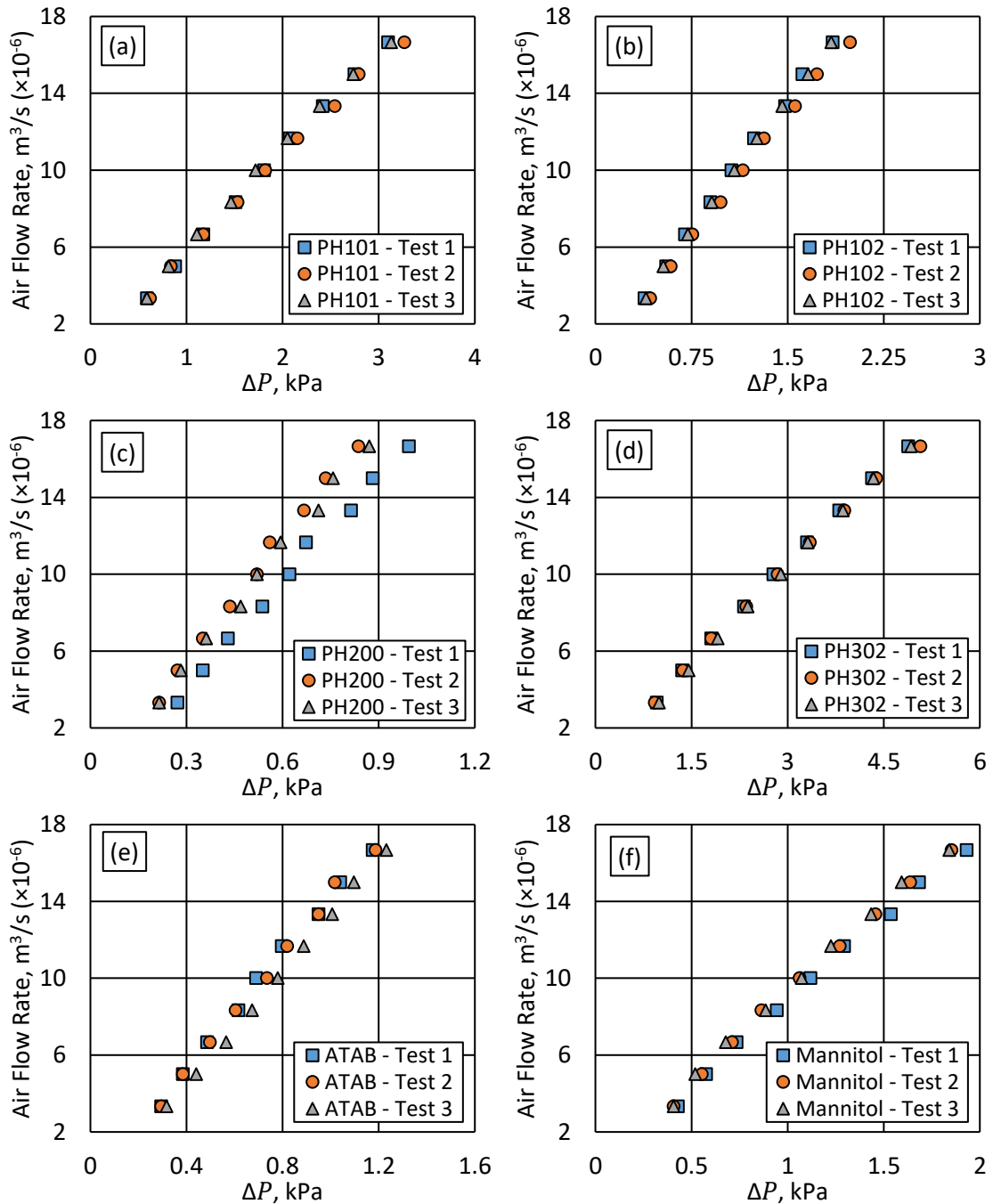


Figure 4-3. Differential pressure vs. air flow rate for a) PH101, b) PH102, c) PH200, d) PH302, e) ATAB and f) Mannitol (markers represent different repeat tests).

Darcy's law (Equation (2-7)) was used to calculate the permeability of the powders in each test. The differential pressures measured for the six powders multiplied by $A/\mu L$ (where A is the cross-sectional area of the powder bed, μ is air viscosity in room temperature and L is the length of the powder samples) and the calculated values were plotted against the air flow rates in Figure 4-4.

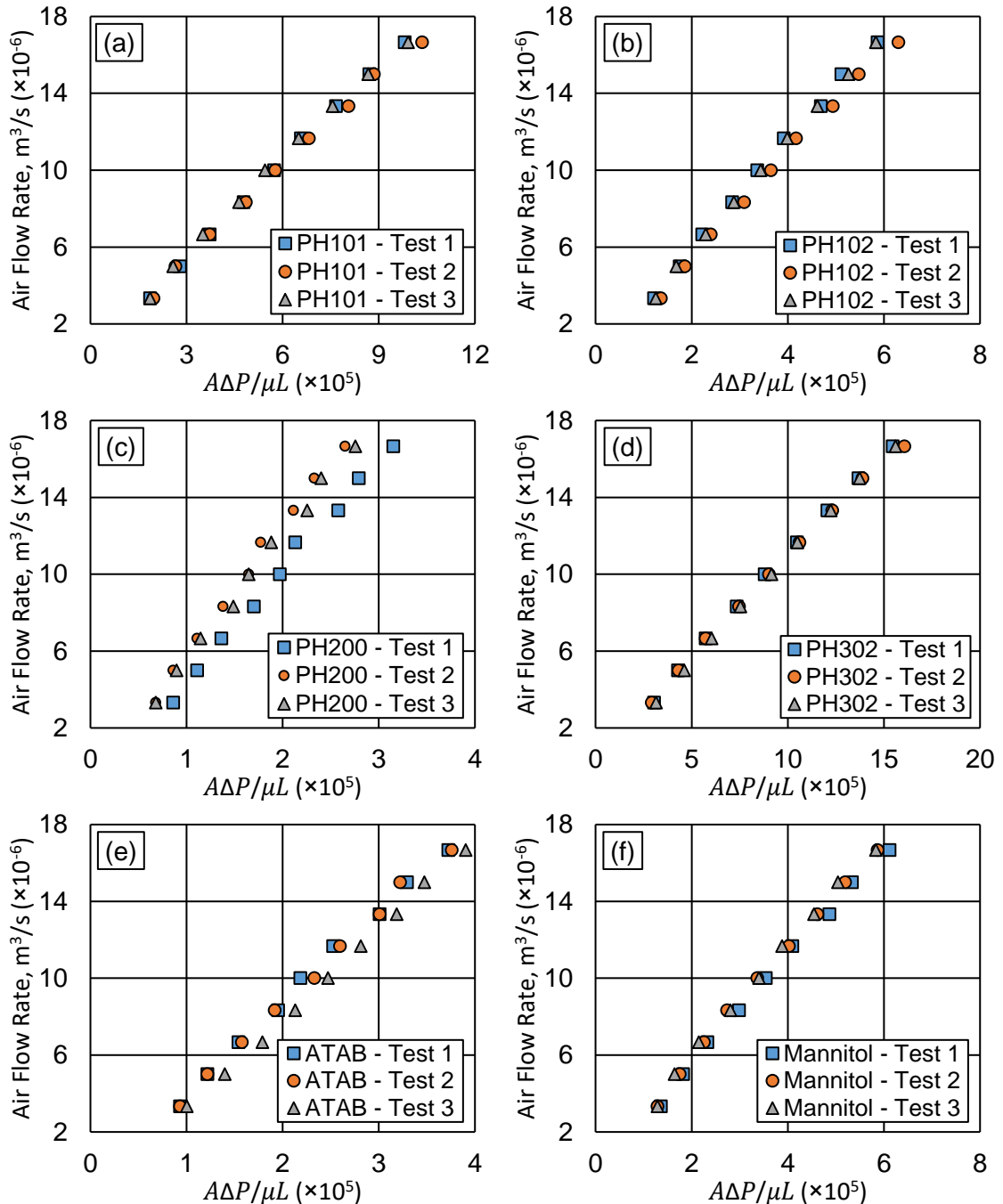


Figure 4-4. $\Delta\Delta P/\mu L$ against air flow rate for a) PH101, b) PH102, c) PH200, d) PH302, e) ATAB and f) Mannitol (markers represent different repeat tests).

Air viscosity was considered to be constant for the tests carried out. Based on Darcy's law the gradient of the best fit line on the data points for each test is equal to the powder permeability.

The permeability of the six materials measured for each experiment and the average permeability for each powder are presented in Figure 4-5. The error bars represent the standard error in fitting the experimental data to Darcy's Law.

According to Kozeny and Carman equation (Equation (2-8)), permeability of a powder is a function of particle size and void fraction. Comparing the permeability values calculated for PH101, PH102 and PH200 shows that for PH101 with the smallest average particle size has the lowest permeability.

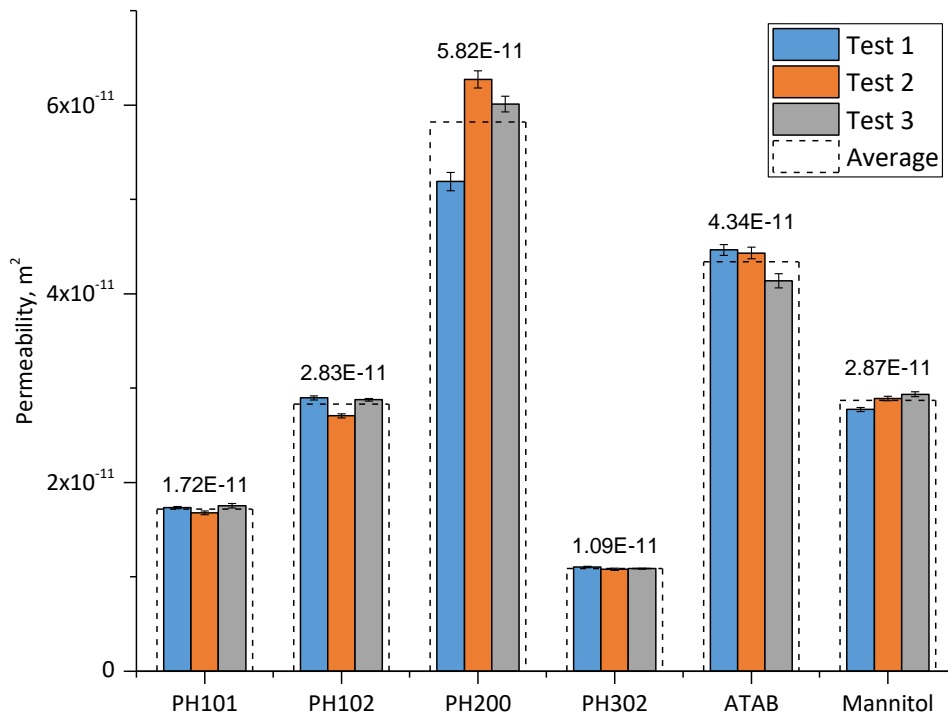


Figure 4-5. Powder permeability measured for the six materials

For PH302 and PH102 with average particle size of 100 μm the values of permeability calculated are significantly different. Also, for ATAB, Mannitol and PH200 with average particle size of 180 μm it is observed that the permeability is larger for PH200 and reduces for ATAB and Mannitol respectively. The difference in the permeability of powders with similar average particle size is due to different void fractions (ϵ). Using the

mass of the powders measured for each test and the volume of the container the bulk density of the materials was calculated and the void fraction of the powders was determined using

$$\varepsilon = 1 - \frac{\rho_b}{\rho_s} \quad (4-1)$$

where ρ_b is the bulk density and ρ_s is the particle density of the material. The average bulk density, void fraction and the permeability calculated for the six powders are presented in Table 4-1.

Table 4-1. Void fraction and permeability for uncompressed materials

Material	PH101	PH102	PH200	PH302	ATAB	Mannitol
Bulk Density, kg/m ³	297	306	328	407	713	486
Void Fraction	0.81	0.80	0.78	0.74	0.75	0.68
Permeability, m ² (×10 ⁻¹¹)	1.72	2.83	5.82	1.09	4.43	2.87

It is shown that for powders of similar particle size, the powder with smaller void fraction has lower permeability. Average permeability of PH302 with void fraction of 0.74 is 1.09E-11 while for PH102 the permeability is nearly 2.5 times higher at 2.83E-11. Similarly, permeability reduces with void fraction for ATAB, Mannitol and PH200.

The bulk densities presented in Table 4-1 are smaller than the values measured using the procedure explained in Section 3.3. The powder container of the permeability apparatus is significantly smaller in diameter (20 mm) compared to the cylinder used to measure the bulk density in Section 3.3 (57.4 mm) and it is more difficult for air inside the container to escape as the powder is introduced and it results in larger voids entrapped between the particles and smaller bulk density.

4.3.2. Influence of compaction on powder permeability

The pressure drops measured for different compaction levels are plotted against the length of the powder sample in the container in Figure 4-6. It is observed that by

compressing the powder, the differential pressure necessary for the same flow rate increased. During compactions, the particles rearrange within the powder bed and fill the voids available within the bed. Reduction of the voidage increases the difficulty of particle movement and results in pressure build up. For higher stresses the particles may undergo plastic deformation and breakage, which reduce porosity and thus the differential pressure increases.

For four grades of MCC, the increase in the differential pressure is more gradual at early stages of compaction and increases rapidly after a certain level. For these materials, as the compaction started due to the existence of large number of irregular and fine particles in the powder bed (illustrated in Figure 3-1) the particles mostly rearranged and little transformation occurred. As the compaction continued, further rearrangement was opposed by particle interlocking and breakage of the particles produced more fines which resulted in a larger increase of the pressure difference.

For ATAB and Mannitol, it is observed that the samples could not be compacted to the same levels (in terms of displacement) compared to four grades of MCC. For these materials, the particles are mostly spherical and the number of fines is smaller (Figure 3-2 and Figure 3-3). Therefore, the initial packing density is larger and the particle rearrangement in the container is limited.

Using the differential pressures measured and Darcy's law (Equation (2-7)) the permeability of the six materials under different levels of compaction were calculated. In different repeat tests the mass of the powder introduced into the container was different. Therefore, the permeability results are compared against the changes in bulk density calculated using the mass of the powder and the volume of the container that the powder occupied (Figure 4-7). It is observed that powder permeability is reduced as the powder is compacted in the container. It is shown that the scatter in the data observed in Figure 4-6 is mostly due to the difference in mass of the powder in the container.

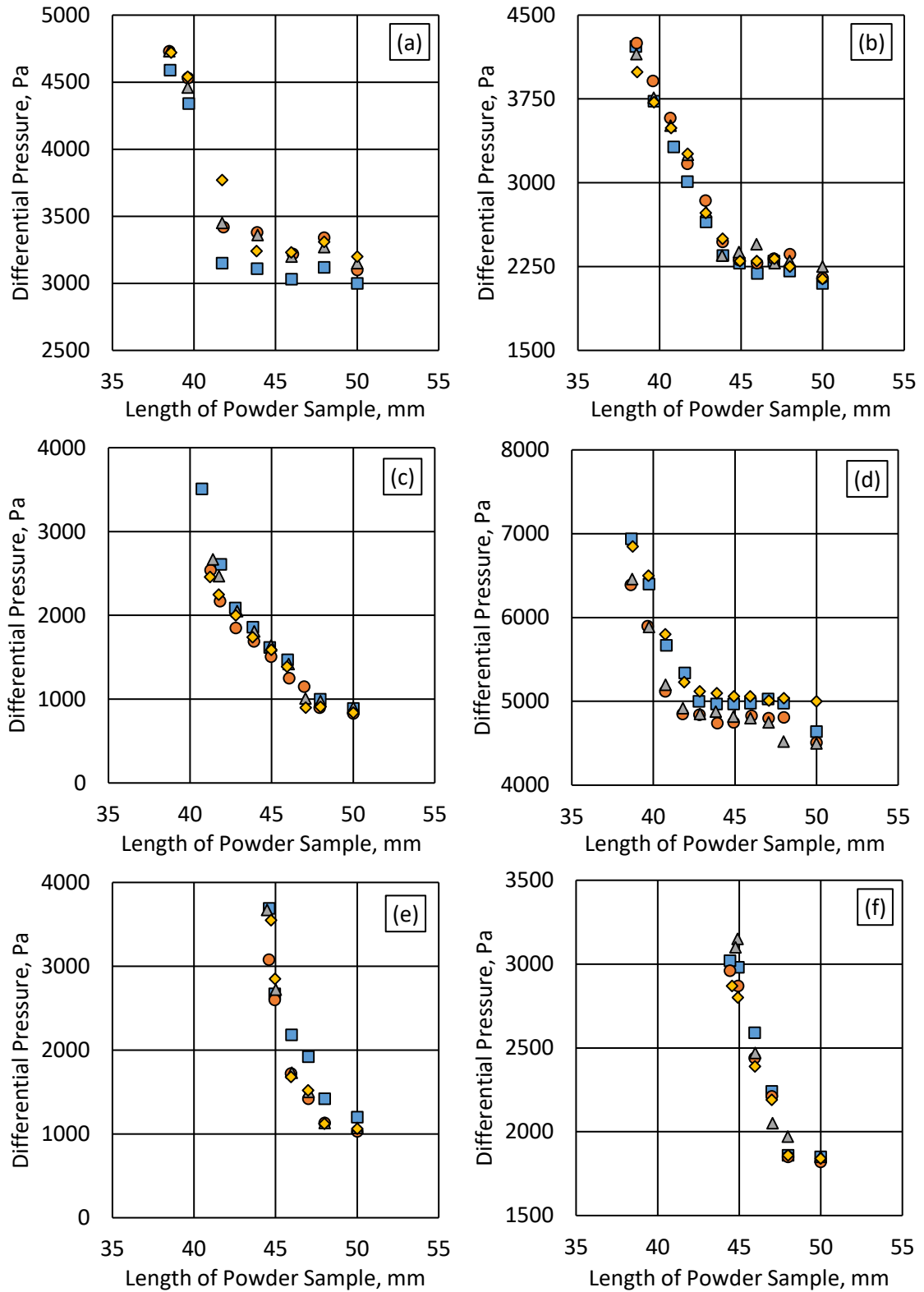


Figure 4-6. Differential pressure vs the length of the powder sample for a) PH101, b) PH102, c) PH200, d) PH302, e) ATAB and f) Mannitol (markers represent different repeat tests)

For MCC, the reduction in permeability is more gradual at the initial stages and accelerate as the powder was compacted beyond a certain level. At early levels of compaction, the particles mostly rearrange within the container and permeability changes mostly because of the change in void fraction. After a certain compaction level, as the particle rearrangement is restricted by interlocking, the stress levels increase inside the container. At this stage, powder permeability will be influenced by both reduction in the void fraction and also the reduction in the particle size of the powder in the container.

The permeability values calculated for different levels of powder compaction are plotted against the void fraction for six materials in Figure 4-8. It is shown that changes in void fraction influence the permeability of each powder differently. In order to compare this influence on different materials, the values of the permeability were normalised by the initial (loose state) permeability of each powder.

$$\text{Normalised Permeability} = \frac{k}{k_0} \quad (4-2)$$

where k is the permeability of the compacted powder and k_0 is the initial permeability of the sample material. Normalised void fraction is similarly defined as the ratio between the void fraction of the compacted powder and the initial void fraction. Normalised permeability of six powders is plotted against the normalised void fractions in Figure 4-9. It is observed that changes in void fraction as a result of applying compaction influences the permeability of the powders differently. For ATAB and PH200 with similar average particle size, the effect of void fraction on powder permeability is similar. While for Mannitol this effect is more limited. This is the result of different mechanism involved when the six powders are compacted. Generally, for powders with more spherical particle shapes and lower number of fines the movement of the particles within the container is limited and upon compaction, the particles break into smaller particles as a result of the contact stresses applied. For powders with more irregular particle shapes and higher number of fines, the particles mainly rearrange which result in a more gradual decrease in the permeability.

As discussed before, the total displacement of ATAB and Mannitol is smaller than the four grades of MCC (Figure 4-6). However, it is observed that the total reduction of powder permeability is similar (Figure 4-9). In other words, for a similar compaction level, the reduction in powder permeability for ATAB and Mannitol is significantly larger. For ATAB in particular, permeability reduces for nearly 75% (similar to PH200) where the sample was compacted by 50% of the displacement of PH200.

For ATAB and Mannitol, the particles are mostly spherical. Therefore, particle rearrangement at initial stages is limited and the permeability is mainly reduced due to particle breakage and increasing the number of fine particles.

4.1. Conclusion

Consistently with Kozeny and Carman relation (Equation (2-8)) permeability reduces for powders with smaller average particle size and void fraction. This is due to narrower passages for air in the powder bed.

By compressing the powder, permeability reduces as the particles rearrange inside the container and the smaller particles move to the gaps between relatively larger particles resulting in reduced void fraction. By compressing the powder further, the particles start to break and more fines are produced. The permeability at this stage reduces more rapidly as a result of higher number of fine particles (smaller average particle size) and a smaller void fraction.

The change in void fraction influences the permeability differently for each material. For some of the materials used, 5% reduction in the voidage resulted in nearly 70% reduction of the permeability while for others, this reduction is limited to 20-50%.

For powders with spherical particle shape, the total compression that could be applied using the current system was smaller compared to powders with irregular particle shape. However, the change in the void fraction for these materials was similar to other powders and permeability was reduced to the same extent by a smaller reduction in the sample length.

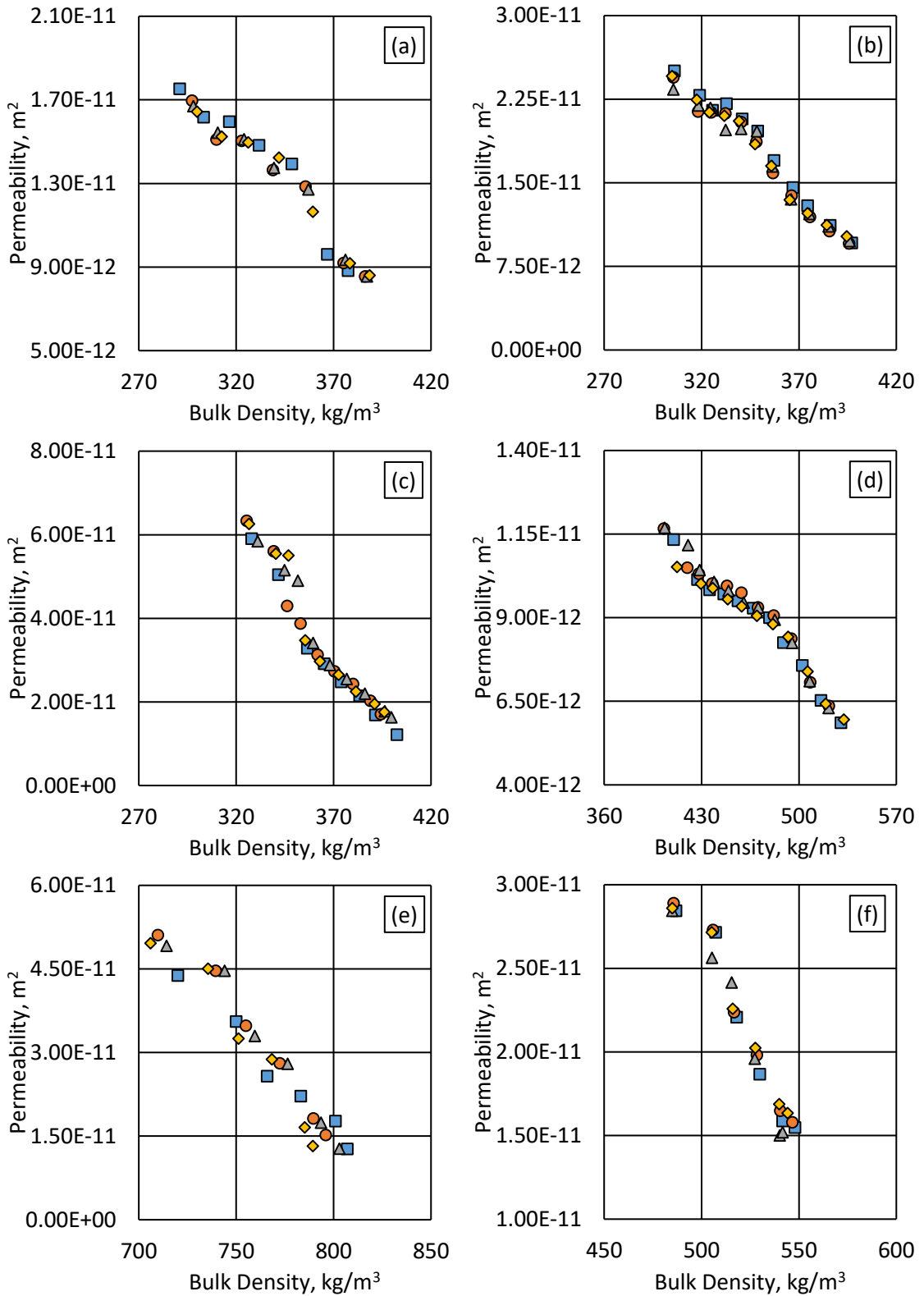


Figure 4-7. Powder permeability vs bulk density for a) PH101, b) PH102, c) PH200, d) PH302, e) ATAB and f) Mannitol (markers represent different repeat tests)

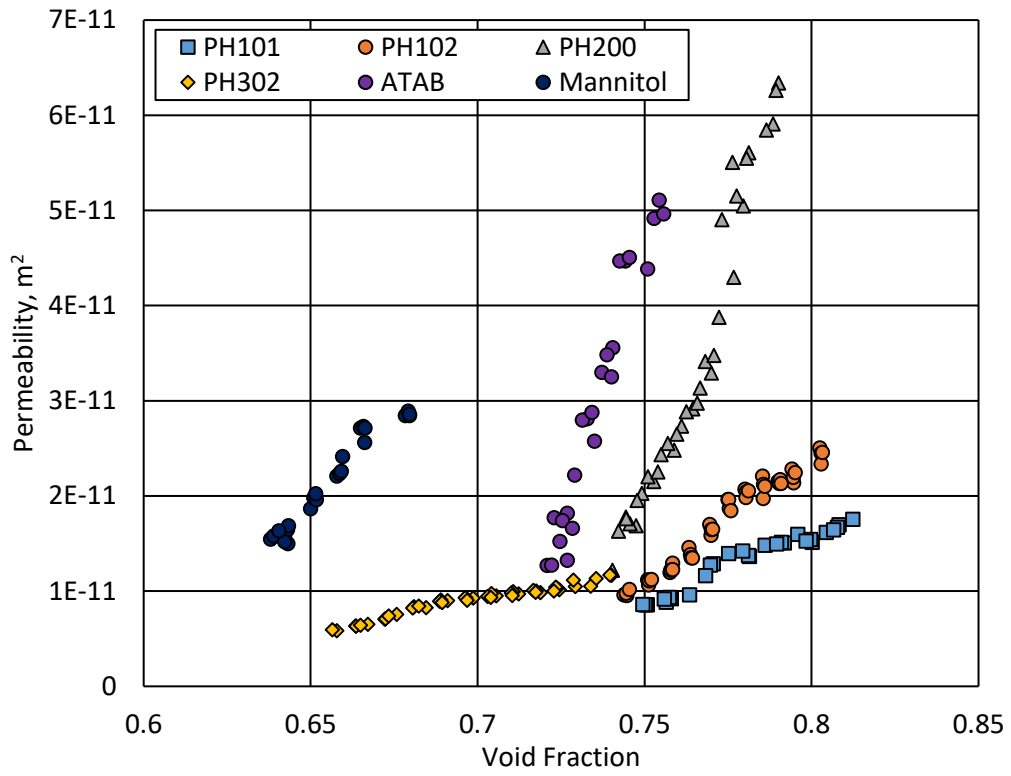


Figure 4-8. Powder permeability vs. void fraction for six materials

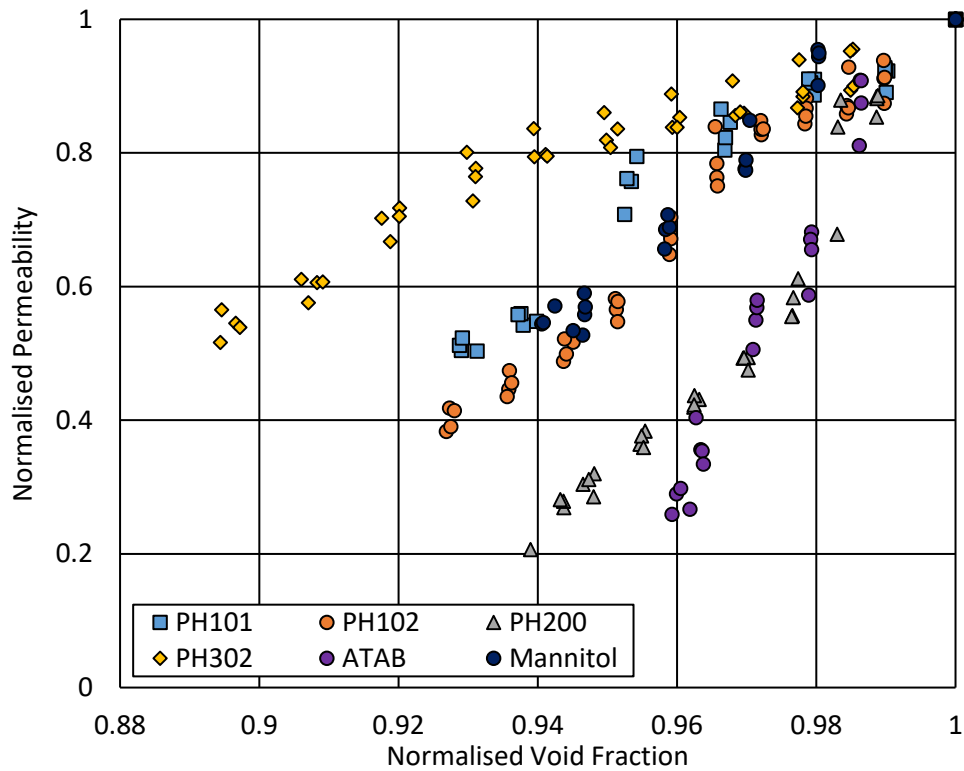


Figure 4-9. Normalised permeability vs. normalised void fraction for six powders

Chapter 5. Vacuum assisted flow initiation from arching state

In this chapter the influence of differential pressure on flow initiation of four grades of MCC from arching state was investigated. The term “differential pressure” refers to the pressure difference between the vacuum chamber and the ambient pressure. The critical orifice diameter measurement apparatus described in Section 3.5 was extended to enable the discharge of the powder into a chamber with controlled pressure and the sensitivity of critical orifice diameter to air pressure at the exit was investigated. The differential pressures required to initiate powder flow for different exit diameters were measured. The results obtained were discussed in terms of the average particle size and bulk density; and with reference to the flowability of the powders characterised in Chapter 3. A dimensional model is developed to predict the differential pressure required to initiate powder flow as a function of orifice diameter and powder properties.

Mannitol and ATAB with small critical orifice diameters (Table 3-4) were not used for the experiments presented in this chapter as the correct analysis of the results would not be possible for a limited number of data points.

5.1. System development

A cylindrical vacuum chamber with internal diameter of 146 mm and height of 100 mm made of acrylic was designed to accommodate the critical orifice measurement device and control the air pressure or vacuum at the exit (Figure 5-1). The pin used to control the shutter was installed on the body of the chamber allowing control of the shutter whilst maintaining vacuum in the chamber. Two standard connecting ports were placed on the top plate of the chamber, one to connect the chamber to the vacuum pump via a pressure regulator (Airtrol V-900-10 W/K) and one port to connect a pressure transducer (Sensirion SDP1000-L). The pressures were logged using a data acquisition device (National Instruments NI USB-6221) and PC software (LabVIEW). Three cylindrical containers with internal diameters of 57.4 mm and heights of 50, 75 and 100 mm were built out of aluminium. The critical orifice diameter measurement disks described in Section 3.5 was used. The base of the vacuum chamber was sealed with an O-ring to enable convenient operating of the device.

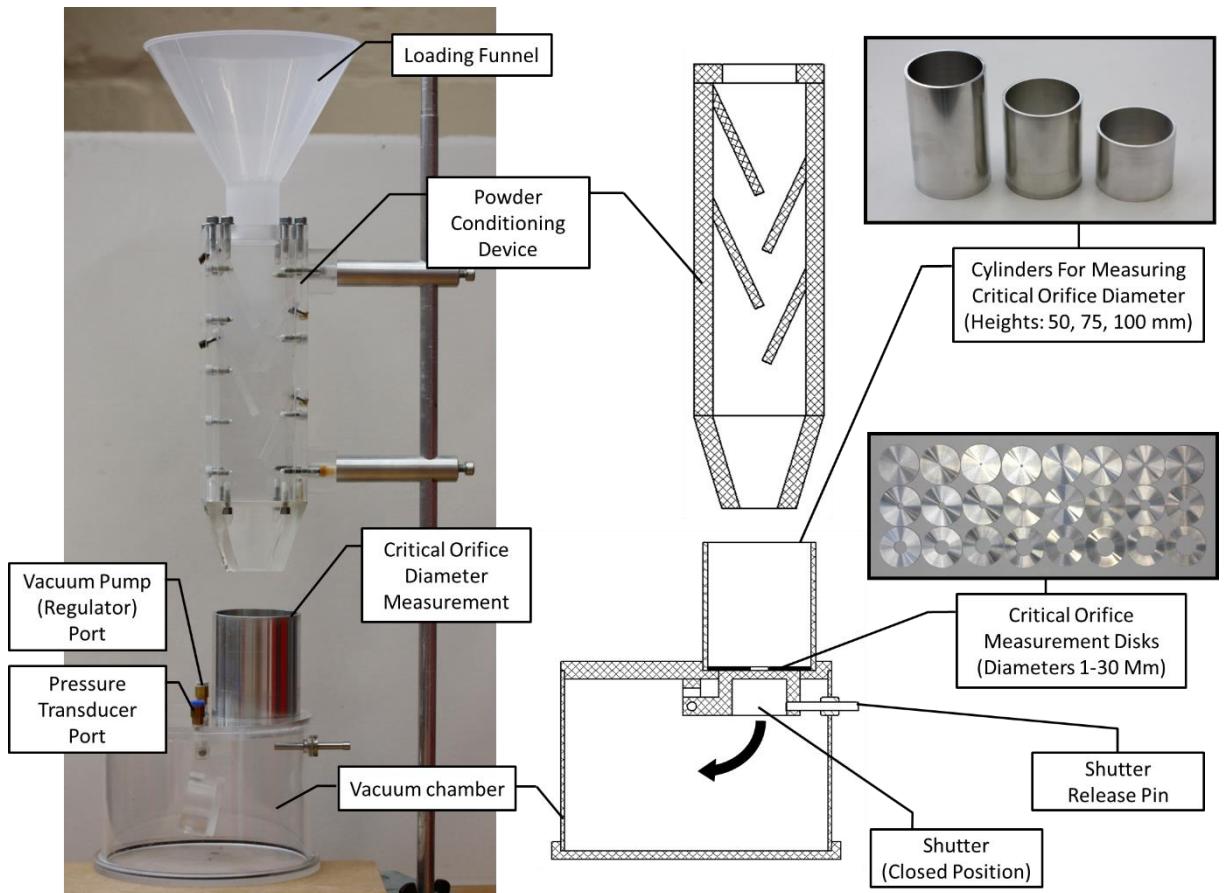


Figure 5-1. Apparatus used to measure the differential pressure required to initiate powder flow from arching state

5.2. Procedure

A disk with a given orifice diameter was placed at the base of the container (Figure 5-1). In order to ensure repeatable and consistent initial condition of the powder in the container, the powder was introduced using the conditioning device described in Section 3.2 and the excess powder was removed using a horizontal blade to meter the same volume of powder in each experiment.

The shutter was opened using the associated pin. If the powder was discharged from the container, the procedure was repeated using a disk with smaller orifice. When arching appeared upon opening the shutter, the differential pressure between the vacuum chamber and ambient atmosphere was increased using the pressure regulator and the vacuum pump. The differential pressure at which powder flow initiated was recorded. The pressure was monitored using the differential pressure transducer. Three powder containers were used to study the effect of powder height. This procedure was

repeated three times for each disk and each cylinder height using a fresh sample for each test.

5.3. Transducer calibration

The schematic experimental setup used to calibrate the differential pressure transducer is presented in Figure 5-2. The pressure inside the vacuum chamber was decreased to -500 Pa using a manual pump (pressure bulb). The differential pressure between the vacuum chamber and the ambient atmosphere was monitored with the differential pressure transducer and a calibrated manometer. The differential pressure was then reduced slowly and the output voltage of the transducer was logged using a data acquisition device (National Instruments NI USB-6221) and PC software (LabVIEW). The output voltage was compared with the pressures measured by the manometer. Using this method the calibration curve to convert the output voltage of the transducer to the corresponding differential pressure was determined.

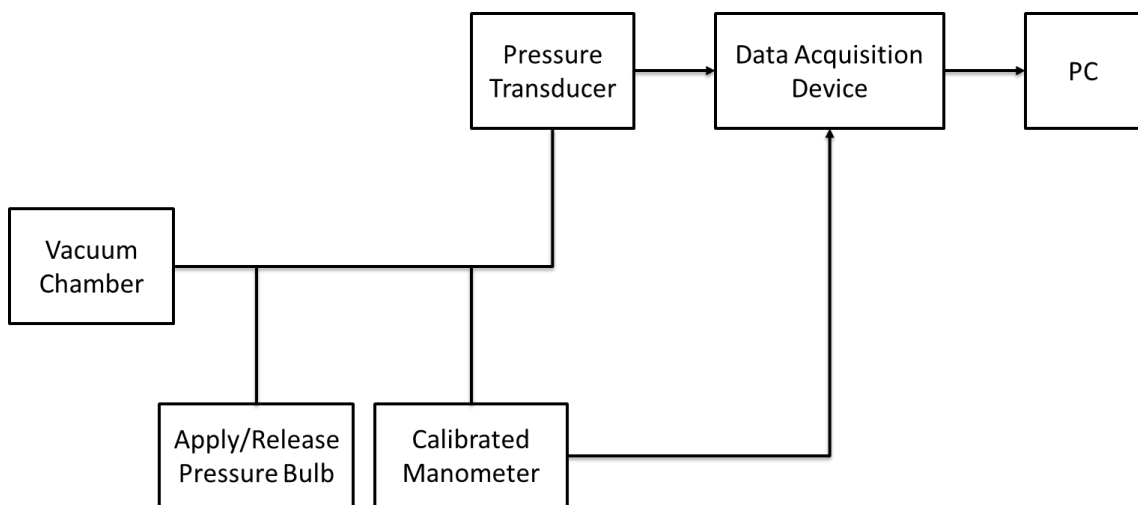


Figure 5-2. Schematic diagram of pressure transducer calibration setup

5.4. Results and discussions

5.4.1. Effect of air pressure at discharge on flow initiation

The averaged differential pressure (calculated from the three repeat experiments) required to initiate powder flow from arching state for the range of orifice diameters using four grades of MCC are presented in Table A - 1 in Appendix and are plotted in Figure 5-3 . In this figure, each colour represent one of the four grades of MCC and

different markers represent the three powder heights used in the experiment. The error bars from averaging the differential pressures are very small and they would not be visible due to the scale of the vertical axis.

It is observed that for a material with critical orifice diameter of around 30 mm, by applying a small differential pressure across the powder bed (100-200 Pa), the critical orifice diameter can be reduced significantly by up to 15 times (e.g. from 30 to 2 mm).

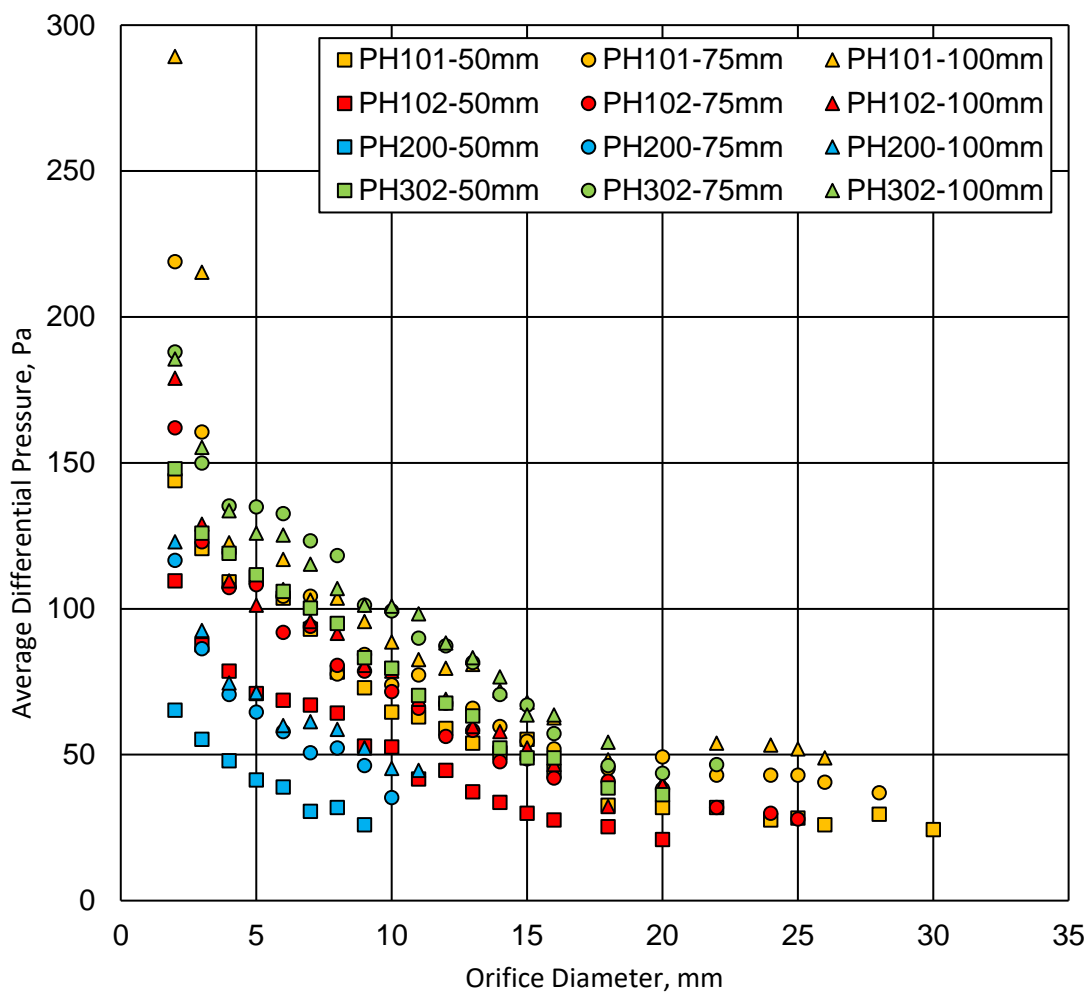


Figure 5-3. Orifice diameter vs. average differential pressure required to break the arch and initiate flow

Figure 5-3, shows that the differential pressure required to initiate powder flow increases when the exit diameter is reduced. For example, for PH102, the differential pressure required to initiate powder flow using exit diameter of 25 mm was recorded as 28 Pa while for orifice size of 5 mm the differential pressure measured was 108 Pa. It is

also evident that an increase in powder height results in an increase in the differential pressure required for flow initiation. This effect is observed for all four powders used in this study.

The differential pressure required for flow initiation for four grades of MCC can be discussed in terms of flowability. It is shown that for powders that are ranked as poor flowing powders using the angle of repose experiment described in Section 3.4, the differential pressure required to initiate powder flow is larger. For PH101 and PH302, with the angle of repose of 45° the differential pressures recorded are significantly larger than the values measured for PH102 and PH200. As discussed in Chapter 3, powder flowability is influenced by average particle size and bulk density. The effects of these parameters on the differential pressure required to initiate powder flow are discussed below.

Figure 5-3 also illustrates that the differential pressure decreases as the average particle size increases. Comparison of the results obtained for PH101, PH102 and PH200, with similar bulk density shows that for PH101 with average particle size of 50 µm, the differential pressures measured are larger and reduces for PH102 and PH200 with average particle sizes of 100 µm and 200 µm respectively (the batch of PH200 used for the experiments presented in this chapter was 200 µm).

Comparing the results obtained for PH102 and PH302 shows that for PH302 with similar average particle size but higher bulk density, the differential pressure required to initiate powder flow is larger.

Based on the results presented in Table A - 1 in Appendix, the critical orifice diameter recorded for a material is consistent with the results measured using the procedure described in Section 3.5.1 when the powder height above the exit was 75 mm. However, it is observed that a different critical orifice diameter was measured when the powder height above the exit was changed. This observation emphasizes on the fact that the flowability measurement techniques are effected by the processing parameters and therefore, the flow measurement must be carried out in similar conditions.

5.4.2. Dimensional model development

Using dimensional analysis, a relation was developed to predict the differential pressure required to initiate powder flow from material properties and the processing parameters involved in this process. The parameters involved in the process are: differential pressure required to initiate powder flow (ΔP); bulk density of powder (ρ_b); acceleration due to gravity (g); particle size (d); height of powder above the exit (H); and orifice diameter (D). There are also other parameters like viscosity of air (μ), coefficient of friction between particles (μ_p) and between particles and the wall (μ_{pw}), shape of the exit and adhesion between particles that contribute. Thus ΔP can be written as a function of $\rho_b, g, d, H, D, \mu, \mu_p, \mu_{pw}$, particle shape and adhesion i.e.

$$\Delta P = f(\rho_b, g, d, H, D, \mu, \mu_p, \mu_{pw}, \text{shape}, \text{adhesion}) \quad (5-1)$$

or

$$F(\Delta P, \rho_b, g, d, H, D, \mu, \mu_p, \mu_{pw}, \text{shape}, \text{adhesion})=0 \quad (5-2)$$

Following the Buckingham Π theorem (Gibbins, 2011) used in dimensional analysis, a model is developed to predict the pressure required to break the arch and initiate powder flow. Three parameters of ρ_b, g and d are selected as the independent variables in the dimensional analysis representing the dimensions of mass, $[M]$, time, $[T]$, and length, $[L]$, respectively.

The unit of differential pressure, ΔP , is N/m^2 or kg/ms^2 which in dimension terms can be written as $[M/LT^2]$. In order to eliminate the mass dimension, the differential pressure is divided by the bulk density with the dimension of $[M/L^3]$

$$\frac{\Delta P}{\rho_b} = \frac{[M/LT^2]}{[M/L^3]} = \left[\frac{L^2}{T^2} \right] \quad (5-3)$$

The time dimension in the expression has the same power as the independent variable selected for time (g). Therefore, the time dimension can be eliminated by dividing Equation (5-3) by g .

$$\frac{\Delta P}{\rho_b g} = \frac{[L^2/T^2]}{[L/T^2]} = [L] \quad (5-4)$$

The dimensionless differential pressure is formed by dividing Equation (5-4) by particle size, d .

$$\overline{\Delta P} = \frac{\Delta P}{\rho_b g d} = \frac{[L]}{[L]} = 1 \quad (5-5)$$

Similarly, the dimensionless groups of powder height above the exit, \overline{H} , and orifice diameter, \overline{D} , can be formed.

$$\overline{H} = \frac{H}{d} \quad (5-6)$$

$$\overline{D} = \frac{D}{d} \quad (5-7)$$

Therefore, it can be written that

$$\overline{\Delta P} = f(\overline{H}, \overline{D}, \mu, \mu_p, \rho_{pw}, \text{shape}, \text{adhesion}) \quad (5-8)$$

According to the results, by increasing the height of the powder, the differential pressure to initiate powder flow increases. Therefore, there is a direct relation between H and ΔP . Also, the differential pressure increases for smaller orifice sizes. So, orifice diameter (D) is inversely proportional to ΔP . The two dimensionless groups of \overline{H} and \overline{D} can be combined to form a new dimensionless group

$$\frac{\overline{H}}{\overline{D}} = \frac{H}{D} \quad (5-9)$$

For a given powder over a range of orifices and powder heights, it is possible to fit a power law relation to the data (Figure 5-4)

$$\frac{\Delta P}{\rho_b g d} = c_i \left(\frac{H}{D} \right)^{n_i} \quad (5-10)$$

where c_i and n_i are empirical constants which depend on the material and processing parameters that are not included in the relationship. The index i refers to “initiation”.

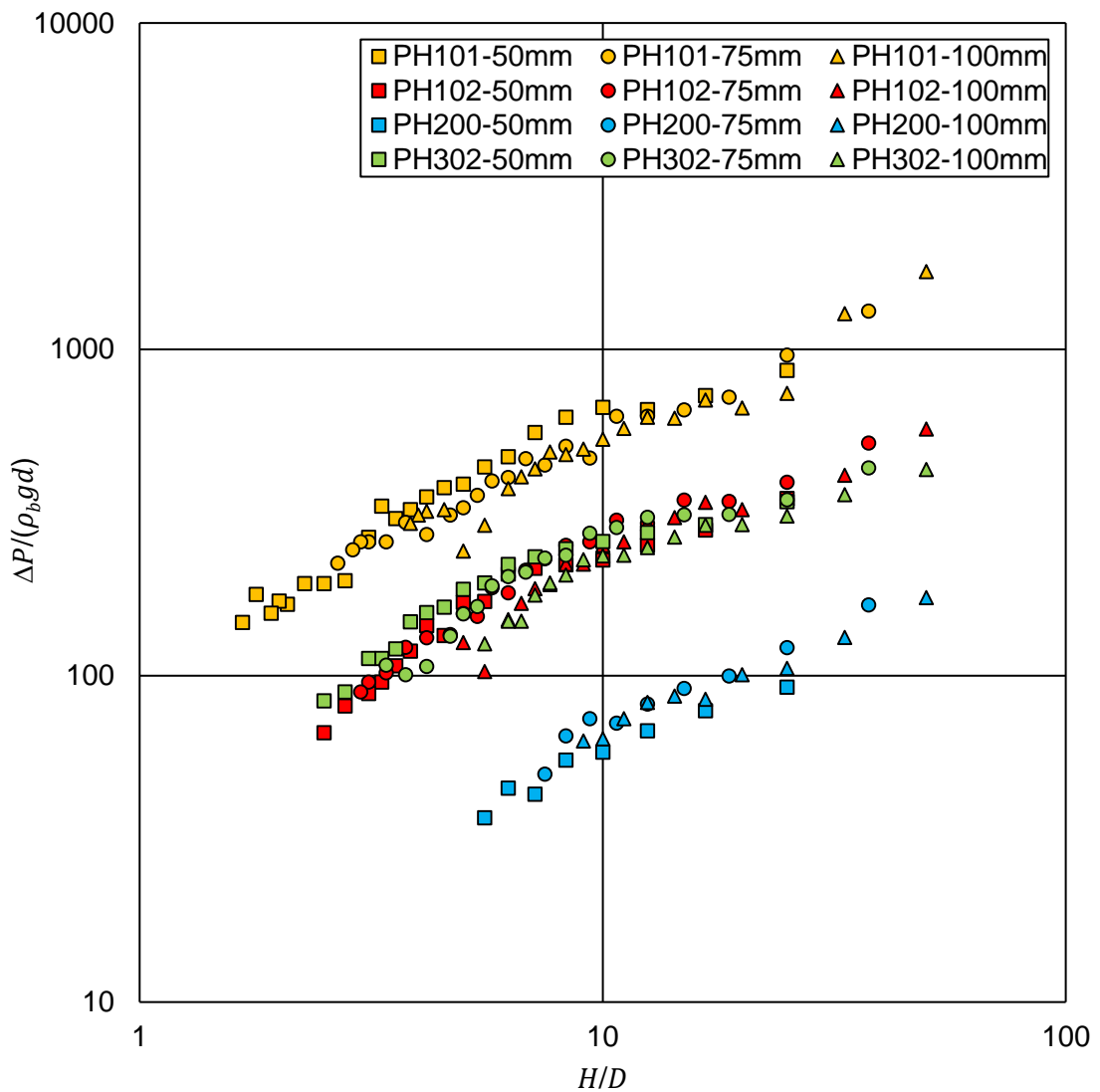


Figure 5-4. Power law relationship between the two dimensionless groups H/D vs. $\overline{\Delta P}$

The values of c_i and n_i obtained from fitting the expression to the data are presented in Table 5-1 and Figure 5-5.

Table 5-1. Values of c_i and n_i for the powders tested

Material	c_i	n_i
PH101	118	0.66
PH102	61	0.57
PH200	15	0.62
PH302	80	0.45

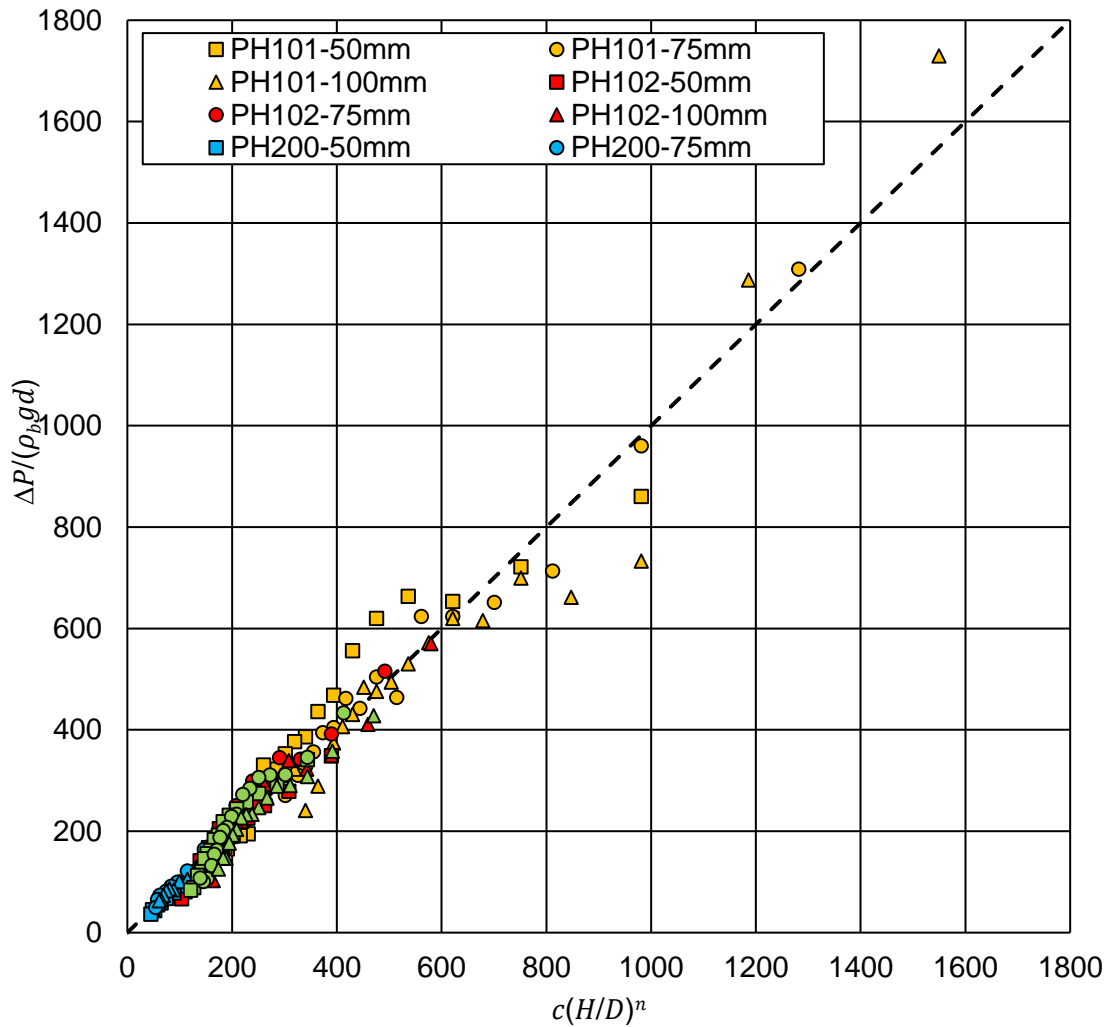


Figure 5-5. Plot of $c_i(H/D)^{n_i}$ vs. $\overline{\Delta P}$ based on the values of c_i and n_i obtained from fitting the relation on the results

Equation (5-10) satisfies the observations made on the effects of orifice diameter (D), bulk density (ρ_b) and height of the powder above the exit (H) on the differential pressure (ΔP). However, as indicated above, a powder with higher average particle size (d) requires a smaller differential pressure to initiate powder flow which is not consistent with the relation between d and ΔP with the expression. This is due to the fact that particle size is a determining factor for other parameters involved in the process that are not considered in this study. For example, the Kozeny – Carman relationship (Kozeny, 1927, Carman, 1937) links particle size to powder permeability (k), where permeability is defined using Darcy's law (Darcy, 1856).

In Equation (5-10) the coefficients c_i and n_i depend on the material dependent parameters and the processing conditions, e.g. geometry of the system. As the processing conditions (except H and D) are fixed for all materials, it is instructive to set the value of n_i to the average value ($n_i = 0.58$). The values of c_i obtained for the materials using a fixed n_i are presented in Table 5-2 and plotted in Figure 5-6. Comparing the coefficients, it is seen that c_i is inversely proportional to average particle size (d). PH200 with the highest d has the smallest c_i while for PH102 and PH302 (with different bulk density but similar average particle size) the value of the coefficient is almost the same.

Once the arch formed in the powder bed was broken and the powder was discharged, three different mechanisms for the remaining powder in the container were observed (Figure 5-7). The mechanism depends on the size of the exit and powder flowability. Generally, for large exit diameters mechanism (b) is observed for all powders where the angle of the remaining powder in the container and horizontal can be related to powder flowability. For powders with good flow behaviour this angle is smaller and most of the powder in the container will discharge while for powders with lower flowability this angle will be larger.

For PH101 and PH302, which are ranked as poor flowing compared to other materials based on the angle of repose experiment, a transition to mechanism (c) and then (d) is observed by reducing the exit diameter. However, for PH200 with the best flowability, mechanism (b) was the only mechanism observed and even for exit diameter of 2 mm the flow of the powder under differential pressure continued until the maximum

amount of powder possible was discharged. Mechanism (d) shows the tendency of poor flowing powder to form arches which are broken by the applied differential pressure.

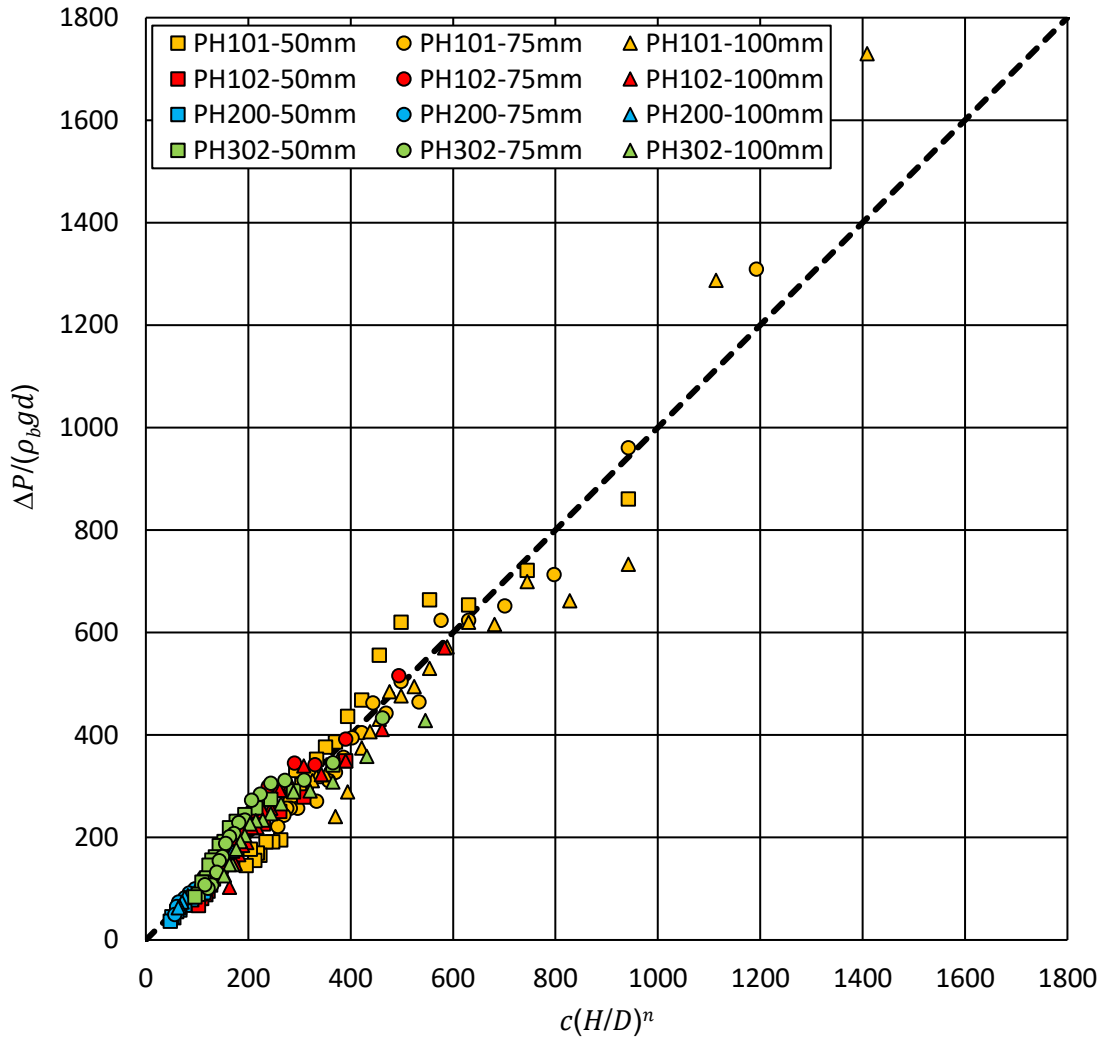


Figure 5-6. Plot of $c_i(H/D)^{n_i}$ vs. $\overline{\Delta P}$ based on the values of c_i obtained for a fixed n_i

Table 5-2. Values of c_i calculated from fitting the expression to the data for a fixed $n_i = 0.58$

Material	c_i
PH101	146
PH102	61
PH200	18
PH302	56

For all powders flowing under the effect of differential pressure it was observed that if the differential pressure was removed then the arch re-formed instantaneously. This indicates that differential pressure is necessary not only for flow initiation but also to maintain the flow. This aspect is examined in detail in Chapter 6.

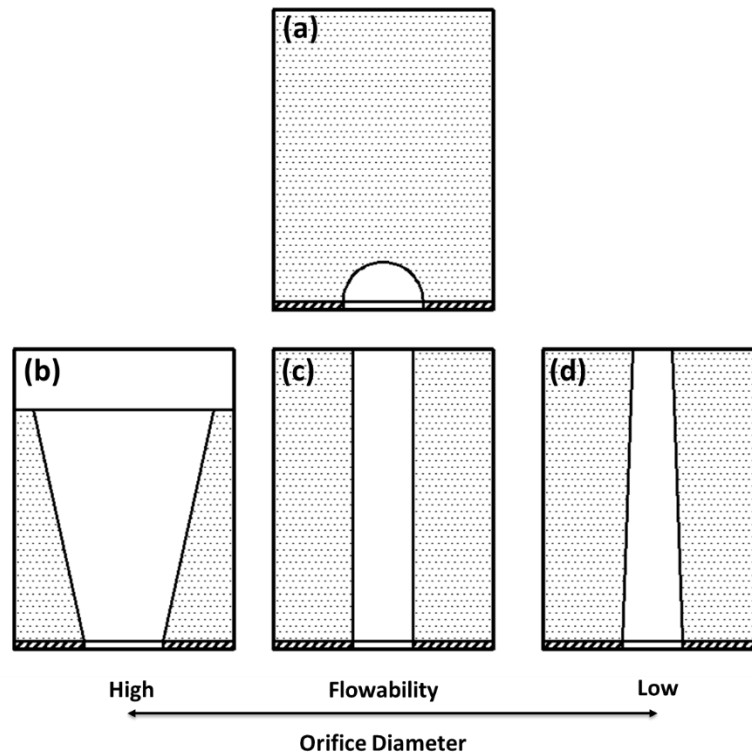


Figure 5-7. Schematic diagram of flow patterns; a) initial state (arching), b) mechanisms for good flowing powder and large orifice diameters, c) transition regime, d) mechanism for poor flowing powders and small exit diameters after discharge under differential pressure

5.5. Conclusions

This research examined the effect of differential pressure conditions on powder flow initiation from an arching state. Arch stability is very sensitive to small variations of pressure. Specifically, it was demonstrated that if the air pressure at the exit is reduced by only a small amount, of the order of 100 Pa (the atmospheric pressure is 100,000 Pa) then it was possible to reduce the critical orifice diameter significantly.

A dimensional model was developed to calculate the pressure difference (ΔP) required to initiate flow for a given exit diameter. Equation (5-10) contains two dimensionless groups (one related to the powder properties and one related to the geometry of the

system) and two empirical parameters (c_i, n_i) which can be determined using simple experiments.

For practical use Equation (5-10) can be calibrated using the system presented in Figure 5-1. by performing 2 experiments to determine the slope and the off-set of the logarithmic relationship in Figure 5-4. Parameter c_i includes powder specific properties, including particle size and more detailed experiments are required to isolate the effect of these properties.

Equation (5-10) can be used in process design provided that the material specific parameter c_i was determined experimentally. The potential practical impact of the proposed flow model is significant in terms of predicting flow initiation and offering a measure for powder flowability.

Chapter 6. Mass flow rate of fine and cohesive powders under differential air pressure

For materials discharging from containers with exit diameters smaller than the critical orifice diameter, arching inhibits powder flow. In Chapter 5 it was shown that by applying a small differential pressure (100-200 Pa) the critical orifice diameter of a material can be reduced significantly by up to 15 times. In this chapter, the influence of differential pressure on mass flow rate of powders is investigated. A new system is designed in order to measure the mass flow rate of the materials under a range of differential pressures using disks with orifice diameters both above and below the critical orifice diameter. The term “differential pressure” refers to the pressure difference between the vacuum chamber and the ambient pressure averaged over the mass flow rate measurement period. The results are compared in terms of powder flowability, average particle size and bulk density. Existing models to predict the mass flow rate of powders under differential pressure are examined. It is shown that these models over predict the mass flow rate of fine and cohesive powders significantly. A new dimensional model is proposed to predict the flow rate of powders under differential pressure.

6.1. System development

Similar to the apparatus used in the previous chapter, a critical orifice diameter measurement system was extended with a large vacuum chamber as illustrated in Figure 6-1. This development is necessary to accommodate the handling of a large amount of powder than in Chapter 5. A circular step with diameter of 57.4 and depth of 1.5 mm (equal to the thickness of the critical orifice diameter measurement disks) was designed on the top plate of the vacuum chamber to place the critical orifice diameter measurement disk. A similar shutter mechanism to that of the critical orifice diameter measurement system (described in Section 3.5) was placed inside the chamber below the measurement disks and the shutter release pin was installed on the chamber wall allowing control of the shutter whilst maintaining vacuum in the chamber. The shutter pin was installed on the side wall of the chamber to be able to control the shutter as well as to maintain the vacuum inside the chamber. A powder container consisting of a

cylindrical section with internal diameter of 68 mm and height of 70 mm attached to a hopper on the top was used to accommodate nearly 1 kg of powder. The pressure inside the chamber was reduced using a vacuum pump controlled with a precision vacuum regulator (Airtrol V-900-10 W/K). The difference between the pressure inside the chamber and ambient atmosphere was measured using a Sensirion SDP2000-L differential pressure transducer. The powder discharging from the container was collected with a beaker placed on a scale inside the vacuum chamber. The pressure in the chamber and the time was logged using a data acquisition device (National Instruments NI USB-6221) and a PC software (LabVIEW) and the weight of the powder was monitored using the scale.

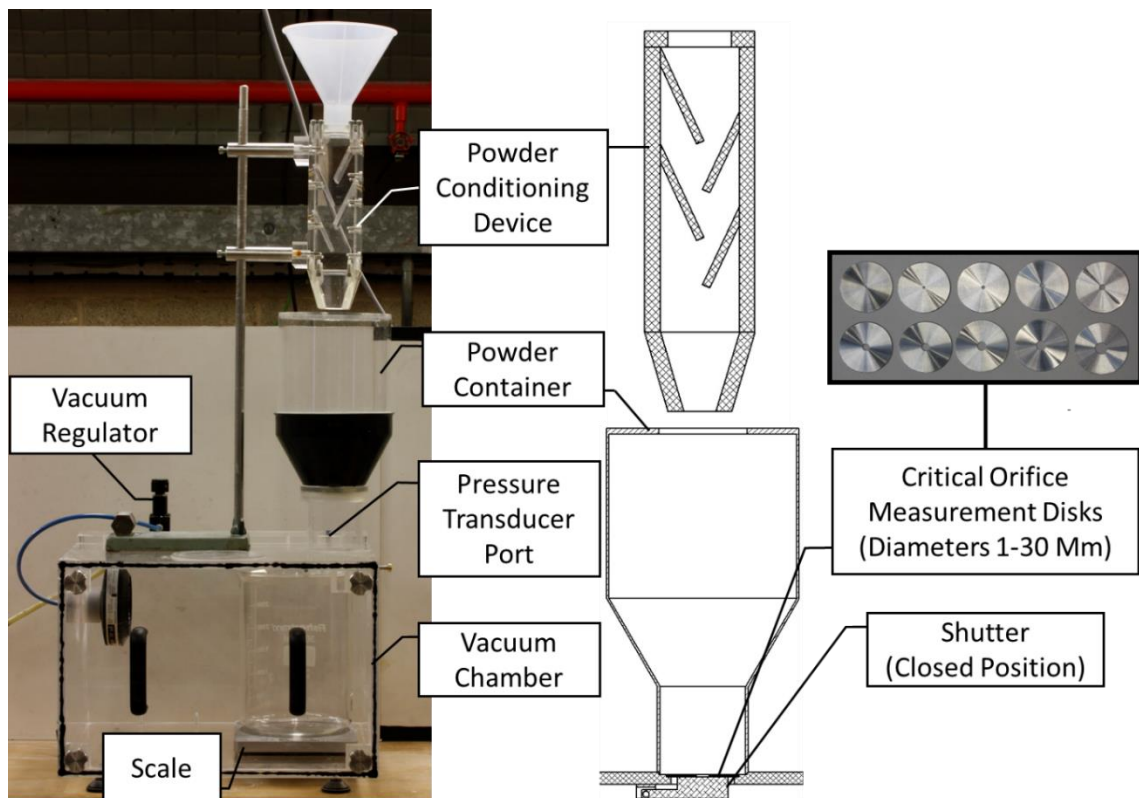


Figure 6-1. Flow rate measurement device

6.2. Procedure

A disk with a given diameter (5, 7 or 10 mm) was placed in position at the bottom of the powder container (Figure 6-1). 800 grams of powder was introduced using the powder conditioning device described in Section 3.2. The shutter was opened using the associated pin. Based on the size of the exit, two cases were occurred:

- 1) If the exit diameter was smaller than the critical orifice diameter of the powder, the material inside the container was not discharged and an arch was formed above the exit. In this case, the differential pressure was increased until the flow was initiated.
- 2) If the orifice diameter was larger than the critical value, the material discharged from the container under no differential pressure (ambient pressure).

In order to measure the flow rate in steady state, time measurement was started once 100 grams of powder was collected and the time taken for 600 grams of powder to discharge was recorded. Powder flow rate was measured three times for each exit diameter.

This experiment was repeated by pre-setting the differential pressure to values above the flow initiation pressure (0-1400 Pa) with increments of 200-300 Pa (for exit diameters above the critical orifice diameter the flow initiation pressure was zero). A minimum of 12 measurements were taken for a given orifice diameter for each of the six materials.

During the experiments the top layers of the powder was agitated manually to avoid “rathole” forming in the powder bed.

6.3. Transducer calibration validation

Calibration of the differential pressure transducer used (Sensirion SDP2000-L) was validated against a calibrated manometer using the procedure demonstrated in Figure 6-2. In this set-up, the pressure transducer and the manometer were connected to a Hot-wire Anemometer calibration unit where the steady flow of air results in a pressure drop inside the unit (Figure 6-2). The air flow rate inside the unit was adjusted using an air velocity control system. The output voltage of the differential pressure transducer and the pressure measured by the manometer were logged using the data acquisition device and PC software described in the previous section. The conversion relation provided by the manufacturer of the transducer was used to calculate the corresponding pressures and the values were compared with the pressures measure by the manometer. A good agreement was observed with errors smaller than 2%.

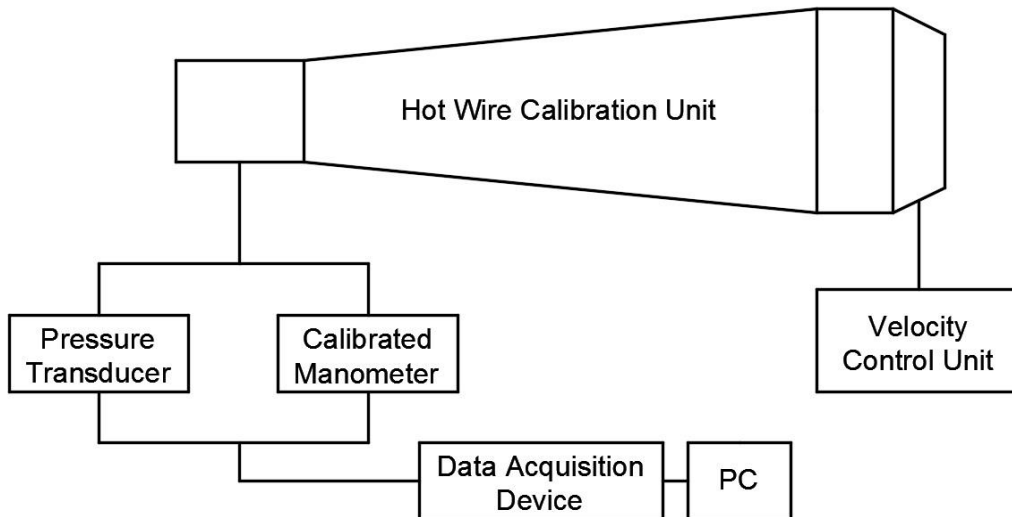


Figure 6-2. Schematic diagram of the transducer calibration setup

6.4. Results and discussions

6.4.1. Flow rate under differential pressure

The mass flow rate of the four grades of microcrystalline cellulose measured under differential pressure is presented in Figure 6-3 for clarity of presentation. Figure 6-4 compares the data for all six powders. In the experiments carried out it was observed that prior to flow initiation the differential pressure was dropped by nearly 10% of the values set before the start of the experiment and the differential pressures used to plot are the average differential pressures during flow rate measurement period.

Based on the results presented in Figure 6-3 and Figure 6-4 the following key observations are made:

- The flow rate increases when the exit diameter is increased
- The flow rate increases when the differential pressure is increased
- Under differential pressure conditions, the mass flow rate of fine and cohesive powders can become higher than of free flowing powders.

These observations are discussed in more detail below. Figure 6-3 presents the data for the four grades of MCC. The three regions correspond to different orifice diameters, 5,

7, and 10 mm as indicated. It is evident that the mass flow rate increases when the orifice diameter is increased, and when the differential pressure is increased, as anticipated.

The critical orifice diameter data presented in Table 3-4 (in ambient atmosphere, without the application of differential pressure) suggest the following rank order of powders in terms of flowability starting from poor flow:

PH101 => PH102 => P302 => PH200 => Mannitol => ATAB.

The orifice diameters considered in this experiment (5, 7 and 10 mm) are below the critical orifice diameters for PH101, PH102 and PH302 which are 30, 26 and 24, mm respectively. Therefore, in ambient pressure, when the shutter was opened the powder was not discharged from the container and the mass flow rate could not be measured. However, powder flow was initiated by applying a differential pressure across the powder bed and mass flow rate was measured. In Figure 6-3, it is evident that as the differential pressure was increased above values necessary for flow initiation, the rank order of MCC powders is changed and for larger differential pressures the new ranking from poor flow becomes:

PH200 => PH102 => PH101

for the differential pressures considered in Figure 6-3. It is important to note that the mass flow rate measured for fine and cohesive powders has become higher than the coarser powders.

The comparison above was limited to PH101, PH102 and PH200 because these powders have similar bulk density but different average particle size. This observation is valid for the three exit diameters in Figure 6-3. PH302, having a higher bulk density, exhibits higher mass flow rate than PH102 which has similar average particle size. Density effects are discussed with reference to volumetric flow rate further on in this section.

Figure 6-4 compares the mass flow rate for all six powders. In terms of mass flow rate, ATAB and Mannitol outperform the other materials, however, it is important to note that their bulk density is also higher. For the exit diameter of 10 mm under high

differential pressures, larger scatter is observed in the data. This is due to increased experimental errors related to measuring higher flow rates.

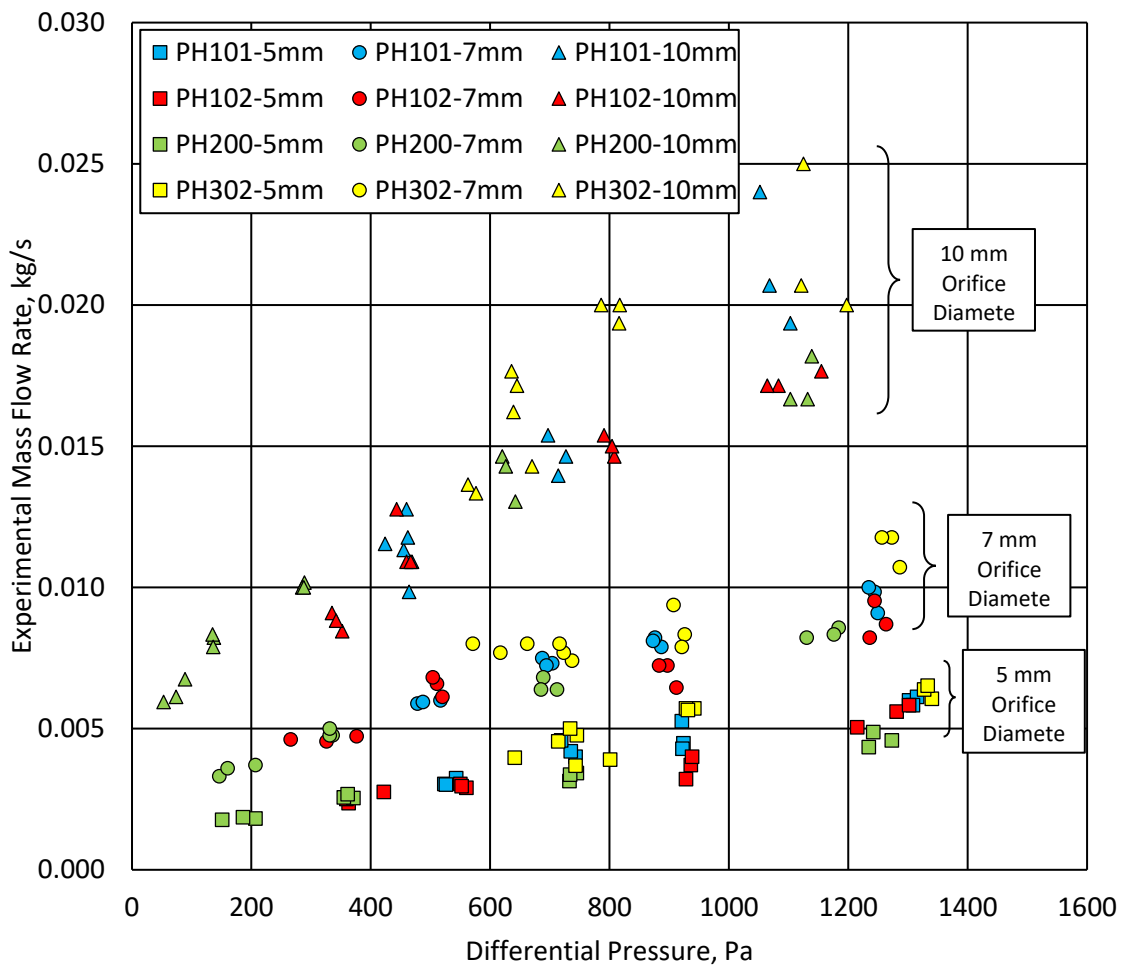


Figure 6-3. Experimental mass flow rate vs. differential pressure for four grades of MCC

For ATAB with critical orifice diameter of 3 mm (Table 3-4), the mass flow rate could be determined with zero differential pressure (ambient pressure) using all three exit diameters. Using the procedure described in Section 3.5.1, the critical orifice diameter of Mannitol was determined as 6 mm. However, in the experiments carried out for arching appeared when the disk with orifice diameter of 7 mm was used and the mass flow rate in ambient atmosphere could only be determined using an orifice of 10 mm. This is due to the difference in the processing parameters (e.g. height of the powder above the orifice) between the critical orifice diameter measurement apparatus and the system used to measure the mass flow rate (Similar to the observations made in Chapter 5).

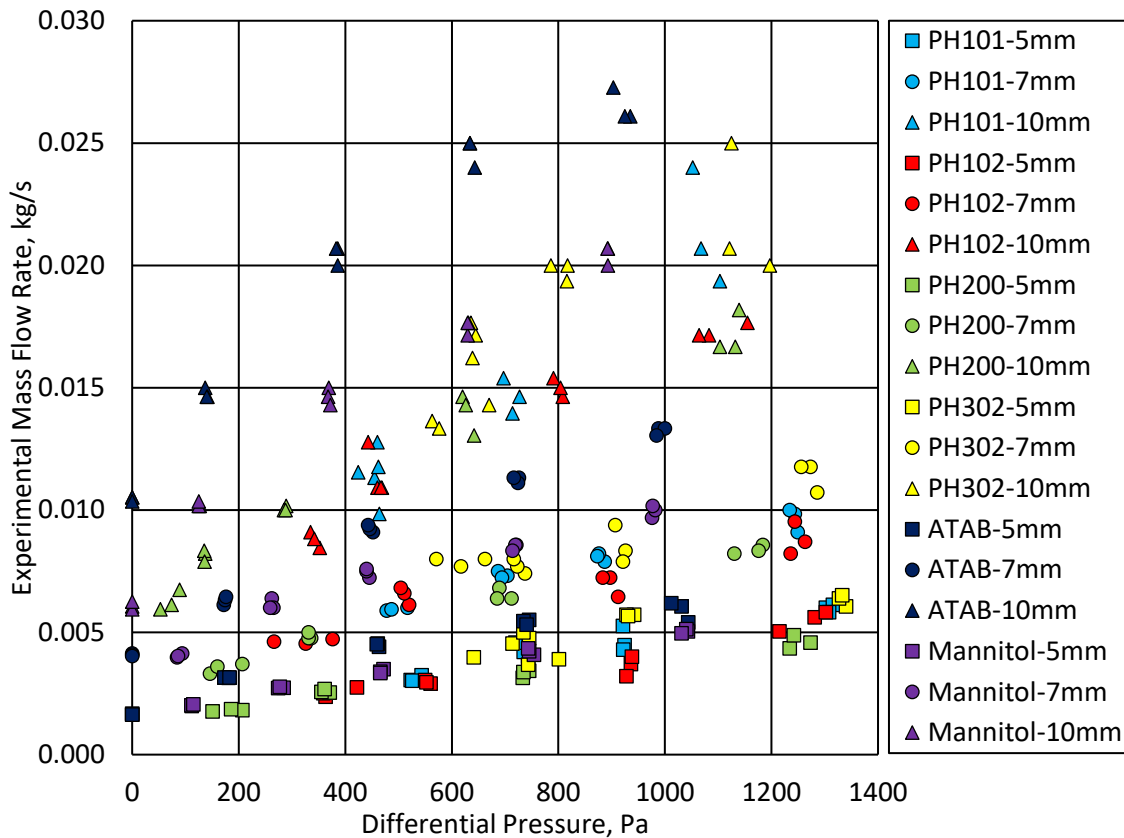


Figure 6-4. Experimental mass flow rate vs. differential pressure measured for all powders

Figure 6-5 presents the measurements in terms of volumetric flow rate for the six materials. It is observed that ATAB which is ranked as the best flowing powder based on the critical orifice diameter results (Table 3-4), has the lowest volumetric flow rate. As before the rank order of the powders in terms of flowability changes as the differential pressure is increased and for higher values of differential pressure the rank order becomes, from the lowest volumetric flow rate:

$$\text{ATAB} \Rightarrow \text{Mannitol} \Rightarrow \text{PH200} \Rightarrow \text{PH302} \Rightarrow \text{PH102} \Rightarrow \text{PH101}$$

The high density powders have low volumetric flow rate, and as before, the application of differential pressure causes the fine and cohesive powders to exhibit higher volumetric flow rate than the coarser and denser powders.

In the next section the existing models are applied to check their ability to capture the observed effects.

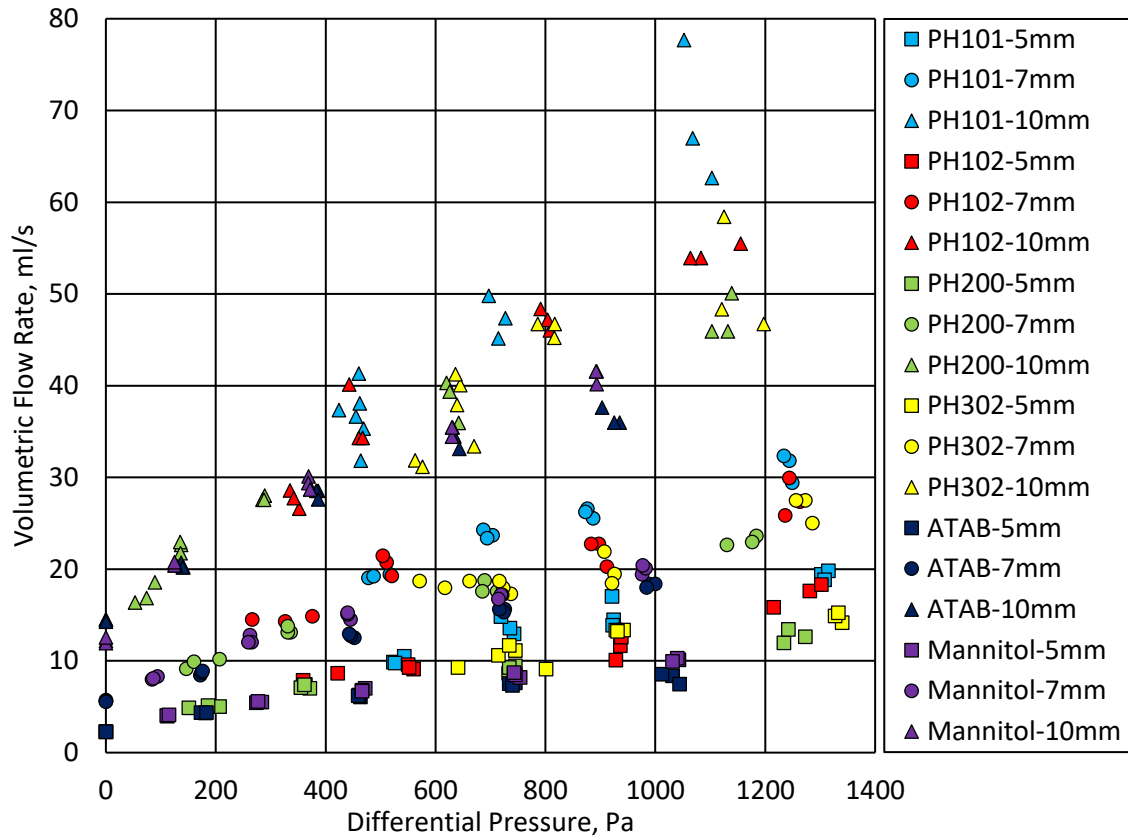


Figure 6-5. Volumetric flow rate vs differential pressure

6.4.2. Analysis of the data using existing models

The modified Crewdson model (Crewdson et al., 1977, Nedderman, 1992) (Equation (6-1) , obtained from Equation (2-18) with $r_0 = D/\sqrt{2}$) was used to predict the mass flow rate of the powders under the same conditions as used in the experiments and the results are presented in Figure 6-6. For each data point the x-coordinate represents the experimentally measured value of mass flow rate and the y-coordinate the value predicted by the Crewdson model which uses the value of 0.58 for the Beverloo constant. The predicted values are above the diagonal line indicating that the Crewdson model significantly over-predicts the flow rate for every test case. Nedderman (Nedderman, 1992) suggested that for fine powders the Beverloo constant ceases to be 0.58 and becomes strongly dependent of particle diameter.

$$\dot{m} = \dot{m}_B \left(1 + \frac{\sqrt{2}\Delta P}{\rho_b g D} \right)^{0.5} \quad (6-1)$$

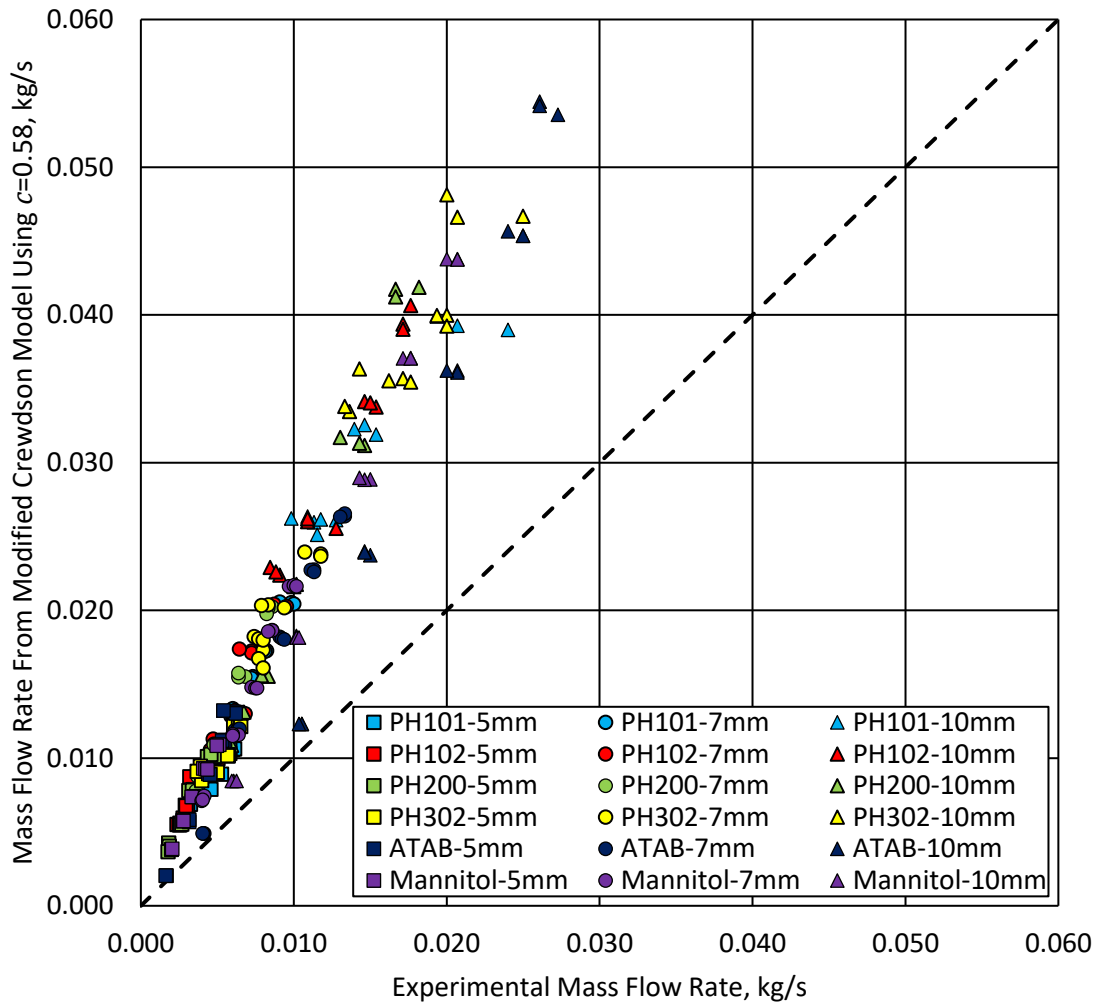


Figure 6-6. Mass flow rates calculated using Crowsdon model with $c_B = 0.58$ vs. mass flow rates measured experimentally for exit diameters of 5, 7 and 10 mm

In the following we examined the possibility of considering c_B as a material dependent parameter. The procedure for obtaining the value of c_B for each material involves measuring the mass flow rate in ambient atmosphere (without applying differential pressure). Given the values of the critical orifice diameter (Table 1) this procedure could be applied only for ATAB and Mannitol as discussed in Section 6.4.1. For PH200 (with critical orifice diameter of 11 mm) an extra set of experiments was carried out using a disk with an orifice diameter of 15 mm and the results are presented in Figure 6-7.

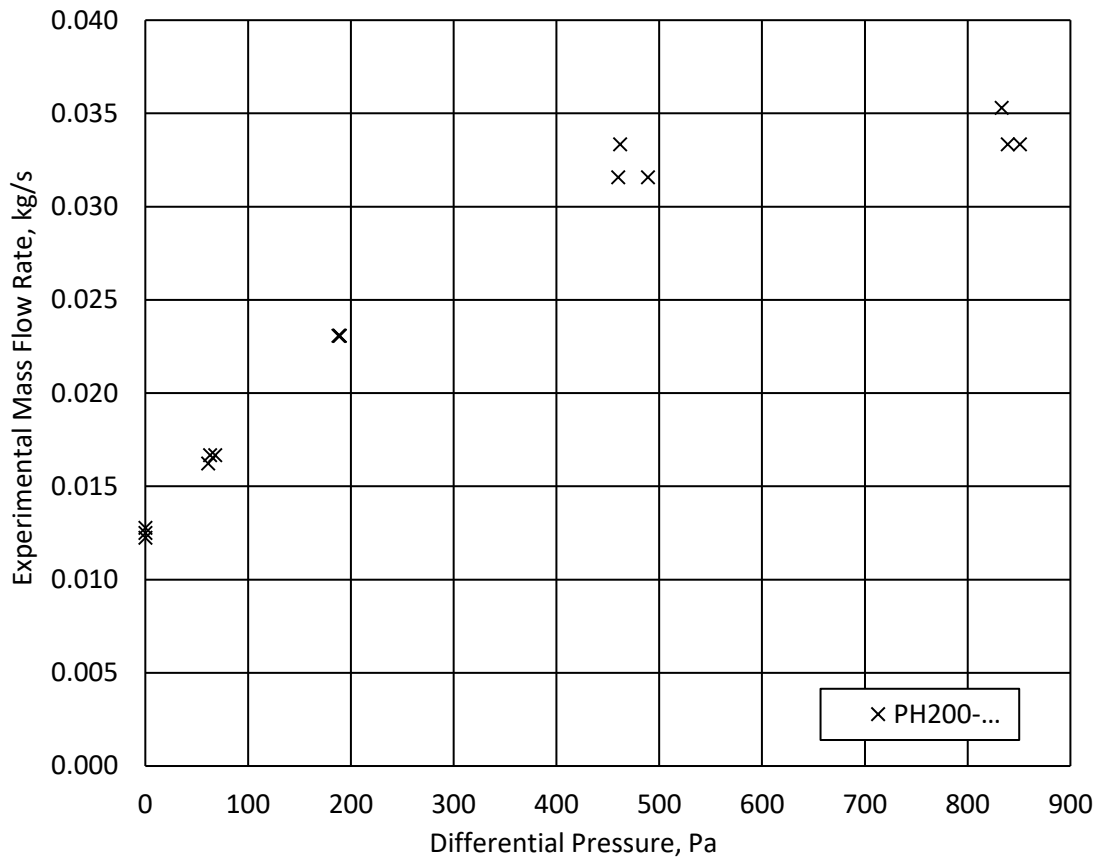


Figure 6-7. Experimental mass flow rate vs. differential pressure for PH200 using exit diameter of 15 mm

The Beverloo coefficients for ATAB, Mannitol and PH200 are $c_B = 0.48, 0.42$ and 0.42 respectively. The predictions of mass flow rate using the Crewdson model for $c_B = 0.58$ and adjusted c_B values are presented for ATAB and Mannitol in Figure 6-8 and for PH200 in Figure 6-9. It is observed that for these materials the mass flow rates predicted by the Crewdson model using the modified value of c_B are still significantly larger than the experimental values for the three exit diameters.

PH101, PH102 and PH302 have large critical orifice diameter (Table 3-4) and their flow rate in air could not be measured using the current system because the flow through a large orifice occurs at a high rate for which the scale described in Section 6.1 was not sufficiently sensitive. Therefore, Beverloo constants adjusted for these three materials were not determined experimentally.

In the next section, a new model is developed using dimensional analysis to predict the mass flow rate of powders under differential pressure.

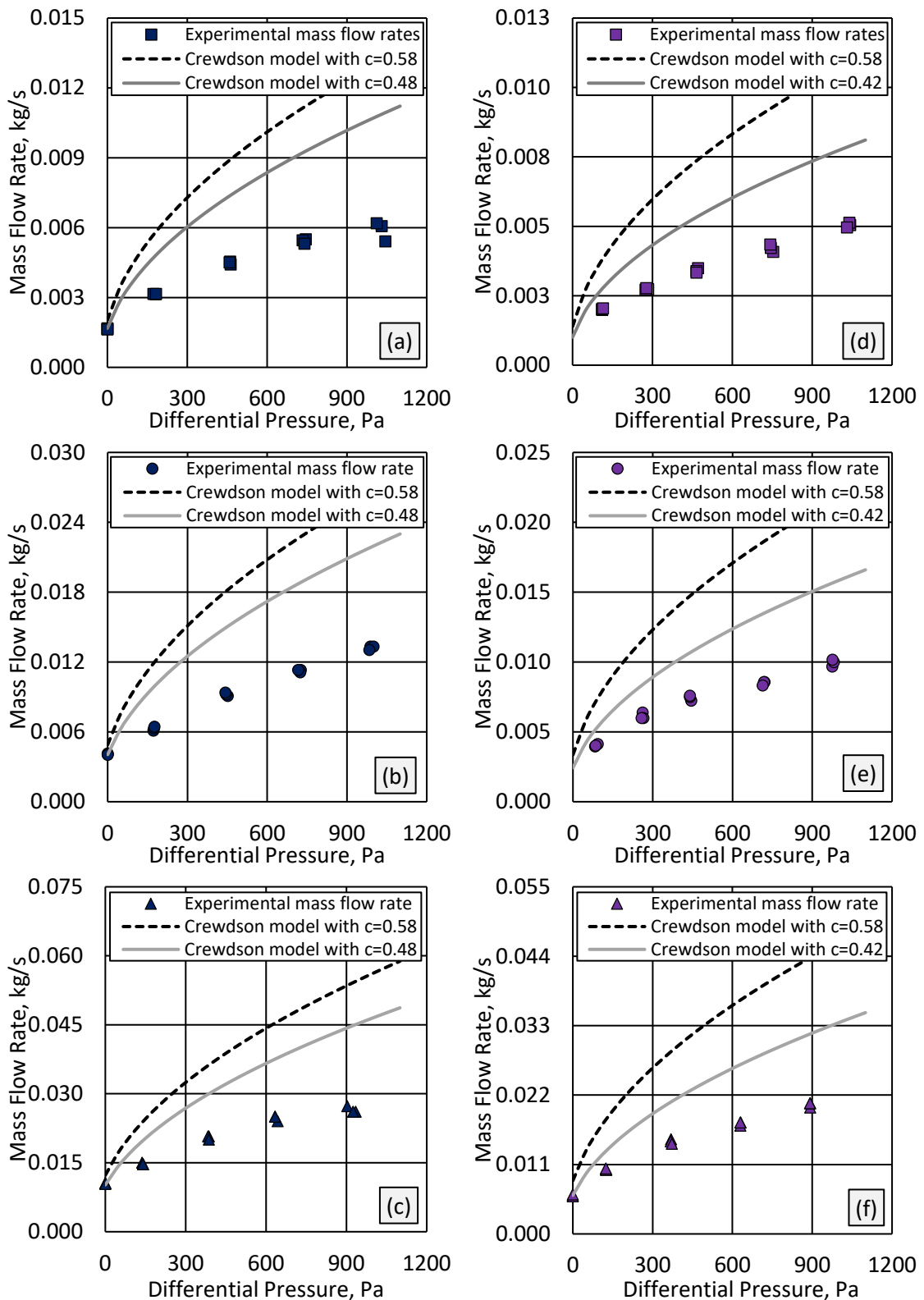


Figure 6-8. Mass flow rate vs. differential pressure for ATAB through orifice diameters of a) 5 mm, b) 7 mm and c) 10 mm (measurement and prediction using the Crewdson model with $c_B = 0.58$ and $c_B = 0.48$) and for Mannitol through orifice diameters of d) 5 mm, e) 7 mm and f) 10 mm (measurement and prediction using the Crewdson model with $c_B = 0.58$ and $c_B = 0.42$)

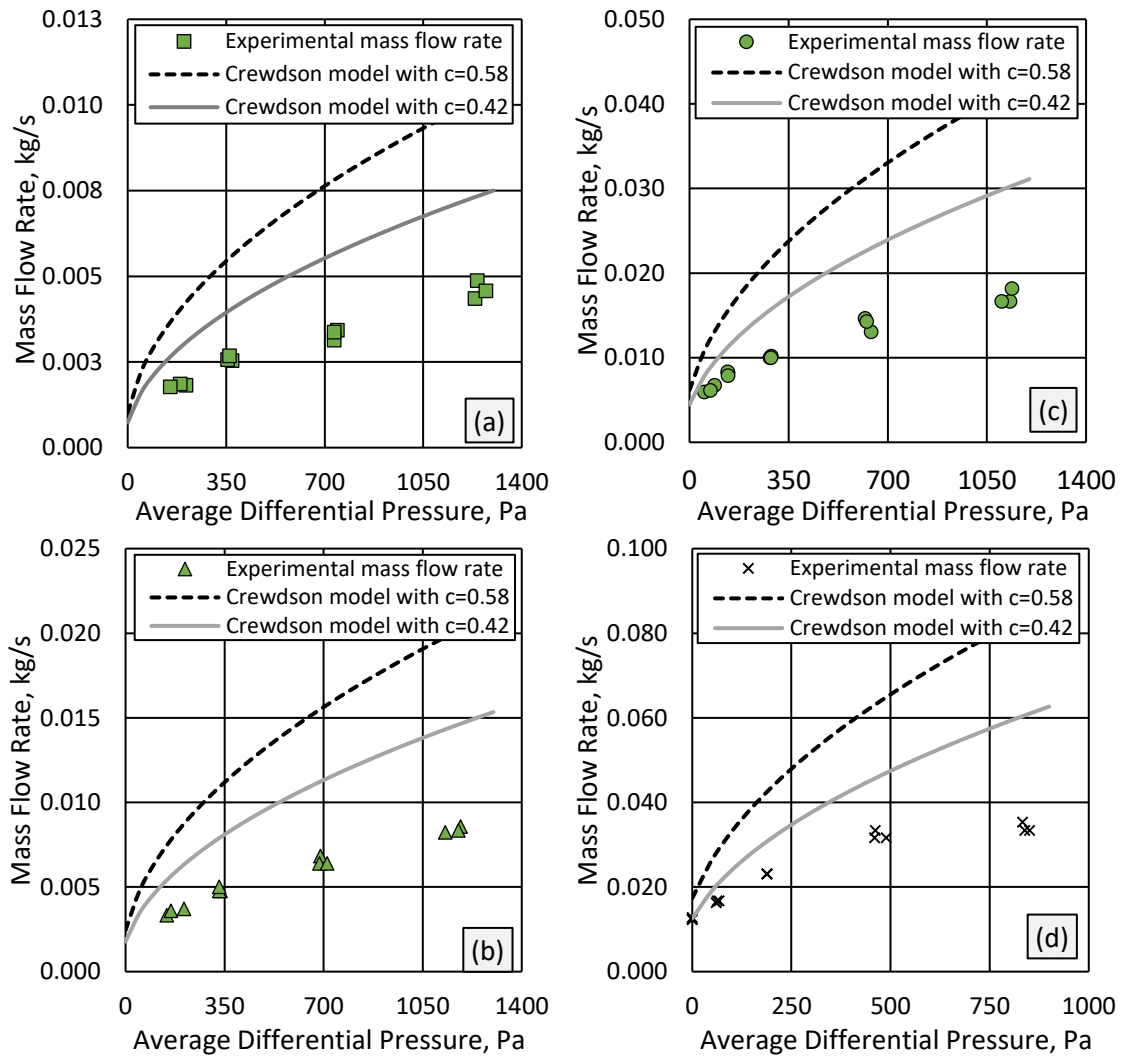


Figure 6-9. Mass flow rate vs. differential pressure for PH200 through orifice diameters of a) 5 mm, b) 7 mm, c) 10 mm and d) 15 mm (measurement and prediction using the Crewdson model with $c_B = 0.58$ and $c_B = 0.42$)

6.4.3. Dimensional model development

The Beverloo model (Equation (2-13)) was developed for flow in ambient atmosphere. To account for the effect of differential pressure Crewdson et al. and Nedderman (Crewdson et al., 1977, Nedderman, 1992) proposed a modification whereby an additional acceleration term was added to gravity. However, as described above, Nedderman (Nedderman, 1992) concluded that c_B must be a function of particle size. As shown in Figure 6-9 and Figure 6-8, this approach does not describe the behaviour of common pharmaceutical excipients. In fact in Equation (6-1) c_B is the only parameter that could be immediately adjusted for a given powder, or considered a material dependent parameter.

The dimensional model proposed below was guided by the following principles: 1) follow the Buckingham Π theorem (Gibbings, 2011); 2) reduce to Beverloo model in absence of differential pressure; and 3) contain material parameters that can be calibrated using simple tests using the methods presented.

The total mass flow rate (\dot{m}) is proposed as the sum of a modified Beverloo correlation (\dot{m}_B) and a term due to the differential pressure applied (\dot{m}_p)

$$\dot{m} = \dot{m}_B + \dot{m}_p \quad (6-2)$$

The method of dimensional analysis is applied. The parameters involved in the process of powder flow rate under differential pressure are: mass flow rate induced by differential pressure (\dot{m}_p); differential pressure (ΔP); bulk density of powder (ρ_b); acceleration due to gravity (g); particle size (d); and orifice diameter (D). There are also other parameters like viscosity of air (μ), coefficient of friction between particles (μ_p) and between particles and the wall (μ_{pw}), shape of the particles and adhesion between the particles that contribute. Thus \dot{m}_p can be written as a function of $\Delta P, \rho_b, g, d, D, \mu, \mu_p, \mu_{pw}$, particle shape and adhesion i.e.

$$\dot{m}_p = f(\Delta P, \rho_b, g, d, D, \mu, \mu_p, \mu_{pw}, \text{shape}, \text{adhesion}) \quad (6-3)$$

or

$$F(\dot{m}_p, \Delta P, \rho_b, g, d, D, \mu, \mu_p, \mu_{pw}, \text{shape}, \text{adhesion})=0 \quad (6-4)$$

Using the Buckingham Π theorem (Gibbings, 2011) and by taking the parameters ρ_b, g and D as the independent variables, two π groups of dimensionless mass flow rate ($\overline{\dot{m}_p}$) and dimensionless differential pressure ($\overline{\Delta P}$) are formed as

$$\overline{\dot{m}_p} = \frac{\dot{m}_p}{\rho_b g^{0.5} D^{2.5}} \quad (6-5)$$

and

$$\overline{\Delta P} = \frac{\Delta P}{\rho_b g D} \quad (6-6)$$

Therefore, it can be written that

$$\overline{\dot{m}_p} = f(\overline{\Delta P}, \rho_b, g, d, D, \mu, \mu_p, \mu_{pw}, \text{shape}, \text{adhesion}) \quad (6-7)$$

The experimental data presented in Figure 6-4 could be fitted with a power law relation.

We write in dimensionless form:

$$\overline{\dot{m}_p} = a_r (\overline{\Delta P})^{n_r} \quad (6-8)$$

or

$$\frac{\dot{m}_p}{\rho_b g^{0.5} D^{2.5}} = a_r \left(\frac{\Delta P}{\rho_b g D} \right)^{n_r} \quad (6-9)$$

where a_r and n_r are material dependent parameters. The index refers to “flow rate”.

Substituting Equation (2-13) (without the inclusion of the empty annulus effect) and (6-9) into Equation (6-2) we have

$$\dot{m} = c_B \rho_b g^{0.5} D^{2.5} + a_r \rho_b g^{0.5} D^{2.5} \left(\frac{\Delta P}{\rho_b g D} \right)^{n_r} \quad (6-10)$$

or

$$\frac{\dot{m}}{\rho_b g^{0.5} D^{2.5}} = c_B + a_r \left(\frac{\Delta P}{\rho_b g D} \right)^{n_r} \quad (6-11)$$

where c_B is the Beverloo coefficient adjusted for the material to give a correct prediction of the mass flow rate under no differential condition, consistent with the condition identified by Nedderman (Nedderman, 1992).

To account for the empty annulus effect (Brown and Richards, 1970) the correction factor $k_B d$ is introduced where k_B is a constant based on the shape of the particles. The proposed model is:

$$\frac{\dot{m}}{\rho_b g^{0.5} (D - k_B d)^{2.5}} = c_B + a_r \left(\frac{\Delta P}{\rho_b g D} \right)^{n_r} \quad (6-12)$$

Using the values of the adjusted Beverloo coefficient c_B determined in Section 6.4.2 for PH200, ATAB and Mannitol, the experimental data was fitted using Equation (6-12) and the values of material dependent parameters a_r and n_r are presented in Table 6-1. In the fit the particles were considered spherical ($k_B=1.5$).

Table 6-1. Flow parameters for the free flowing materials

Material	c_B	a_r	n_r	R^2
PH200	0.42	0.135	0.65	0.98
ATAB	0.48	0.162	0.61	0.98
Mannitol	0.42	0.169	0.61	0.99

For PH101, PH102 and PH302 the Beverloo coefficient could not be measured (Section 6.4.2). Fitting all three parameters c_B, a_r and n_r using Equation (6-12) leads to unreasonably small values for c_B (of order of 10^{-9}) which does not describe the finite flow rate of these materials in ambient atmosphere through exit diameters above the critical orifice diameter. Therefore, it can be concluded that it is necessary to measure c_B before fitting a_r and n_r to the experimental data.

In absence of flow rate measurements in ambient air for PH101, PH102 and PH302 the following procedure was used to estimate values for c_B for these materials. When fitting the values for a_r and n_r for PH200 it was observed that equally good fits (in terms of the coefficient of determination) could be obtained by using $a_r = 0.16$. In the following

it is assumed that $a_r = 0.16$ for the other three MCC materials, PH101, PH102 and PH302. Having fixed a_r , the values of c_B and n_r can be determined from fitting the experimental data with Equation (6-12).

For PH200, ATAB and Mannitol, whilst c_B was measured, constant values for $a_r = 0.16$ could be used to fit n_r with equally good correlation factors. The values are presented in Table 6-2 for all materials.

Table 6-2. The values of the coefficients used to predict the mass flow rate

Material	c_B	a_r	n_r	R^2
PH101	0.17	0.16	0.68	0.93
PH302	0.19	0.16	0.68	0.86
PH102	0.22	0.16	0.65	0.90
PH200	0.42	0.16	0.60	0.98
Mannitol	0.42	0.16	0.63	0.99
ATAB	0.48	0.16	0.62	0.98

Using the parameters in Table 6-2 the mass flow rate predicted by Equation (6-12) for all materials is compared with the experimental measurements as presented in Figure 6-10. It is evident that the proposed model (Equation (6-12)) provides a good approximation of the data.

6.4.4. Discussion

The exponent ($n_r = 0.5$) in the model of Crewdson (Crewdson et al., 1977) (developed for 90 – 850 μm diameter powders with interstitial pressure gradient) cannot be changed for reasons of dimensional consistency. The Beverloo coefficient ($c_B = 0.58$) used in this model was adjusted to reproduce the mass flow rate of fine and cohesive powders in ambient atmosphere following the remark of Nedderman (Nedderman, 1992). However, the flow behaviour of fine and cohesive powders was significantly over-predicted by the Crewdson model.

The dimensional model developed provides the basis for constructing a relationship to describe powder flow under differential pressure. Equation (6-12) includes three material parameters:

- c_B is a proportionality constant for the flow of powder in ambient atmosphere. The values listed in Table 6-2 are generally smaller for poor flowing powders and increases for free flowing powders according to the measures in Table 3-3 and Table 3-4 (with the exception of the high density PH302 which has smaller critical orifice diameter).
- a_r is a proportionality constant in the term that includes the differential pressure. Its value was considered constant for the powders used in this work, however, a_r offers increased flexibility to the model for use with a wider range of powders.
- n_r is an exponent to account for the effect of differential pressure. n_r is relatively small for good flowing powders but generally the values are similar for the materials considered in this study.

The differential pressure in Crewdson's model (Equation (6-1)) affects all powder materials in the same way. However, in Section 6.4.1 it was shown that the effect of pressure influences the flowability of powder differently, or in simple terms the poor flowing powders "benefit more" than free flowing powders. The proposed model (Equation (6-12)) has a general form suitable to discern this effect, particularly because n_r is an adjustable, rather than fixed exponent. The proportionality material constant a_r then ensures good reproduction of the trends observed experimentally.

Equation (6-12) reduces to a Beverloo type equation provided that c_B is determined experimentally from flow measurement in ambient atmosphere. For exit diameters smaller than the critical orifice diameter the mass flow rate in ambient atmosphere will be zero. To calibrate a_r and n_r it is necessary to perform flow rate measurements under differential pressure.

The calibrated model can be used for practical applications where the exit diameter can be larger or smaller than the critical orifice diameter. The latter case is of significant

practical importance. For example, many pharmaceutical formulations are poor flowing due to the cohesive nature of typical active pharmaceutical ingredients, e.g. the critical orifice diameter of active ingredients can be larger than 20 mm (Cai et al., 2013). Pharmaceutical tablets are made by compressing the powder in dies of typical diameters under 10 mm. Die filling is made possible (Sinka and Cocks, 2009, Jackson et al., 2007) by the suction fill effect, whereby the downward movement of the lower punch creates a low pressure environment during die fill. Typical tablet presses produce 0.5-1 million tablets per hour (Jackson et al., 2007); such productivity is enabled by the enhanced mass flow rate into the die under differential pressure. The proposed model has therefore use in the design of powder handling and dosing processes operating by differential pressure.

The model has three empirical parameters which can be determined from simple experiments as described above. The flow of powders in ambient atmosphere is complex and involves a large number of particle characteristics such as particle size and size distribution, particle shape, morphology, friction and adhesion between particles, etc. The flow process is further complicated by interactions between air and powder. The contributing material and process parameters cannot be de-convoluted at the present time in order to develop mechanistic models for powder flow. However, the dimensional model proposed can be of significant practical use.

6.1. Conclusions

Orifice flow experiments under differential pressure show that the flow rate increases when the exit diameter is increased, and when the differential pressure is increased. Depending on the magnitude of differential pressure applied, rank order of powders in terms of flowability evolves and at higher differential pressures the mass flow rate of fine and cohesive powders can become higher than of free flowing powders.

A model for flow of coarse free flowing sands under differential pressure has been developed (Crewdson et al., 1977). However, this does not describe adequately the flow of fine and cohesive powders which represent an important class of materials used in pharmaceutical formulations. Using dimensional analysis a model was proposed

(Equation (6-12)) and validated to predict the mass flow rate of powders under differential pressure.

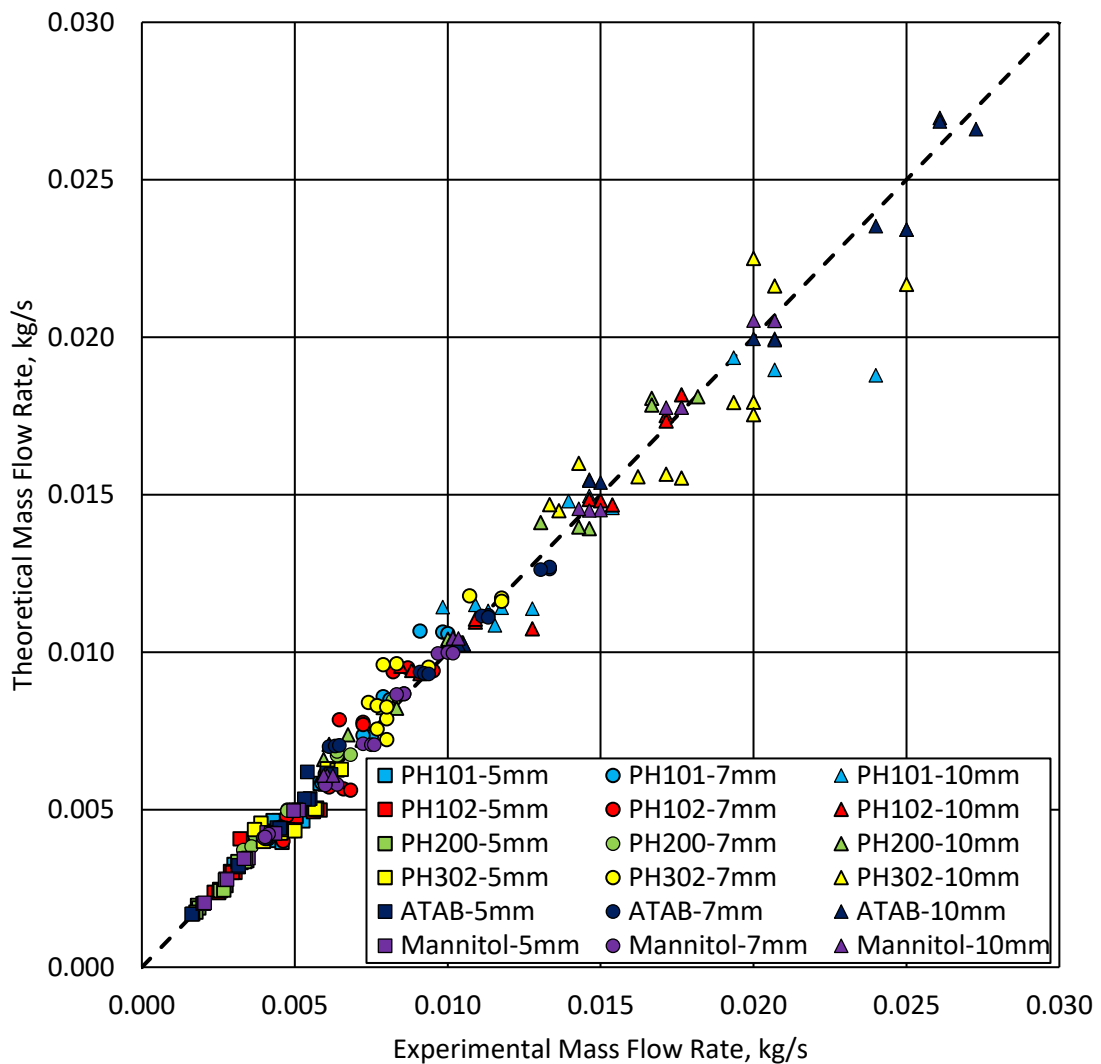


Figure 6-10. Theoretical mass flow rates calculated from the dimensional model vs experimental mass flow rates for all powders using exit diameters 5, 7 and 10 mm

Due to the complex nature of powder flow and the multitude of interrelated material and process parameters the development of a mechanistic model is not yet practical. A small magnitude of differential pressure (e.g. a few hundred Pa) reduces the critical diameter and increases the flow rate significantly for all powders tested. This effect can be utilised advantageously in a number of practical powder handling and dosing operations. The proposed model for powder flowability (Equation (6-12)) can therefore be of significant use for powder and process design.

Chapter 7. Linear shoe-die system under gravity fill mechanism

In this chapter, a pneumatically driven linear shoe-die system (Figure 7-1) developed at the University of Leicester was used to study the effects of material properties and processing parameters on the mass of the powder introduced into the die. A range of experiments were carried out for four grades of MCC (described in Section 3.1.1) using different shoe velocities, die height and height of the powder in the shoe. The mass of the powder introduced into the die and the differential pressure between the die and ambient atmosphere developed by the introduction of powder mass into the die was measured. The experimental data was used to examine the model developed by Schneider et al. (Schneider et al., 2007). This model was modified to include the influences of the differential pressure.

7.1. Description of the system

The linear shoe-die system was originally developed by Wu et al (Wu et al., 2003) and later used by Schneider et al. (Schneider et al., 2007). Jackson et al. (Jackson et al., 2007) modified the system to include the suction effect by releasing the lower punch under its own weight. The punch was then fitted with a pneumatic actuator to control the suction velocity by Mills and Sinka (Mills and Sinka, 2013). For this research two differential pressure transducers were fitted to enable pressure measurement during die filling.

The system consists of a rectangular shoe passing over a square die (14 × 14 mm). The experiments were carried out using two different shoes. The first shoe with the internal length of 65 mm, width of 31 mm and height of 38 mm was used to carry out the experiments where the powder height in the shoe was set to 15 or 30 mm while the second shoe (with the internal length of 65 mm, width of 31 mm and height of 40 mm) was used to carry out the experiments where the powder height was 40 mm. The height of the die was adjusted to 10 and 20 mm by lowering the punch inside the die. The shoe and the punch are moved using servo-pneumatic actuators controlled with a FESTO SPC-200/P02 controller and WinPISA software. In this system, the shoe is associated to the x-coordinate and the punch is associated to the y-coordinate of the controller. The velocity of the servo-pneumatic actuators can be set to the maximum of 1 m/s and their

acceleration can be adjusted to the maximum value of 100 m/s^2 . The system is supplied with compressed air with the pressure set to 3 bars. For the experiments carried out, the acceleration of both axis is set to 10 m/s^2 . As illustrated in Figure 7-2, the velocity of the shoe is increased to the specified value (v_s) linearly with fixed acceleration (10 m/s^2) and reduced linearly back to zero at the end of the travel. The pressure inside the die was measured using two differential pressure transducers (Sensirion SDP1000-L) one attached to the top left hand of the die and the second one attached to the bottom of the punch. A small hole is drilled into the punch to allow pressure measurement inside the die. The pressures measured are logged using a data acquisition device (National Instruments NI USB-6221) and PC software (LabVIEW). The mass of the powder was measured using a Mettler Toledo PL83-S scale.

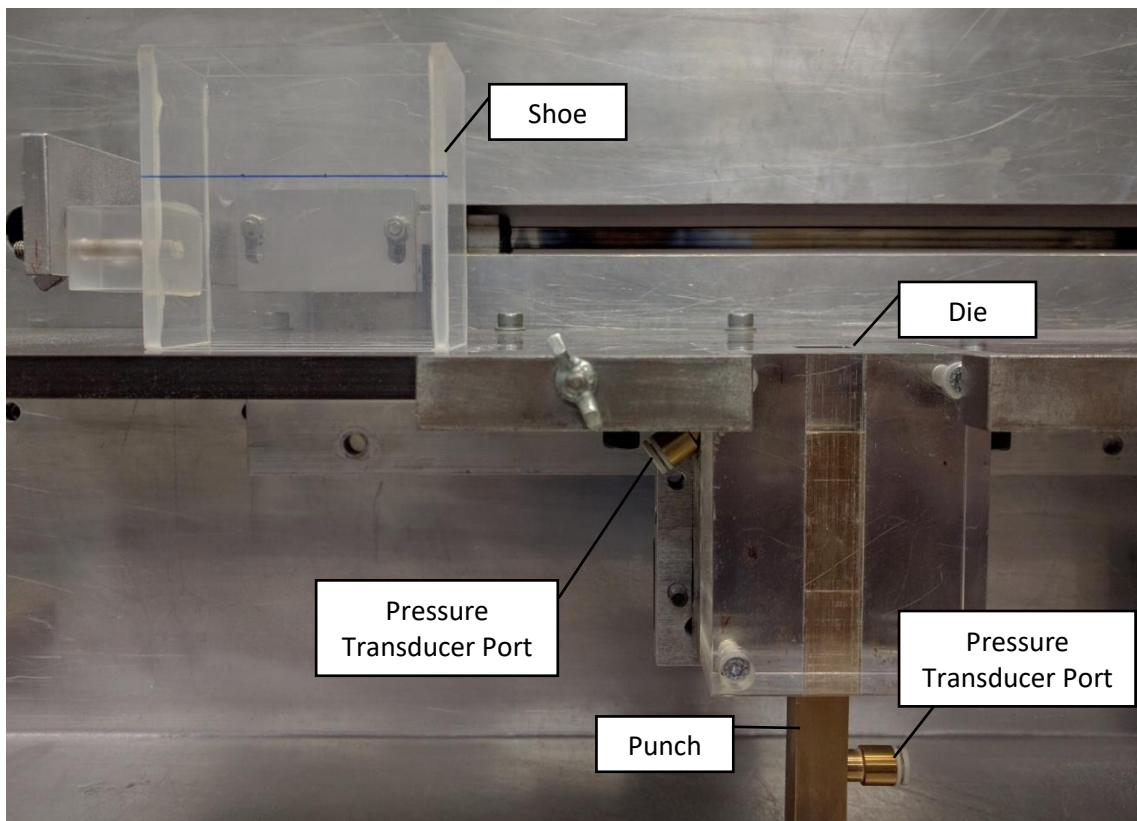


Figure 7-1. Linear shoe-die system

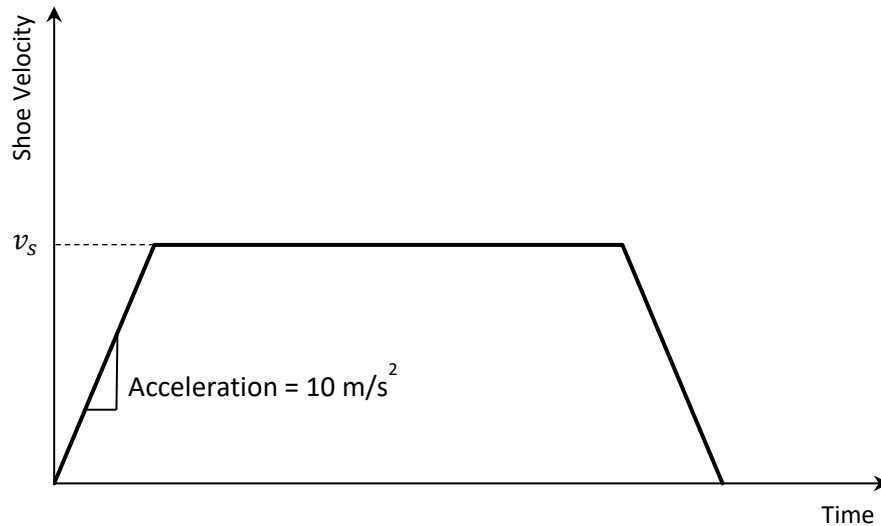


Figure 7-2. Velocity profile of the motion of each axis in the linear shoe-die system

7.2. Procedure

The powder material was introduced into the shoe described in the previous section and an L-shaped rod was used to level the top layer of the powder to set the powder height inside the shoe to 15, 30 or 40 mm. In order to obtain repeatable and consistent initial condition for the powder, the shoe was shaken prior to translating over the die. Each shake involves moving the shoe back and forth for ± 5 mm with velocity of 100 mm/s and the acceleration of 10 m/s^2 . The height of the die was adjusted to 10 or 20 mm by lowering the punch. The shoe was translated over the die opening with a constant velocity (30 – 250 mm/s) and the powder was delivered into the die as a result. The mass of the powder introduced was measured after the experiment using the scale. This procedure was repeated three times for each shoe velocity for the four grades of MCC. The differential pressure between the atmosphere and the die was logged for each test.

7.3. Results and discussions

7.3.1. Mass of the powder delivered into the die

The mass of the powders introduced into the die for different shoe velocities (v_s) is presented for PH101 and PH102 in Figure 7-3 and for PH200 and PH302 in Figure 7-4. The error bars are generated using the standard deviation of the mass introduced. For the majority of the results the errors are negligible. In order to study the influence of

material properties and the processing conditions on the process, the results are plotted in terms of fill ratio (δ) calculated by dividing the mass delivered into the die by the mass of the full die for each powder (Figure 7-5 and Figure 7-6). In the experiments carried out it is observed that the mass of the powder introduced into the die are similar when the height of the powder in the shoe was set to 30 mm while the fill ratios calculated for die height of 10 mm are larger than the die height of 20 mm (due to smaller mass of the full die). Therefore, comparison of the results based on the fill ratio must be made with caution.

The results obtained are used to characterise powder flowability where a powder with better flow behaviour have larger fill ratio. In Figure 7-5 and Figure 7-6, it is shown that the fill ratios measured for PH200 are larger for different shoe velocities. The flowability of the powders can be ranked as below starting with poor flowing.

PH101 => PH302 => PH102 => PH200

This is similar to the ranking obtained from the angle of repose results presented in Table 3-3. It is shown that the fill ratio increases for powders with larger average particle size and for denser powders smaller fill ratio is recorded.

In Figure 7-3 and Figure 7-4, it is observed that the mass delivered into the die reduces by increasing the shoe velocity. Comparing the results obtained for each material shows that the mass introduced into the die is independent of the die height. Also, when the height of the powder in the shoe is 15 mm, larger mass of the powder is delivered. Powder conditioning by the initial back and forth motion of the shoe creates a heap inside the shoe. At low powder heights, this heap facilitates the nose flow of powder into the die. As the tip of the nose enters the die, the die opening would not be fully covered with powder and air can escape easily resulting in higher fill ratio. Larger powder height in the shoe exerts higher body force on the powder at the die opening and a larger driving force for powder to enter the die; however, the pressure exerted by the weight of the material results in local densification of the powder (specifically at lower layers of powder) and particle interlocking which inhibit powder flow. For large powder heights, nose flow does not appear and the particles discharge into the die under bulk and intermittent flow mechanisms. Also, the powder bed is less permeable

at larger heights (due to densification) and it would be more difficult for air inside the die to escape. As more powder enters the die, air pressure built up opposes further flow of the material and results on the reduction of the mass delivered. The measurement of the differential pressure in the die and its influence on the mass delivered is discussed in more detail in the next section.

In Figure 7-3 and Figure 7-4, it is observed that the mass of the powder introduced into the die when the powder height is set to 30 and 40 mm are similar. When the height of the powder is 2.5 times larger than opening size, the flow becomes independent of height and the flow rate under gravity is constant (Deming and Mehring, 1929).

The comparison of the flowability of the powders can also be made in terms of the critical velocity (v_c) which was first introduced by Wu and co-workers (Wu et al., 2003). Critical velocity is the maximum shoe velocity at which the die is completely filled with powder and for a powder with better flow behaviour the critical velocity is larger. The relation between the fill ratio and the shoe velocity (Equation (7-1)) was used to calculate the critical velocity and the constant $1 + n$ for each materials under each specific set of processing conditions.

$$\delta = \left(\frac{v_c}{v_s} \right)^{1+n} \quad (7-1)$$

The values of $1 + n$ and the critical velocity calculated for each set of experiments are presented in Table 7-1. Comparison of the critical velocities calculated shows that for powders that are ranked as good flowing, the critical velocity is higher. For PH200, which is characterised as the best following powder based on the critical orifice diameter measurement and the angle of repose experiments (described in Chapter 3) the critical velocities calculated are 2-3 times larger than the critical velocity of PH102. The critical velocity and the exponent could not be determined for PH101 when the height of the powder in the shoe was set to 40 mm as the mass delivered was constant across the range of shoe velocities used. The values of the critical velocity obtained are specific to the system and the processing parameters used and as the critical velocity is not a material dependant parameter, it cannot be used for process design.

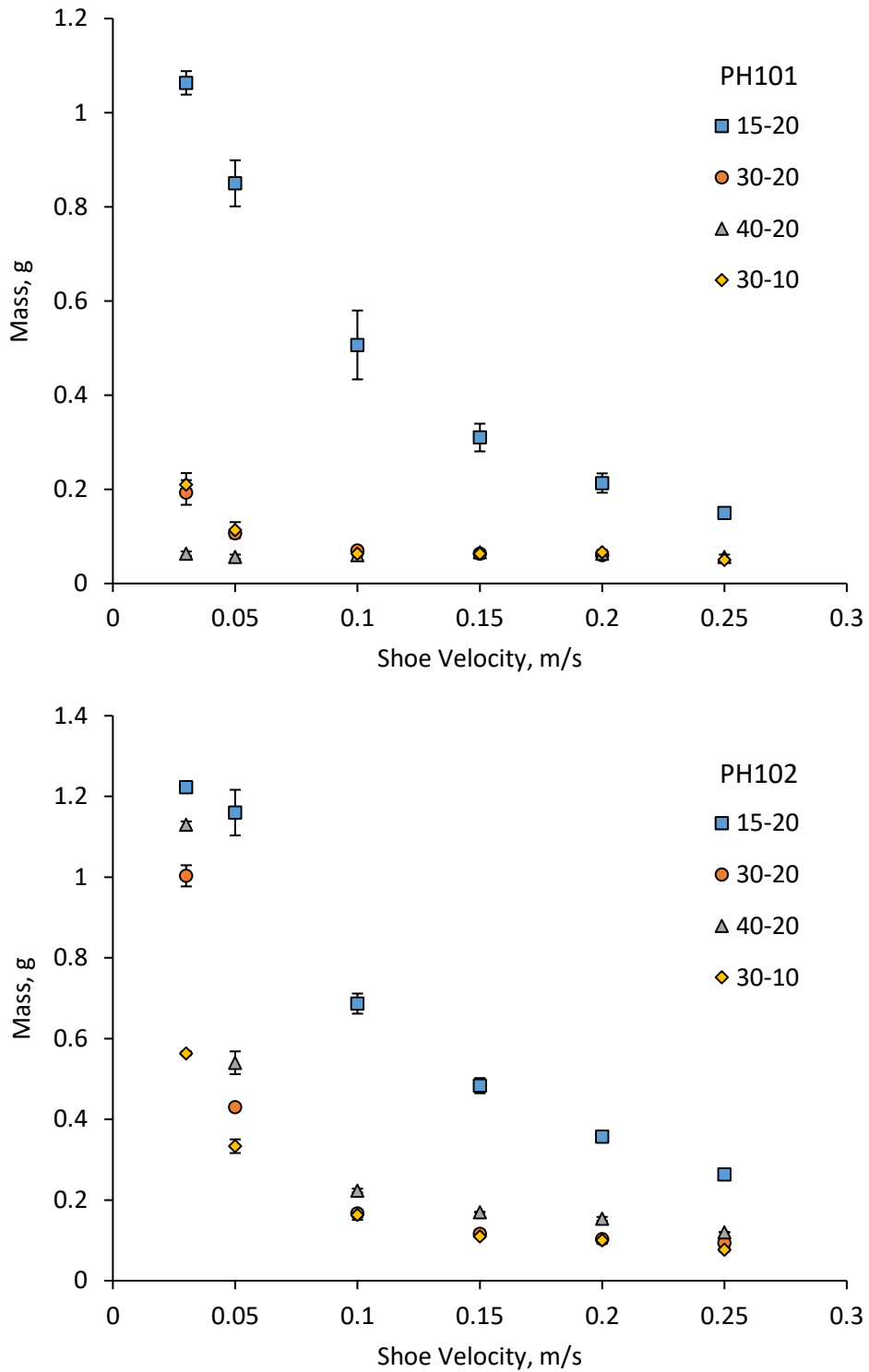


Figure 7-3. Mass of the powder introduced into the die for vs. shoe velocity for PH101 and PH102 using different processing conditions. In the legends, the first number is the powder height in the shoe and the second value is the height of the die.

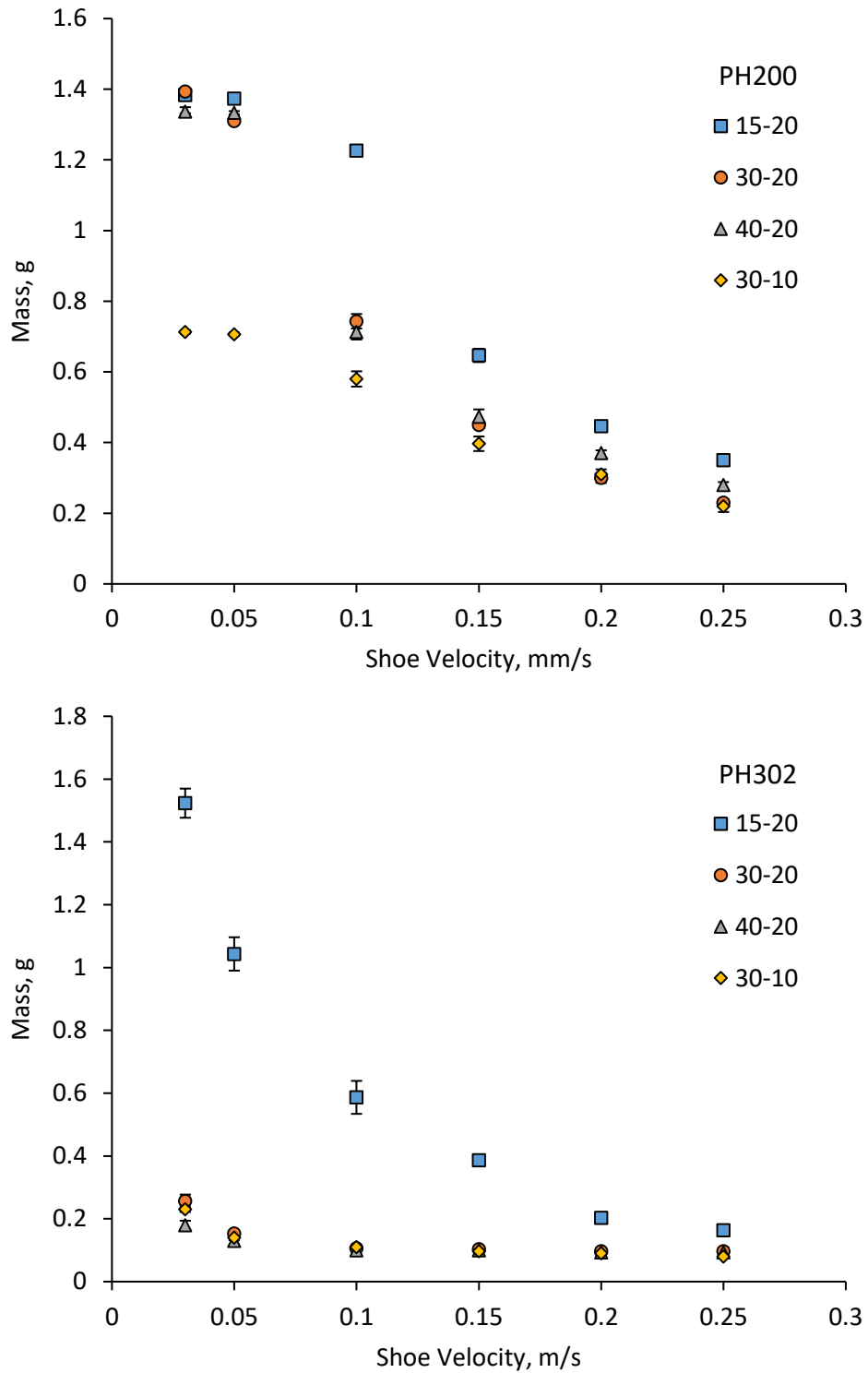


Figure 7-4. Mass of the powder introduced into the die for vs. shoe velocity for PH200 and PH302 using different processing conditions. In the legends, the first number is the powder height in the shoe and the second value is the height of the die.

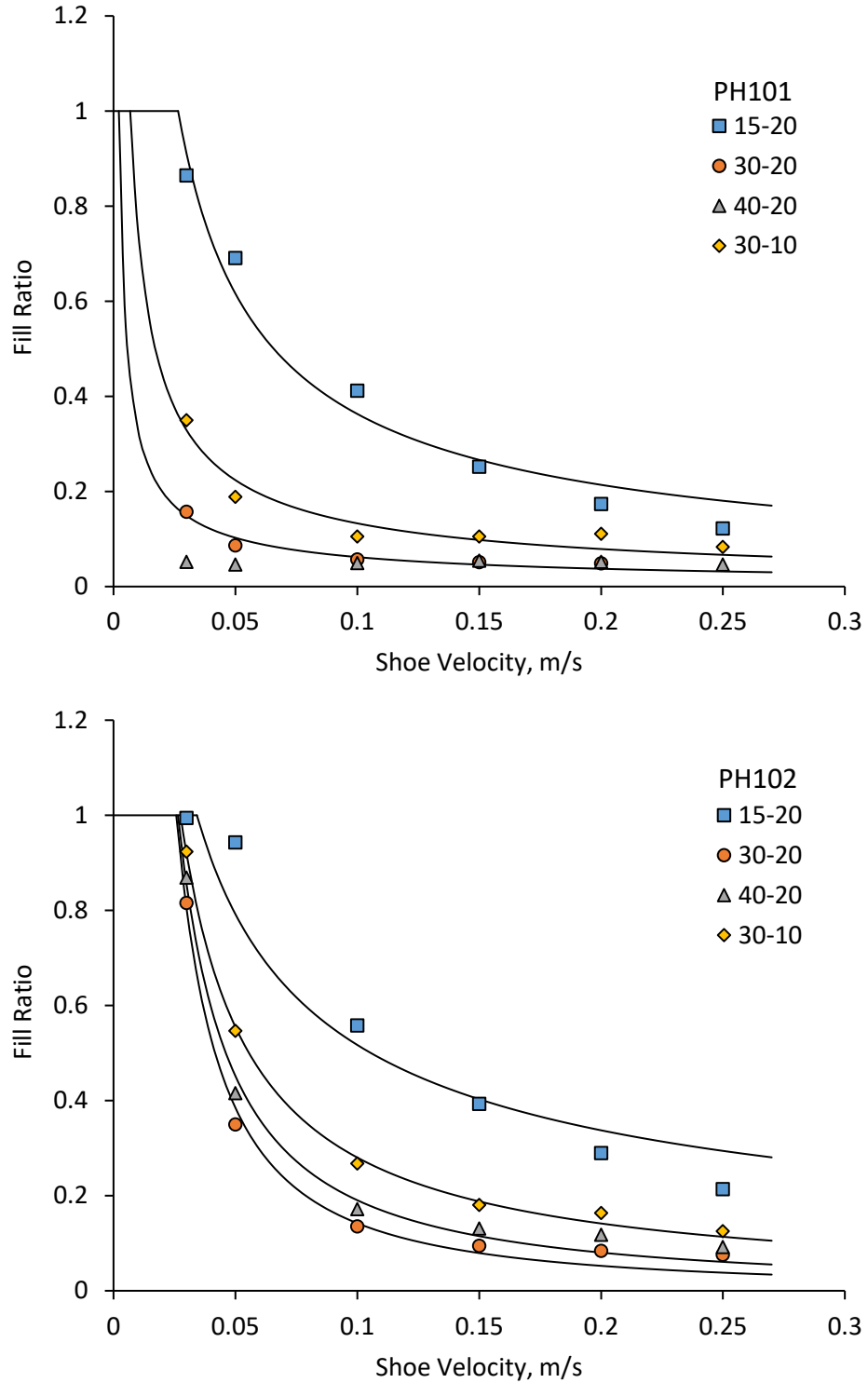


Figure 7-5. Fill ratio of the powder in the die vs. shoe velocity for PH101 and PH102 using different processing conditions. In the legends, the first number is the powder height in the shoe and the second value is the height of the die.

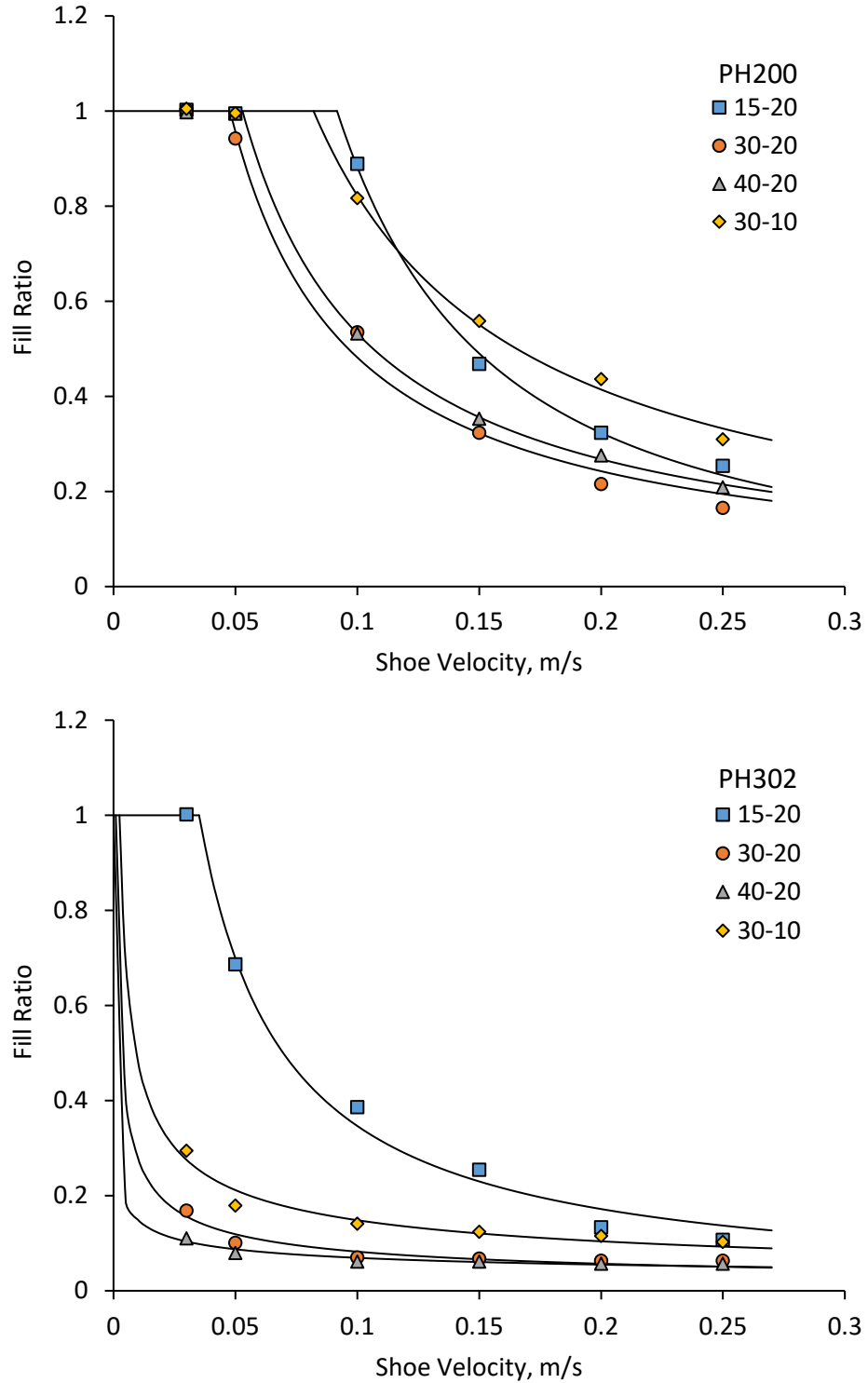


Figure 7-6. Fill ratio of the powder in the die vs. shoe velocity for PH200 and PH302 using different processing conditions. In the legends, the first number is the powder height in the shoe and the second value is the height of the die.

Table 7-1. The values of $1 + n$ and v_c calculated from fitting the experimental data to Equation (7-1).

Materials	15 - 20		30 - 20		40 - 20		30 - 10	
	v_c , mm/s	$1 + n$						
PH101	26	0.763	2	0.727	-	-	7	0.752
PH102	34	0.615	26	1.437	26	1.246	28	0.985
PH200	92	1.449	48	0.990	53	0.991	82	0.989
PH302	35	1.012	1	0.532	0	0.334	2	0.513

7.3.2. Measurement of differential pressure in the die

The changes in the differential pressure between the die and the ambient atmosphere was logged for the experiments carried out. The differential pressure profile for the four grades of MCC were similar to each other. The selected graphs are presented in Figure 7-7. The pressure inside the die increased sharply as the mass delivery initiated. This pressure then dissipated through the powder bed and the clearances in the system during the delivery period before going back to zero as the shoe passed over the die completely. At some stage during the delivery process, there will be a balance between pressure dissipation and pressure build up (due to further introduction of powder mass) and the pressure remained nearly constant. This is more evident for PH101 under the shoe velocity of 50 mm/s. At higher shoe velocities, the delivery period is shorter and this effect is not significant.

For PH102, when the shoe velocity was set to 30 mm/s, the differential pressure profile was different from the rest of the experiments carried out. For this test, the pressure increased gradually to the maximum value. For higher shoe velocities, the differential pressure profiles observed for PH102 were similar to the other grades of MCC (Figure 7-8).

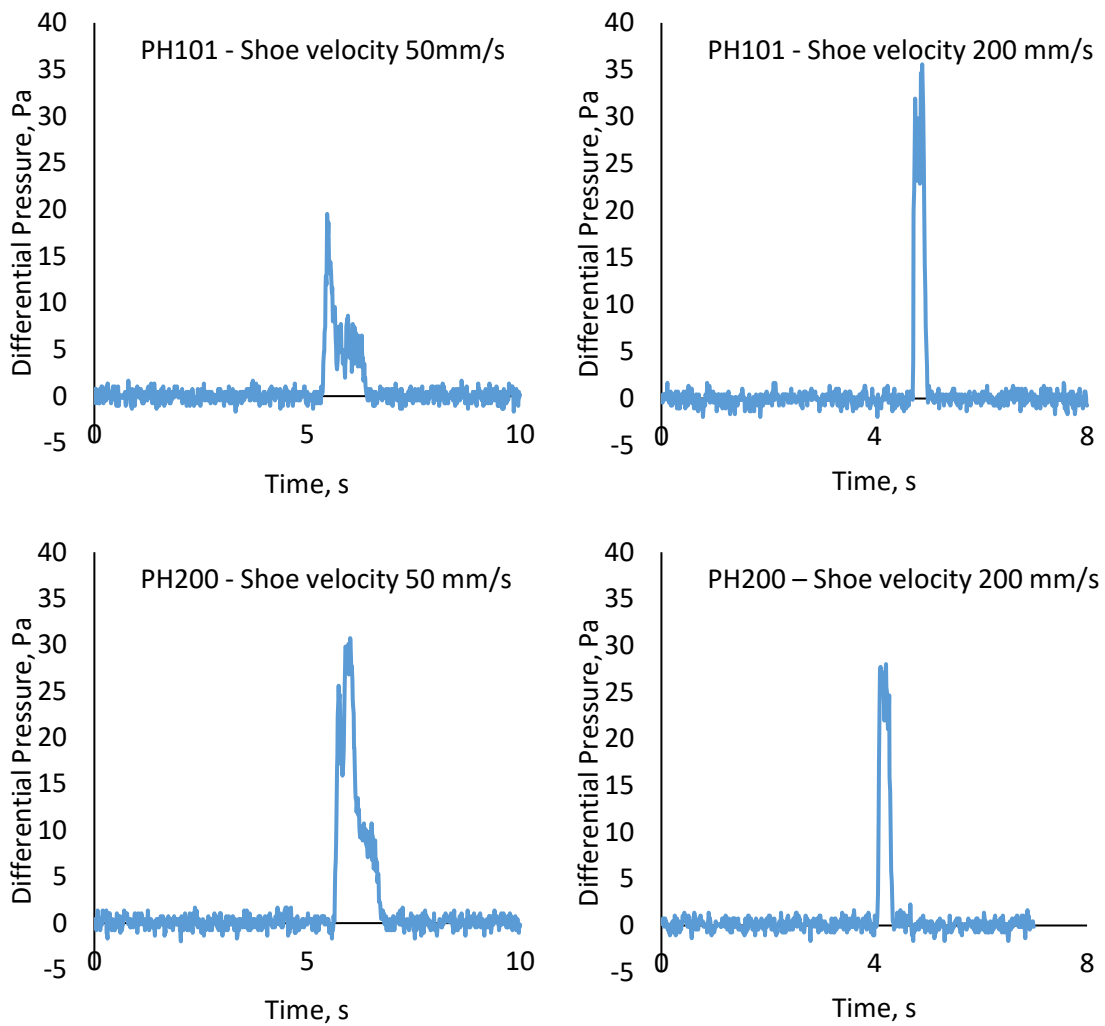


Figure 7-7. Differential pressure profile measured during the delivery period for PH101 and PH200 under shoe velocities of 50 and 200 mm/s.

The average differential pressure between the die and the ambient atmosphere measured for four grades of MCC are presented in Table 7-2 and are plotted against shoe velocity in Figure 7-9 and Figure 7-10. The values of the differential pressures presented in the figures are the maximum values reached during the delivery period. The two numbers in the legends describe the powder height in the shoe and the height of the die in mm respectively. The air pressure effects are not similar for all the materials used. For PH101 and PH302 the differential pressure is increased significantly by the shoe velocity while for PH200 the increase in pressure is less significant especially at high shoe velocities.

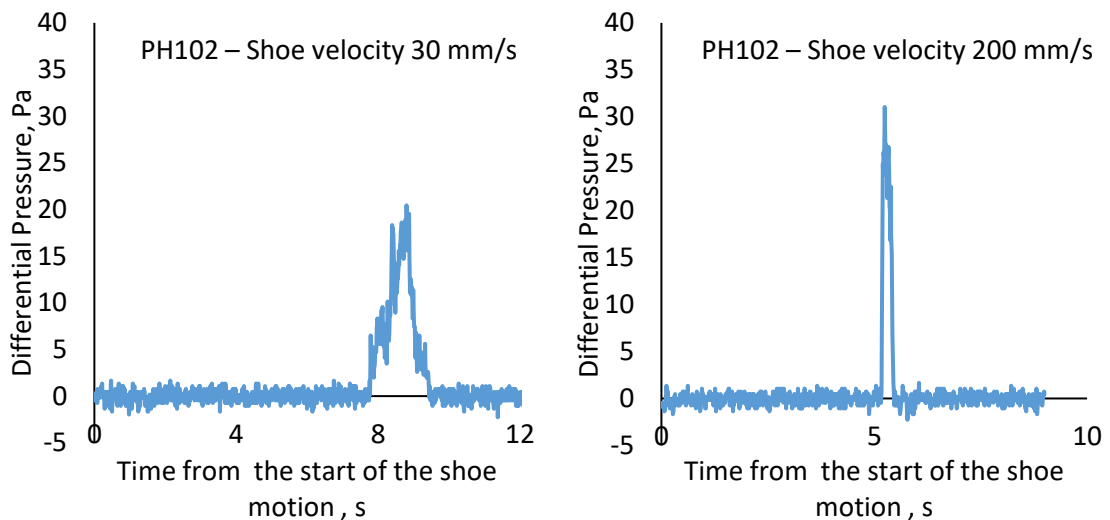


Figure 7-8. Differential pressure profile measured during the delivery period for PH102 under shoe velocities of 30 and 50 mm/s

The differential pressure is a function of several distinct parameters some of which are coupled with each other. As powder is introduced, the volume of the air inside the die is decreased which result in an increase in the pressure. The air pressure build up opposes further flow of powder. Also, it is shown in Figure 7-9 and Figure 7-10 that for high shoe velocities where the mass of the powder delivered into the die is nearly constant, the differential pressure increases with shoe velocity.

The pressurised air can escape through 1) the powder inside the shoe, and 2) the clearances in the system. For materials with smaller permeability it is more difficult for air to escape through the bed and the pressure is mainly dissipated through the clearances. When the powder height in the shoe is larger, the lower levels of the bed are packed denser due to self-weight of the material and initial shaking of the shoe, which result in reduction of permeability and air flow through the powder bed.

Table 7-2. The differential pressures between the die and ambient atmosphere measured for four grades of MCC under different processing parameters.

Test	Shoe Velocity, m/s	Differential Pressure, Pa			
		PH101	PH102	PH200	PH302
15-20	0.03	9	7	8	17
	0.05	13	11	12	25
	0.1	21	21	23	30
	0.15	22	22	27	41
	0.2	28	26	32	41
	0.25	25	26	31	42
30-20	0.03	11	19	24	15
	0.05	18	16	31	21
	0.1	22	20	30	32
	0.15	26	25	28	51
	0.2	35	26	28	55
	0.25	35	34	27	56
30-10	0.03	8	18	15	13
	0.05	14	17	22	22
	0.1	21	18	24	31
	0.15	29	29	26	42
	0.2	32	30	27	45
	0.25	30	29	25	52
40-20	0.03	10	6	9	5
	0.05	13	9	15	7
	0.1	19	17	21	12
	0.15	25	20	20	17
	0.2	26	21	23	20
	0.25	26	22	24	21

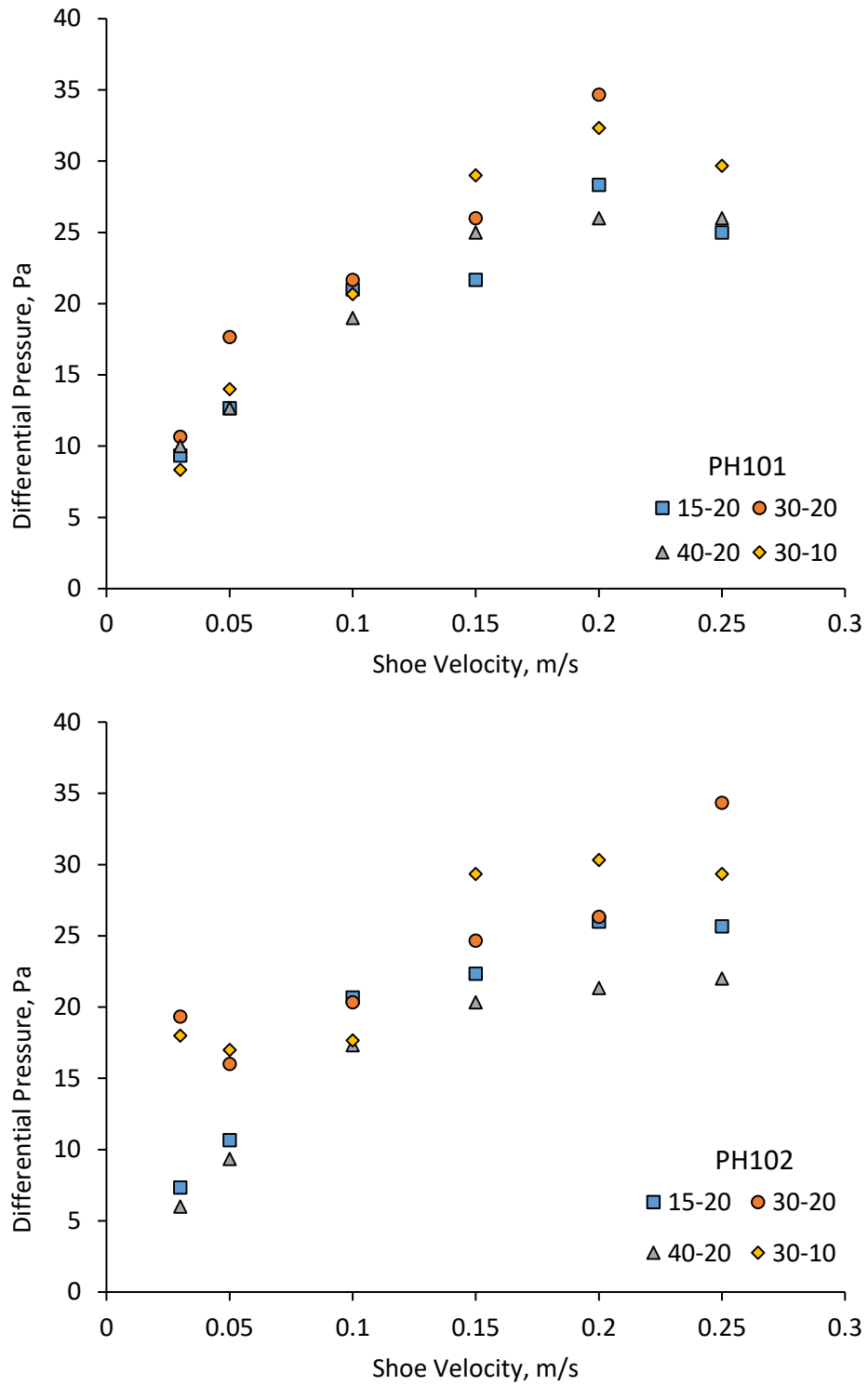


Figure 7-9. Differential pressure between the die and ambient atmosphere vs. shoe velocity for PH101 and PH102 under different processing conditions.

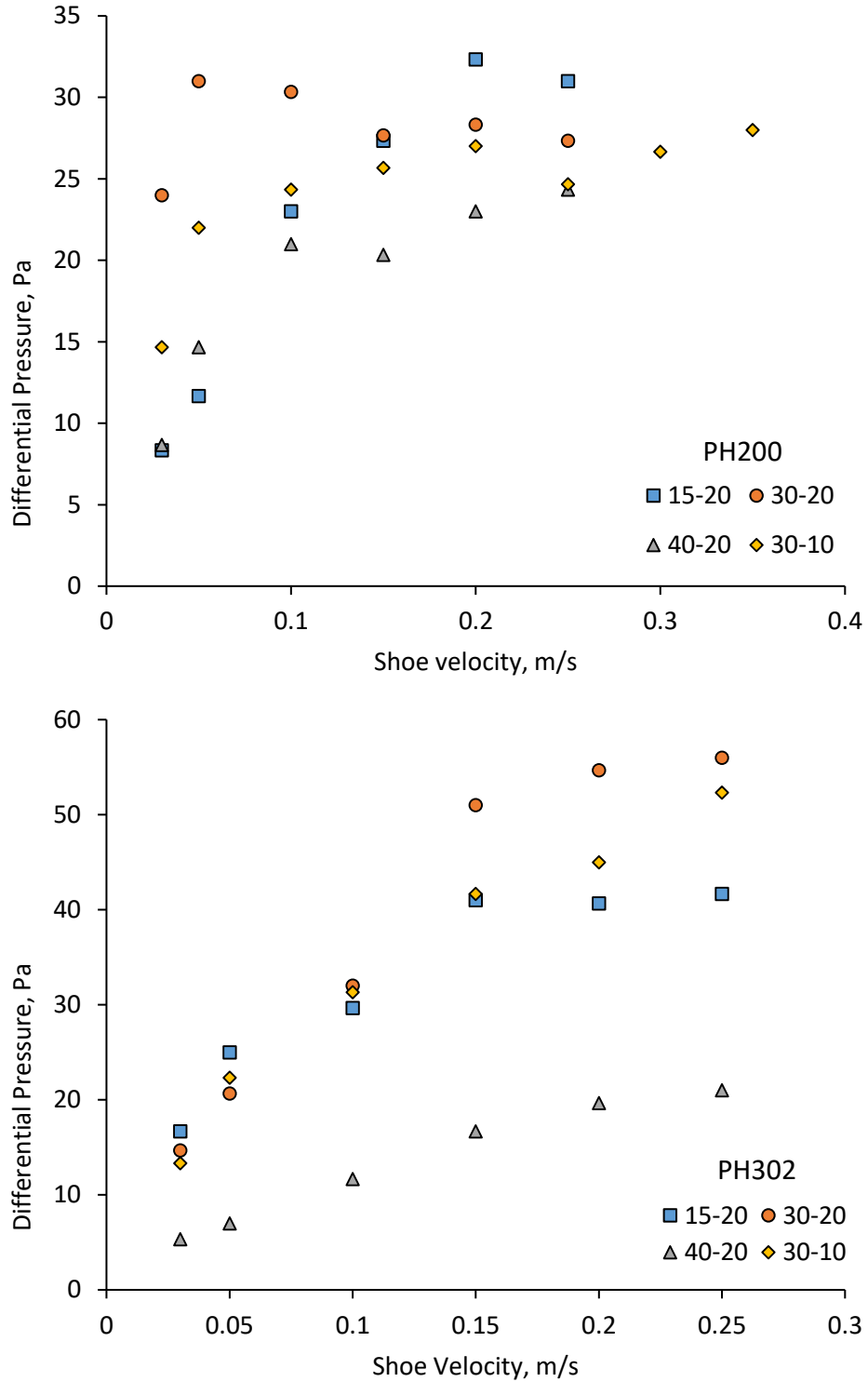


Figure 7-10. Differential pressure between the die and ambient atmosphere vs. shoe velocity for PH200 and PH302 under different processing conditions.

7.3.3. Existing model on prediction of the mass delivered

A dimensional model was developed by Schneider and co-workers (Schneider et al., 2007) to predict the mass of the powder delivered into the die as a function of shoe velocity (Equation (2-20)). This relation was developed from an assumed power law relation between mass flow rate and shoe velocity by considering a consistent mass flow rate into the die over the delivery period.

The experimental data were fitted to Equation (2-20) and the values of the coefficients were determined. The exponent $(1 + n)$ has the same value as those obtained from Equation (2-21). The coefficient c and the values of the exponent are presented in Table 7-3

Table 7-3. The values of c and $1 + n$ calculated from fitting the experimental data to Schneider model.

Materials	15 - 20		30 - 20		40 - 20		30 - 10	
	c	$1 + n$						
PH101	0.041	0.763	0.007	0.727	-	-	0.008	0.752
PH102	0.071	0.615	0.007	1.437	0.011	1.246	0.012	0.985
PH200	0.041	1.449	0.041	0.990	0.045	0.991	0.035	0.989
PH302	0.028	1.012	0.013	0.532	0.014	0.334	0.012	0.513

The model developed by Schneider was originally validated for the results measured in vacuum and gave good predictions of the mass delivered in the die. However, large scatter in the data was observed for the experiments carried out in air.

Here, it is shown that the values of the coefficients in the model not only depend on the properties of the powder but also they change for different processing parameters (i.e. powder height in the shoe). The model developed by Schneider does not incorporate the effect air pressure built up inside the die and the influence of the powder height in the shoe on densification of the particles and on powder permeability. To use this

relation, the coefficients have to be determined for each material and set of process conditions.

In developing Schneider's relation, it was assumed that the mass flow rate is consistent during powder delivery period. However, in the experiments carried out it was observed that most of the powder mass is introduced into the die at the early stages of delivery due to smaller packing density at the front of the heap formed in the shoe. Therefore, the delivery time is smaller than the values considered.

Schneider's model can give a good prediction of the mass flow rate (assuming that the mass flow rate is consistent during delivery period) for some of the experiments carried out over the range of velocities considered. For example, for PH302 with powder height of 40 mm and die height of 20 mm the theoretical mass flow rates calculated from Equation (2-20) are similar to the experimental values (Figure 7-11).

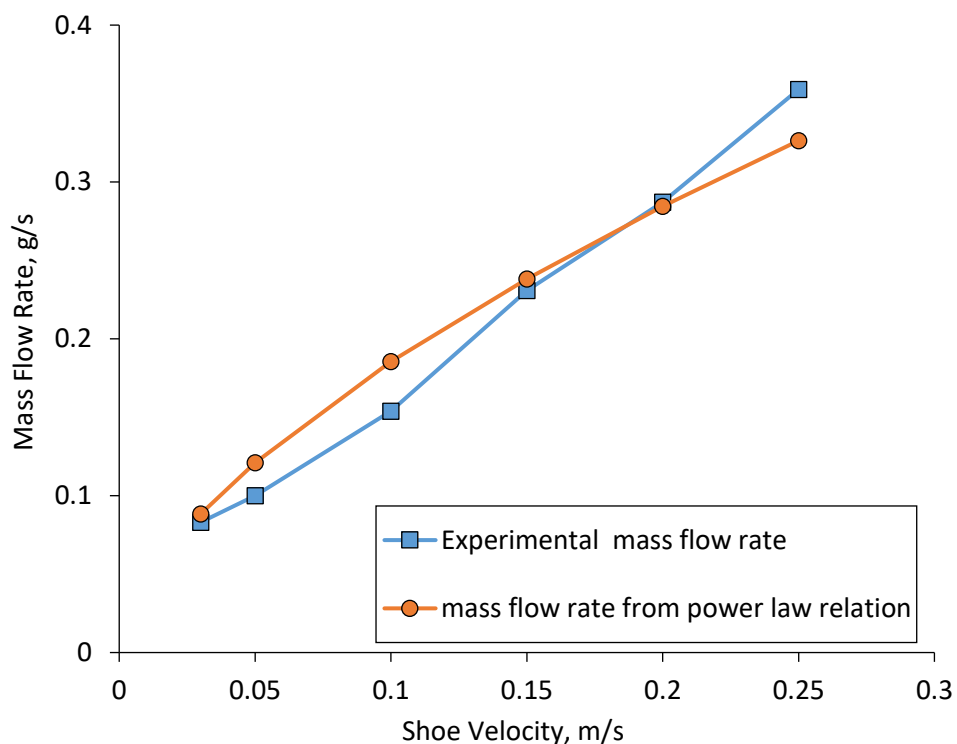


Figure 7-11. Mass flow rate of PH302 with powder height of 40 mm and die height of 20 mm measured and the theoretical flow rates calculated from the power law using the coefficients from fitting the experimental data to Equation (2-20).

The powder law relation proposed between the mass flow rate and the shoe velocity suggest that the mass flow rate always decreases by increasing the shoe velocity. However, as it was observed in Figure 7-3 and Figure 7-4, the mass of the powder does not change significantly prior to a specific shoe velocity and by taking the assumption above the reduction in delivery time exceeds the change in mass delivered resulting in an increase in the mass flow rate. For example, the mass flow rate calculated from the powder law relation using the coefficients presented in Table 7-3 and the experimental mass flow rates calculated from dividing the mass delivered by the delivery time (considering the mass flow rate is consistent) are compared for PH102 with powder height of 30 mm and die height of 20 mm in Figure 7-12. At low shoe velocities, the mass of the powder introduced reduces by increasing the velocity and therefore the mass flow rate of the powder reduces. At high shoe velocities, the reduction in the mass delivered is minimal and it remains nearly constant. As the delivery time reduces with increasing the velocity the mass flow rate increases. To calculate the mass flow rate of the powder, the delivery time should be determined accurately.

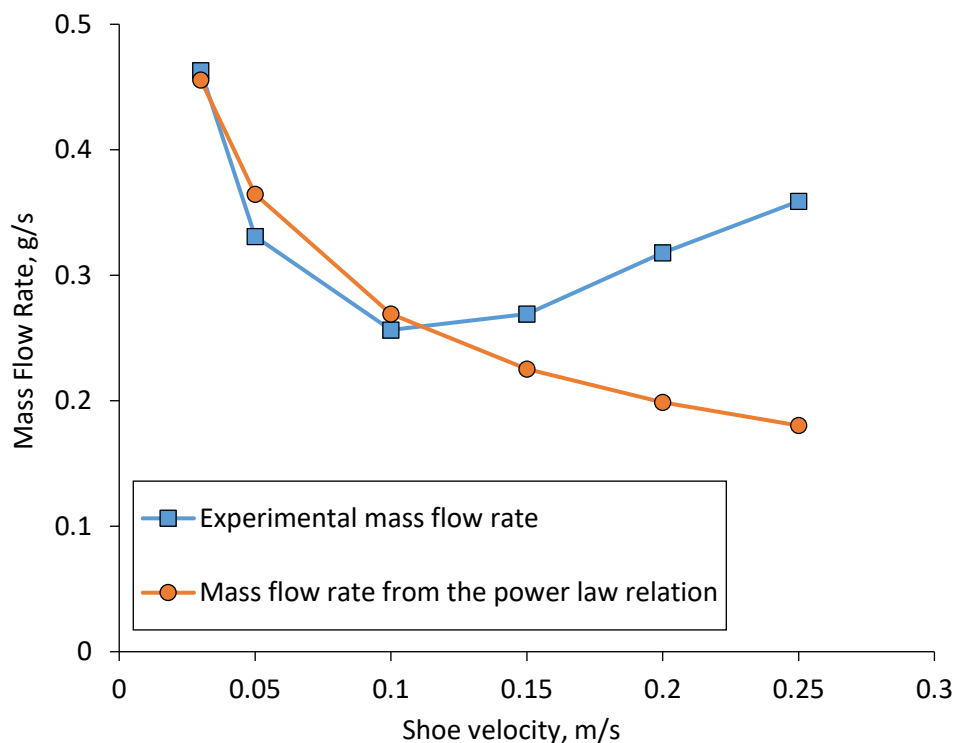


Figure 7-12. Mass flow rate of PH102 with powder height of 30 mm and die height of 20 mm measured and the theoretical flow rates calculated from the power law using the coefficients from fitting the experimental data to Equation (2-20).

In the next section, the model developed by Schneider (Schneider et al., 2007) is modified to include the powder height in the shoe and the differential pressure in the die to isolate the effect of these parameters on powder flow and find coefficients that only depend on material properties.

7.3.4. Modification of the model developed by Schneider

In order to use the model developed by Schneider (Schneider et al., 2007) and predict the mass of the powder delivered into the die as a function of shoe velocity, the values of the coefficients c and n should be determined experimentally. However, it was shown in Section 7.3.3 that for the experiments carried out in air the coefficients change for each material under different processing conditions. Therefore, for each set of processing parameters, these coefficients have to be calibrated for the material in order to give a correct prediction of the mass.

As mentioned in the previous section, in developing Schneider's model it was assumed that the mass flow rate into the die was consistent during delivery period and the power law relation proposed between the dimensionless mass flow rate in gravity fill mechanism (\overline{m}_g) and dimensionless shoe velocity (\overline{v}_s) π groups was expressed in terms of the mass delivered into the die (m_g).

$$\frac{m_g}{\rho_b D^2 L} = c \left(\frac{v_s}{\sqrt{gD}} \right)^{-(1+n)} \quad (7-2)$$

Here, this model is modified to include the powder height (H) and the differential pressure between the die and ambient atmosphere developed in gravity fill mechanism (ΔP). Other parameters that are involved in this process are: viscosity of air (μ), coefficient of friction between particles (μ_p) and between particles and the wall (μ_{pw}), powder permeability (k), shape of the particles, adhesion between the particles and clearances in the system. Using the same independent parameters taken in the dimensional analysis carried out by Schneider (bulk density (ρ_b), acceleration due to gravity (g) and the width of the die (D)) the dimensionless groups of \overline{H} and $\overline{\Delta P}$ were formed as

$$\bar{H} = \frac{H}{D} \quad (7-3)$$

and

$$\overline{\Delta P_g} = \frac{\Delta P_g}{\rho_b g D} \quad (7-4)$$

Therefore, it can be written that

$$\overline{m_g} = f(\bar{v}_s, \bar{H}, \overline{\Delta P_g}, \mu, \mu_p, \mu_{pw}, k, \text{shape, adhesion, clearances}) \quad (7-5)$$

where \overline{m} and \bar{v}_s are

$$\overline{m_g} = \frac{m_g}{\rho_b D^2 L} \quad (7-6)$$

and

$$\bar{v}_s = \frac{v_s}{\sqrt{gD}} \quad (7-7)$$

Based on the experimental results, it is observed that similar to shoe velocity the mass delivered into the die is inversely proportional to the differential pressure. A relation is proposed between the π groups in the form of Equation (2-21) where \bar{v}_s and $\overline{\Delta P}$ are multiplied and formed a new dimensionless group. The experimental results were fitted to this relation and the values of the coefficients where determined for each material (Table 7-4).

$$\frac{m_g}{\rho_b D^2 L} = c_g \left(\frac{H}{D} \right)^{a_g} \left(\frac{v_s \Delta P_g}{\rho_b g^{1.5} D^{1.5}} \right)^{n_g} \quad (7-8)$$

Table 7-4. The values of the coefficients c_g , a_g and n_g calculated from fitting the experimental data to Equation (2-21).

Material	c_g	a_g	n_g	R^2
PH101	0.047	-2.446	-0.485	0.97
PH102	0.037	-0.970	-0.651	0.88
PH200	0.043	-0.697	-0.911	0.92
PH302	0.040	-3.043	-0.673	0.98

The fitting was carried out only for the experimental results with fill ratios of less than one. For PH200 under different processing conditions and for PH302 with powder height of 15 mm and die height of 20 mm, the fill ratio of one or two of the shoe velocities was recorded as one and the curve fitting could not be carried out accurately using the remaining data points. For these experiments, an additional data point was added with the velocity set to the critical velocity presented in Table 7-1 while the mass of the powder in the die was considered as the mass of full die. For these data points, the values of differential pressure were estimated from the nearby results.

The values of the coefficients obtained from fitting the results to Equation (2-21) was used to calculate the theoretical mass delivered into the die. The theoretical values obtained are compared with the experimental measurements in Figure 7-13. It is shown that the model can predict the mass with sufficient accuracy.

The scatter in the data presented in Figure 7-13 is caused by errors in differential pressure measurement which is highly influenced by the initial condition of the powder in the shoe.

Unlike the model developed by Schneider (Schneider et al., 2007), it is shown that fixed coefficients can be used for each material under different processing conditions and it would not be required to calibrate the model for different powder heights in the shoe. It is also shown that the values of c_g calculated for different grades of MCC are similar to each other. This suggest that in Equation (2-21) the coefficient c_g is independent of

the material properties. Equally good fits (in terms of coefficient of determination, R^2) can be obtained by using the average $c_g = 0.042$. The values of a_g and n_g calculated from fitting the experimental results to the relation with $c_g = 0.042$ are presented in Table 7-5 and the theoretical masses predicted are compared with the experimental values in Figure 7-14.

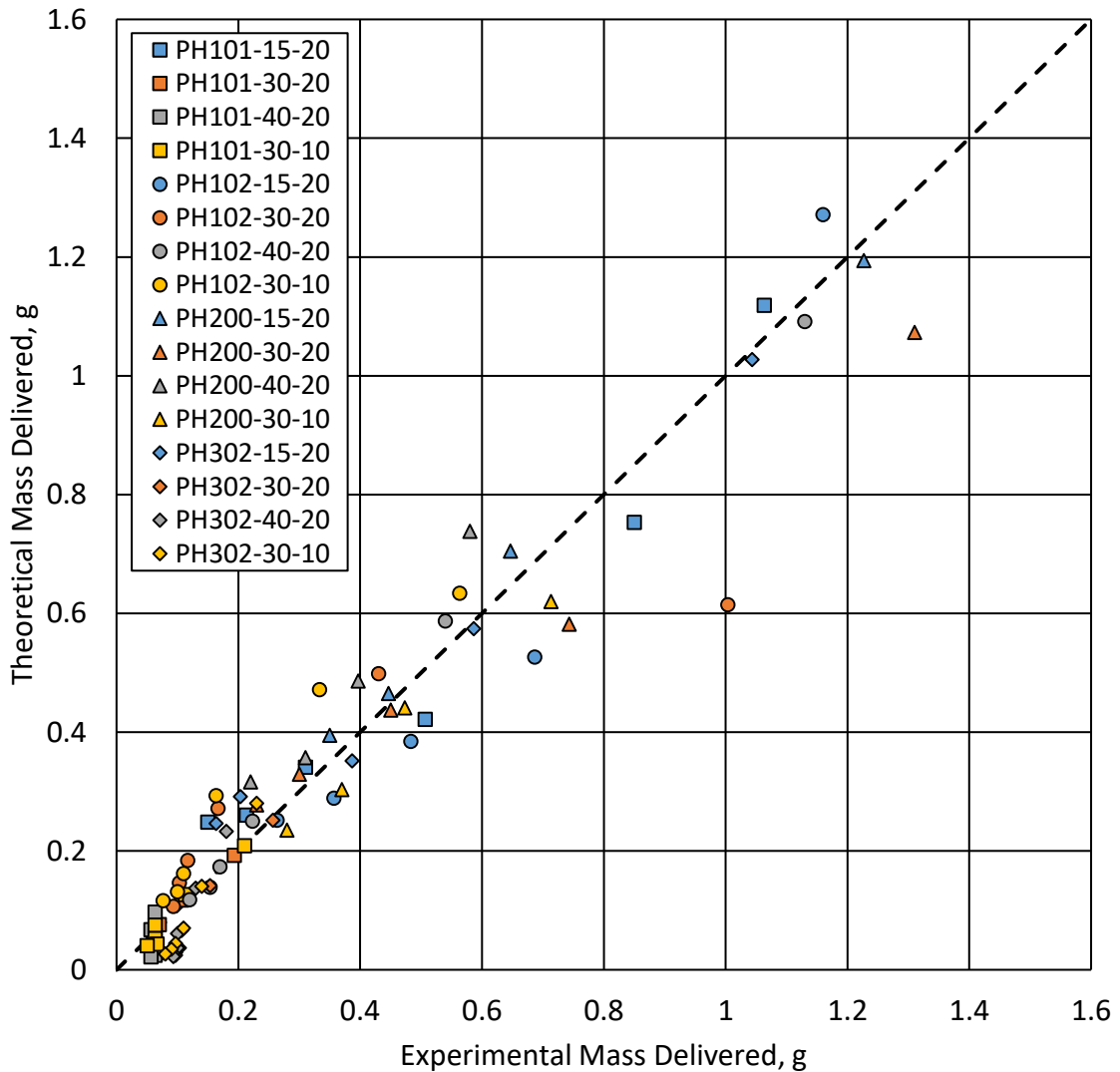


Figure 7-13. Experimental mass delivered into the die vs. the theoretical values calculated from Equation (2-21) for four grades of MCC.

Table 7-5. The values of coefficients calculated from fitting experimental data to Equation (2-21) with $c_g = 0.042$.

Material	c_g	a_g	n_g	R^2
PH101	0.042	-2.415	-0.514	0.97
PH102	0.042	-0.973	-0.618	0.88
PH200	0.042	-0.700	-0.925	0.92
PH302	0.042	-3.029	-0.659	0.98

Comparison of the coefficients obtained (Table 7-5) shows that the influence of powder height on the mass delivered is larger for powders with smaller powder permeability. Based on the results presented in Figure 4-5, the value of the coefficient, a_g , calculated for PH302 with lowest permeability is the smallest and it increases for PH101, PH102 and PH200 respectively. Also, the exponent n_g is changing inversely with average particle size. PH101 with smallest average particle size (50 μm) has the highest n_g while the coefficient calculated for PH200 with average particle size of 180 μm is the smallest. For PH302 and PH102 with similar average particle size, the values calculated for the coefficient are very similar.

In order to use the model developed (Equation (2-21)), the coefficients should be determined experimentally for the desired material. Also, the differential pressure developed in the die must be measured for the powder in use under the specific velocity to predict the mass introduced. The magnitude of the differential pressure depends on the permeability of the powder and the clearances in the system. In the absence of data, the differential pressure in the die should be estimated based on the material and the system in use. In future, the model can be modified to include powder permeability and other parameters affecting the process in the model to use it without the need of experimentation.

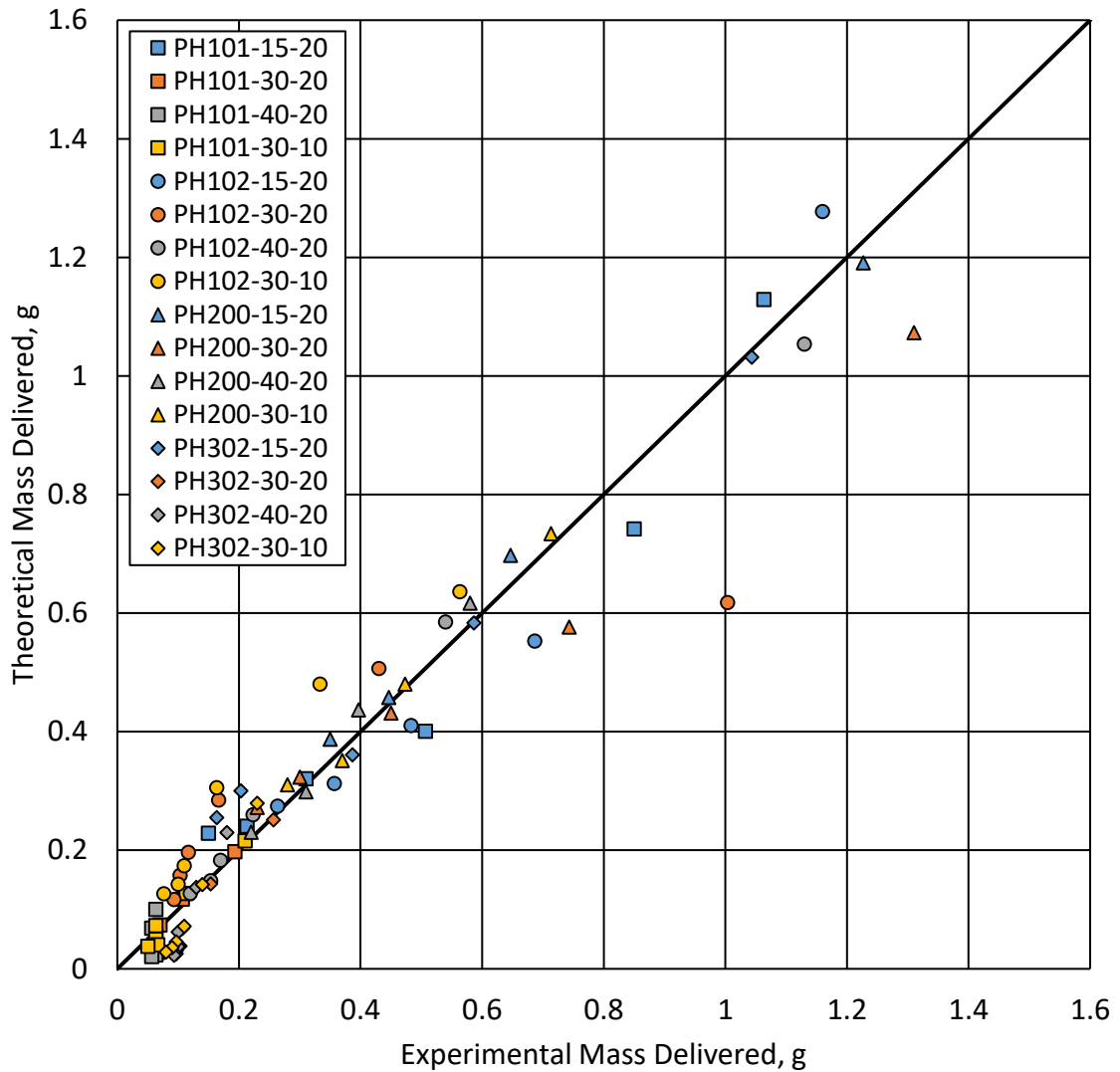


Figure 7-14. Experimental mass delivered into the die vs. the theoretical values calculated from Equation (2-21) with $c_g = 0.042$ for four grades of MCC.

7.4. Conclusion

The mass of the powder delivered into the die reduces by increasing the shoe velocity and the powder mass introduced is inversely proportional to the height of the powder in the shoe. It is also shown that the mass of the powder introduced is independent of the height of the die. The comparison of the results in terms of the fill ratio should be made with caution as different fill ratios are obtained by changing the height of the die (due to different mass of the full die) while the mass delivered in both cases might be similar.

Powders ranked as good flowing based on the critical orifice diameter measurement and the angle of repose experiments have larger critical velocity showing improved flow behaviour in the linear shoe-die system.

The differential pressure (between the die and ambient atmosphere) is influenced by a range of parameters involved in the process. As the powder is introduced into the die, the differential pressure increases as the volume that can be occupied by air is decreased. The increasing differential pressure, inhibits further flow of material. The differential pressure is also influenced by the height of the powder in the shoe as more powder results in densification of the particles and inability of air to escape from the die.

A dimensional model developed to predict the mass of the powder discharged into the die as a function of shoe velocity was examined for the experiments carried out. The model includes two empirical constants. It was shown that the values of the coefficients change for each material under different processing conditions.

The dimensional model was modified to include the height of the powder in the shoe and the differential mode. The new model was examined for the materials and it was observed that the mass of the powder introduced into the die can be predicted with sufficient accuracy. There are three empirical coefficients (c_g , a_g and n_g) included in the model developed. The value of c_g was found to be fixed for the range of powders used and the values of a_g and n_g were found to be changing with powder permeability and the average particle size respectively.

The coefficients can be determined for the desired material using simple experiments. The differential pressure in the die should also be determined to use the model. In the absence of necessary data, the differential pressure can be estimated based on the permeability of the material and the clearances in the system.

Chapter 8. Linear shoe-die system under suction fill mechanism

In this chapter, the system described in Section 7.1 was used to study powder mass flow rate in suction fill mechanism. The mass of four grades of MCC delivered into the die was measured for a range of shoe and suction velocities. The suction mechanism was achieved by lowering the punch as the shoe was passing over the die. The pressure inside the die was measured at two different locations. The results obtained were compared to identify the influence of shoe and suction velocity on the mass of the powder delivered. A dimensional model was developed to predict the mass introduced into the die during suction fill mechanism as a function of shoe velocity, suction velocity and the differential pressure between the die and open atmosphere.

8.1. Procedure

The powder was introduced into the shoe (65×31×38 mm) presented in Figure 7-1 and an L-shaped rod was used to level the top layer of the powder and set the height to 15 mm. The powder was preconditioned by moving the shoe in a back and forth motion (± 5 mm) to ensure consistent and repeatable initial state of the material inside the shoe. The punch was adjusted to cover the opening of the die completely. The shoe travelled over the die with a specific velocity (100, 200 or 300 mm/s) and the punch was lowered with a set velocity (100 - 300 mm/s) precisely when the die opening was fully covered by the front of the powder bed. The velocity profiles of the motion of the shoe and the punch are similar to the profile presented in Figure 7-2. After the shoe passed the die opening completely, the punch was raised to eject the powder and the mass delivered was measured using a Mettler Toledo PL83-S scale. The differential pressure between the die and ambient atmosphere was measured using two Sensirion SDP1000-L transducers. The first transducer measured the pressure at the opening of the die and the second one measured the differential pressure at the bottom of the die (through the small hole in the punch). The pressures measured were logged using a National Instruments data acquisition device (NI USB-6221) and the NI LabVIEW PC software. This procedure was repeated three times for each suction velocity under the three shoe speeds using the four grades of MCC described in Section 3.1.1.

8.2. Results and discussions

8.2.1. Measurement of the mass delivered into the die

In developing the procedure, the minimum suction velocity was selected based on the shoe velocities chosen to ensure that the suction time was smaller than the time in which the die was fully covered by the shoe (equal to the length of the die subtracted by the die opening). The mass of powder measured for four grades of MCC under different shoe and suction velocities are presented in Figure 8-1 and Figure 8-2. The error bars are generated using the standard deviation of the three repeat experiments.

Comparing the mass of four grades of MCC delivered into the die in suction fill with the results obtained in Chapter 7, shows that the suction fill increases the efficiency of the process significantly. It was observed that the mass of the powder delivered into the die under gravity fill mechanism decreases by increasing the shoe velocity. However, it is shown in the figures that under suction fill mechanism, the influence of shoe velocity on the mass delivered changes based on the suction velocity. The extent of these effects varies for different materials.

In Figure 8-1, it is shown that for PH101 with shoe velocity of 100 mm/s, the mass of the powder initially increased with increasing the suction velocity and decreased when the suction velocity was increased further. For the shoe velocity of 200 mm/s there was no increase in the mass delivered for the range of suction velocities considered and the mass decreased continuously with suction velocity. When the shoe velocity was set to 300 mm/s although the mass of the powder introduced into the die using suction velocity of 100 mm/s was smaller than the mass delivered for shoe velocities of 100 and 200 mm/s with similar suction velocity, increasing the suction velocity resulted in a large increase in the mass delivered such that at suction velocity of 200 mm/s the mass of the powder introduced exceeded the mass delivered for shoe velocities of 100 and 200 mm/s under the same suction velocity. Similar observations in terms of the influence of shoe and suction velocity on the mass of the powder delivered were made for PH102 and PH302.

For PH200, when the shoe velocity was set to 100 mm/s, the die was completely filled with powder under the suction velocity of 100 mm/s and increasing the suction velocity

further had no effect (Figure 8-2). For shoe velocity of 200 mm/s minor changes in the mass introduced was observed. Increasing the suction velocity had a larger influence on the mass delivered when the shoe velocity was set to 300 mm/s. At this shoe velocity, the mass of the powder increased with suction velocity up to 150 mm/s before reducing for higher suction velocities. The increase in the mass delivered is not as significant as the increase observed for other grades of MCC and the mass couldn't reach the same values as the mass introduced for lower shoe velocities (100 and 200 mm/s).

8.2.1. Remarks on suction fill

In gravity fill mechanism, the mass of the powder deposited into the die tends to reach a constant value by increasing the shoe velocity. This means that the mass flow rate of powder delivered from the shoe into the die would increase.

In suction fill the flow rate is dependent not only on the suction velocity but also on the shoe velocity. The shoe can be considered as providing the supply and suction velocity is considered as a demand or driving force. For a specific supply level, increasing demand results in larger mass of the powder delivered into the die. This is observed for the three grades of MCC, PH101, PH102 and PH302 under the shoe velocity of 300 mm/s (Figure 8-1 and Figure 8-2). This suggests that increasing suction velocity results in increased mass flow rate. This is not always the case, but only when the "supply" or shoe velocity is sufficiently high. In other words, for a given shoe velocity, there exist an optimum suction velocity at which the mass of the powder introduced is the largest and the reduction in the mass delivered at suction velocities above the optimum value is due to the reduction in the mass of the powder available above the die opening to be sucked into the die during the suction fill period.

In the study carried out by Mills and Sinka (Mills and Sinka, 2013), they observed that the flowability rank order (based on the critical velocity) changed for the materials used. For the range of shoe and suction velocities considered, the mass of the powder deposited decreased for higher shoe velocities which allowed for the determination of the critical velocity. However, in Figure 8-1 and Figure 8-2 it is shown that the mass delivered at a high shoe velocity can exceed the mass introduced under smaller shoe velocities using the optimum suction velocity. Therefore, it would not be possible to

determine the critical velocity for suction fill mechanism using the relation proposed by Wu and co-workers (Wu et al., 2003) and the flowability ranking cannot be obtained.

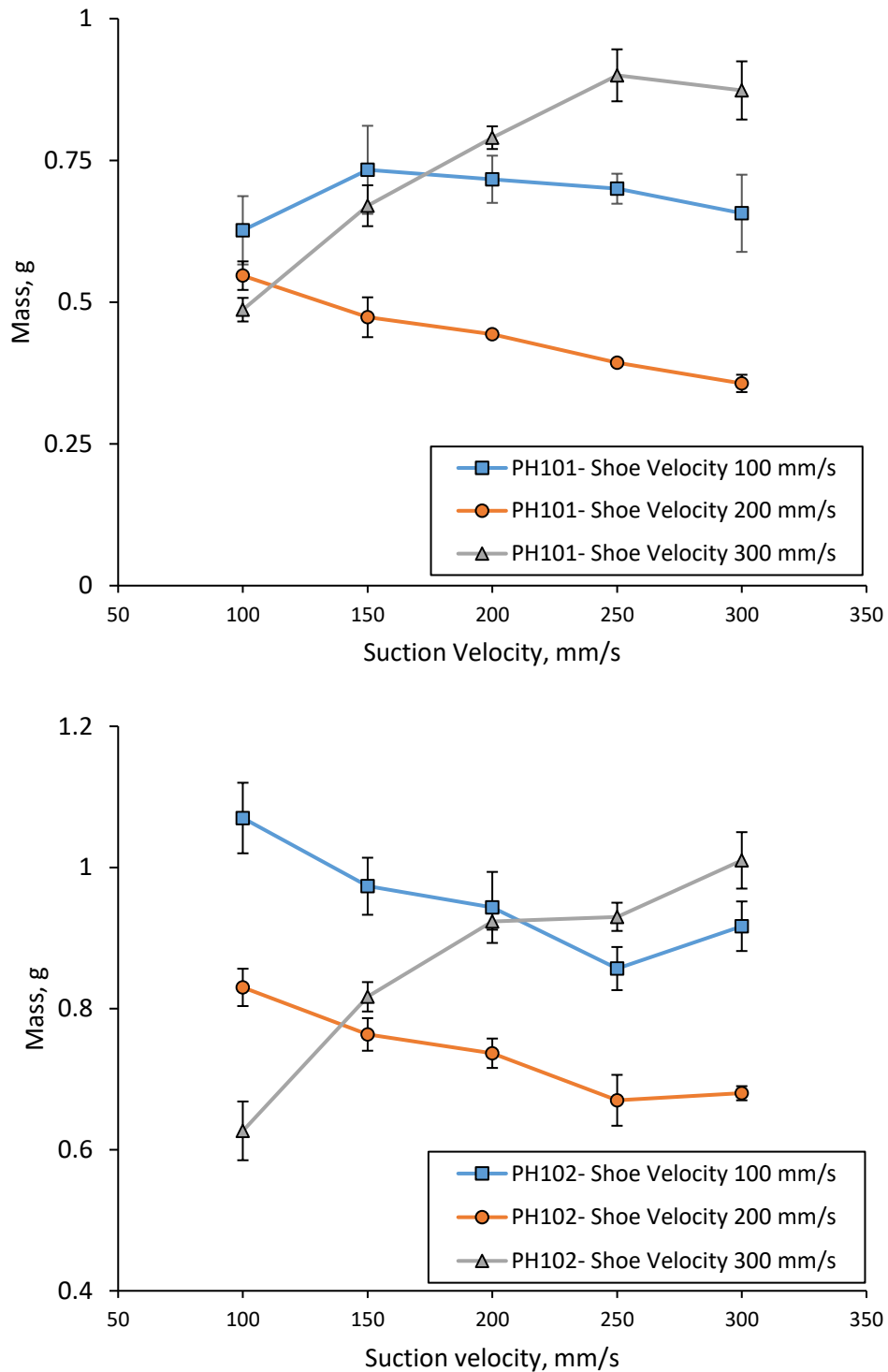


Figure 8-1. Mass of the powder delivered into the die in suction fill using different shoe velocities vs. suction velocity for PH101 and PH102.

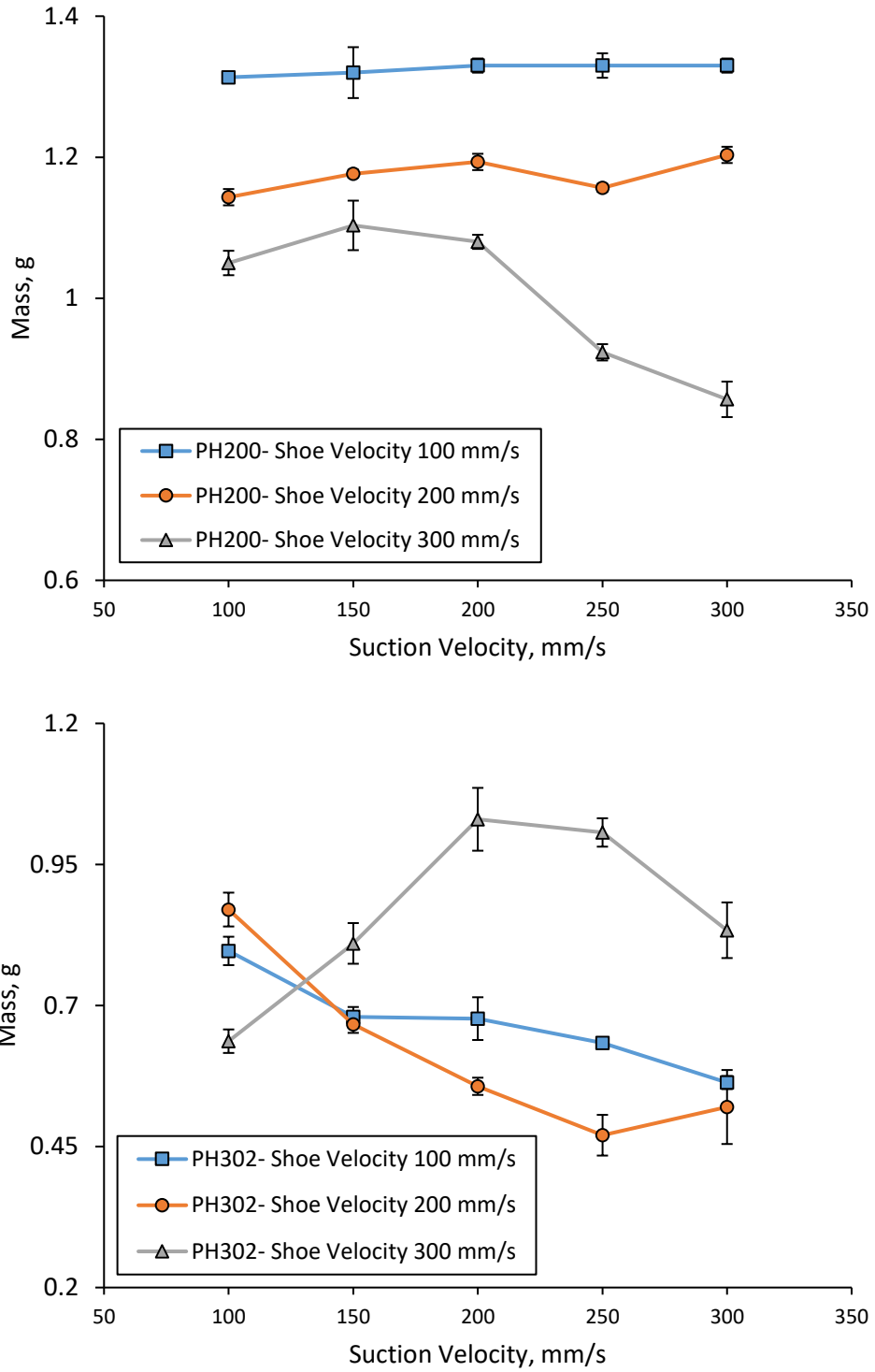


Figure 8-2. Mass of the powder delivered into the die in suction fill using different shoe velocities vs. suction velocity for PH200 and PH302.

8.2.2. Differential pressure measurement in the die

The changes in the differential pressure between the die and ambient atmosphere can be described by the schematic diagram presented in Figure 8-3. There are four important features on the differential pressure profile: 1) the total delivery time which depend on the shoe velocity and the length of the shoe, 2) the suction fill delivery time which is determined by the velocity of the punch in the die and height of the die, 3) the gravity fill delivery time which depends on the total delivery time and the suction fill delivery period, and 4) the magnitude of the differential pressure in suction and gravity fill mechanisms.

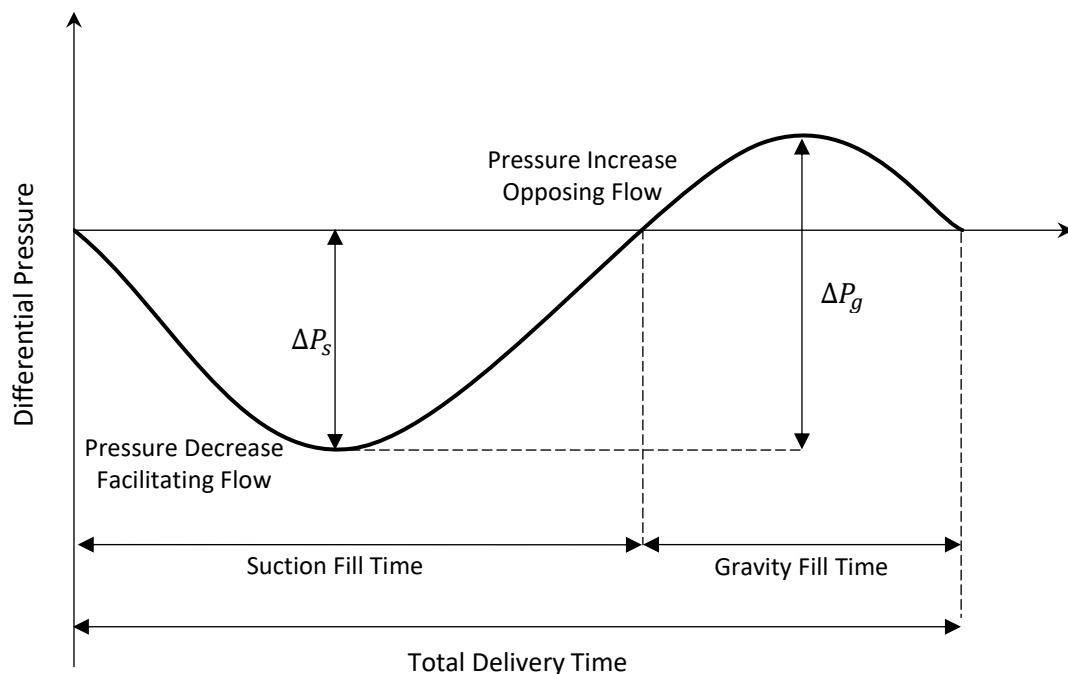


Figure 8-3. Schematic diagram of differential pressure changes between the die and ambient atmosphere during suction fill and gravity fill mechanisms.

Initially, the downward motion of the punch in the die creates a suction effect which reduces the pressure inside the die and results in a pressure gradient in the direction of the flow which facilitates powder flow into the die. Due to the inertial effect there exist a small delay between the downward motion of the punch and powder flow initiation. When the initial acceleration of the punch is finished and the punch velocity reaches the specified value, the motion of the punch continues with constant velocity before

decelerating to velocity of zero. During this period, the velocity of the particles are still increasing due to the initial acceleration while the punch moves with a constant velocity. The air that has entered the die through the powder bed and clearances in the system is therefore compressed between the particles and the punch; and although the suction fill period is not over yet, the pressure starts to increase. Increasing pressure in the die opposes further flow of powder. The pressure increase continues when the suction fill is over and powder material is discharged under gravity fill mechanism.

Selected pressure profiles for PH101 are presented in Figure 8-4 for reference. It is shown that the differential pressure reduces to the minimum value quickly when the suction fill mechanism starts. Using the velocity of the shoe and the height of the die, the suction full time can be calculated. For suction velocities of 100, 200 and 300 mm/s the suction times are 0.2, 0.1 and 0.067 seconds respectively (the actual times are somewhat longer due to acceleration and deceleration of the punch). It is observed that the pressure inside the die starts to rise before the suction period is over. For higher shoe velocities, the mass of the powder delivered to the die prior to the initial mass delivered under suction effect is smaller and the rise in the pressure is not as significant as the pressure increase for smaller shoe velocities (the mass delivered in gravity fill reduces for higher shoe velocities as demonstrated in Chapter 7). The magnitude of the minimum and maximum pressures reached changes for different shoe and suction velocities. Similar pressure profiles were observed for other materials.

The magnitude of the differential pressures developed between the die and ambient atmosphere depend on powder permeability, the clearances in the system, the mass of the powder introduced into the die and the shoe velocity. The influence of some of these parameters is coupled with each other. For powders with higher permeability, it is easier for air to enter the die during suction fill resulting in a smaller negative pressure gradient in the die and reduced suction effect. In gravity fill mechanism, as the air inside the die can escape through the powder bed, the inhibiting pressure is smaller and larger mass is delivered into the die.

The average differential pressures for the suction and gravity fill mechanisms are presented in Table 8-1 and are plotted against the suction velocity in Figure 8-5 and Figure 8-6. For suction fill, the differential pressure (ΔP_s) was taken as the minimum

pressure recorded in the profile. For gravity fill mechanism as the opposing pressure gradient is developed prior to the initial suction effect, the differential pressure (ΔP_g), was taken as the difference between the minimum and the maximum pressures recorded. These differential pressures are demonstrated in Figure 8-3.

In Figure 8-6, it is shown that for PH200 (with the highest powder permeability based on the results presented in Figure 4-5) the differential pressures measured for suction fill mechanism for different shoe velocities are similar to each other while for the other grades of MCC the differential pressures measured under the shoe velocity of 300 mm/s are significantly larger than the values recorded for lower shoe velocities. This explains why the mass of PH200 delivered into the die is not highly influenced by the suction effect. This has also been observed by Mills and Sinka previously (Mills and Sinka, 2013).

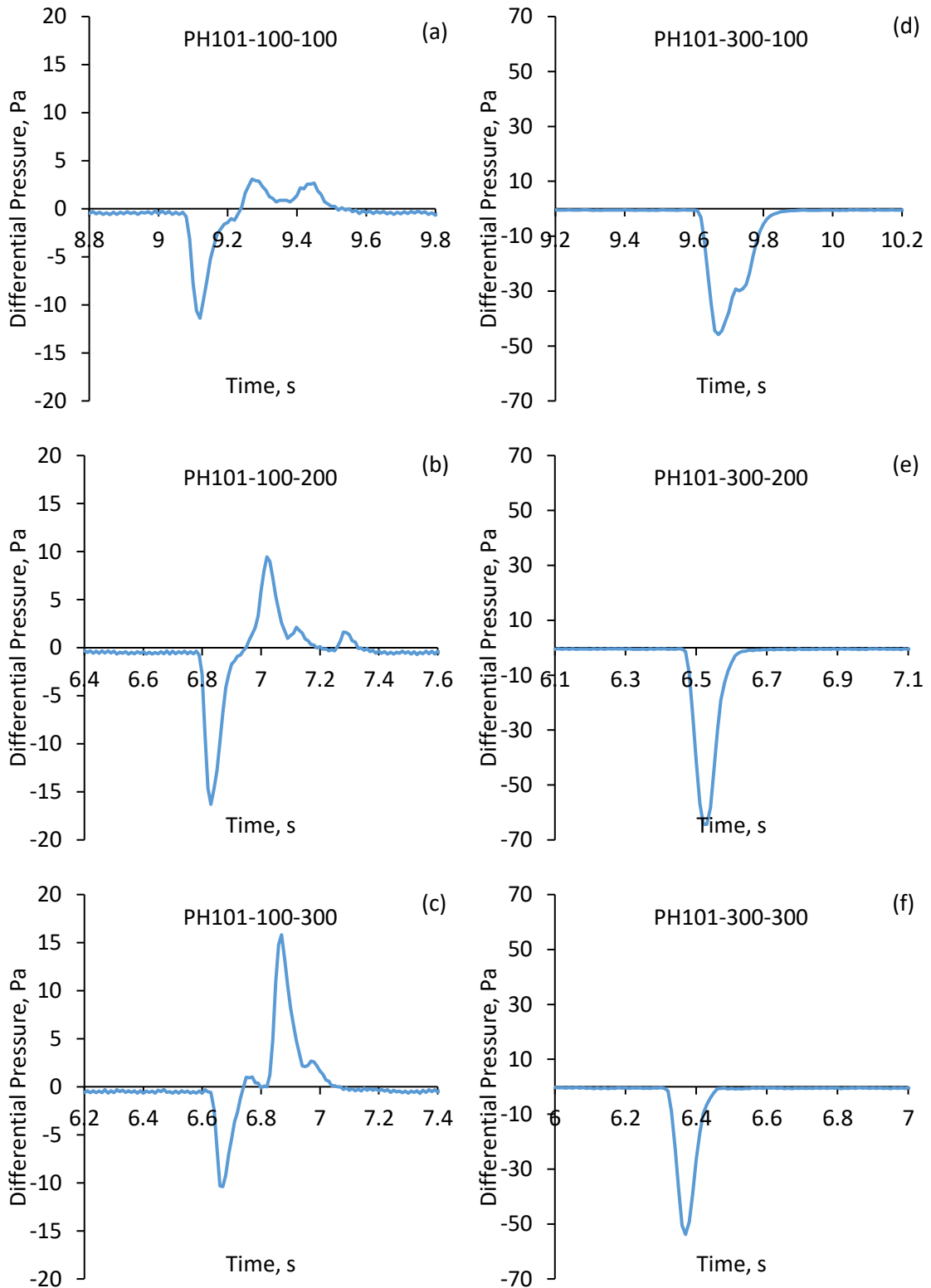


Figure 8-4. Differential pressure measured for PH101 using a) shoe velocity 100 mm/s and suction velocity 100 mm/s, b) shoe velocity 100 mm/s and suction velocity 200 mm/s, c) shoe velocity 100 mm/s and suction velocity 300 mm/s, d) shoe velocity 300 mm/s and suction velocity 100 mm/s, e) shoe velocity 300 mm/s and suction velocity 200 mm/s and shoe velocity 300 mm/s and suction velocity 300 mm/s.

Table 8-1. Differential pressures measured for four grades of MCC in suction and gravity fill mechanisms under different shoe and suction velocities.

Material	Shoe Velocity, m/s	Suction Velocity, m/s	Differential Pressure, Pa		Material	Shoe Velocity, m/s	Suction Velocity, m/s	Differential Pressure, Pa	
			Suction Fill	Gravity Fill				Suction Fill	Gravity Fill
PH101	0.1	0.1	15	21	PH200	0.1	0.1	13	22
	0.1	0.15	23	28		0.1	0.15	14	25
	0.1	0.2	25	32		0.1	0.2	16	30
	0.1	0.25	22	34		0.1	0.25	15	27
	0.1	0.3	19	35		0.1	0.3	12	28
	0.2	0.1	20	21		0.2	0.1	24	31
	0.2	0.15	16	18		0.2	0.15	20	29
	0.2	0.2	12	17		0.2	0.2	20	33
	0.2	0.25	7	19		0.2	0.25	12	24
	0.2	0.3	10	20		0.2	0.3	14	26
	0.3	0.1	62	62		0.3	0.1	19	21
	0.3	0.15	61	61		0.3	0.15	22	28
	0.3	0.2	58	59		0.3	0.2	19	24
	0.3	0.25	65	68		0.3	0.25	14	25
0.3	0.3	60	61	0.3	0.3	12	25		
PH102	0.1	0.1	21	30	PH302	0.1	0.1	20	27
	0.1	0.15	15	24		0.1	0.15	21	29
	0.1	0.2	17	26		0.1	0.2	19	27
	0.1	0.25	15	28		0.1	0.25	18	28
	0.1	0.3	14	27		0.1	0.3	15	35
	0.2	0.1	24	25		0.2	0.1	47	47
	0.2	0.15	17	21		0.2	0.15	24	25
	0.2	0.2	22	25		0.2	0.2	21	22
	0.2	0.25	15	19		0.2	0.25	6	14
	0.2	0.3	15	20		0.2	0.3	21	21
	0.3	0.1	56	56		0.3	0.1	52	52
	0.3	0.15	54	55		0.3	0.15	53	53
	0.3	0.2	48	51		0.3	0.2	69	70
	0.3	0.25	40	44		0.3	0.25	68	69
0.3	0.3	61	66	0.3	0.3	50	50		

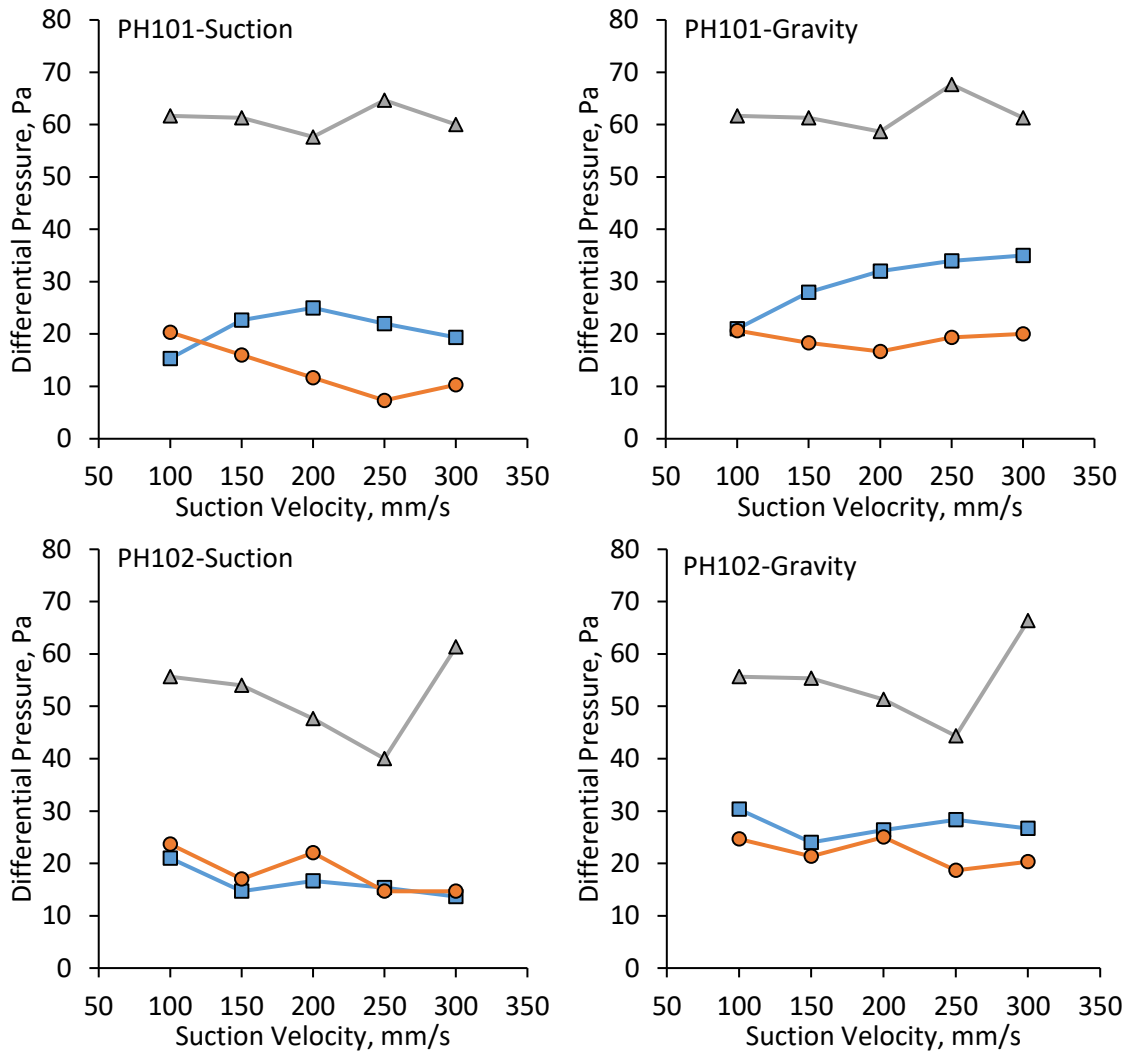


Figure 8-5. Differential pressures between the die and ambient atmosphere measured for PH101 and PH102 during suction fill and gravity fill mechanisms for the experiments carried out using different shoe and suction velocities.

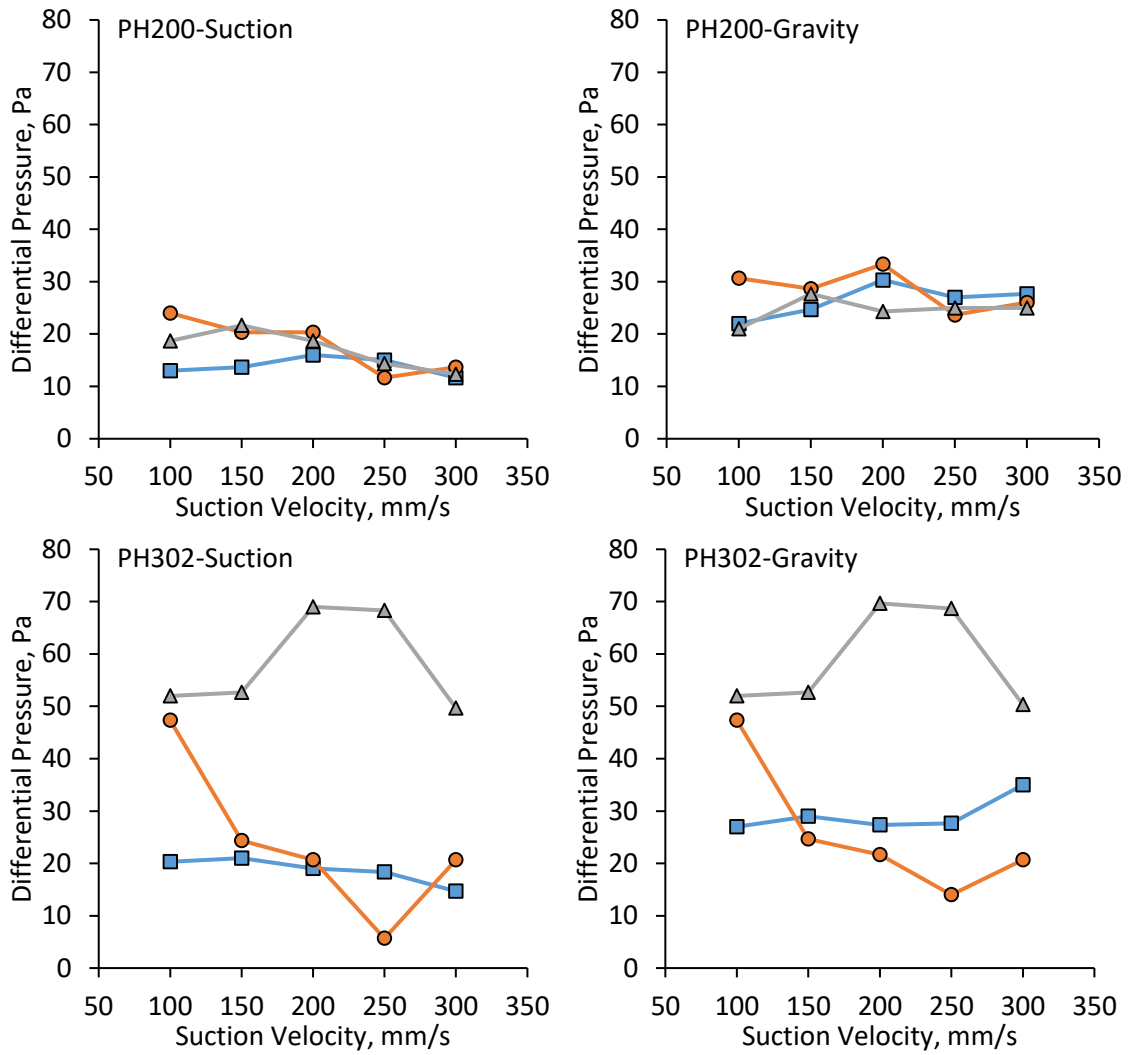


Figure 8-6. Differential pressures between the die and ambient atmosphere measured for PH200 and PH302 during suction fill and gravity fill mechanisms for the experiments carried out using different shoe and suction velocities.

In the following section, dimensional analysis is used to develop a model to predict the mass of the powder delivered into the die as a function of shoe and suction velocities.

8.2.3. Dimensional model development

The total mass of powder introduced into the die (m) can be stated as the sum of mass delivered under suction fill mechanism (m_s) and the mass delivered under gravity fill mechanism (m_g).

$$m = m_s + m_g \quad (8-1)$$

In Section 7.3.4, a model was developed to predict the mass of the powder delivered into the die under gravity fill mechanism (Equation (2-21)). Combining Equation (7-8) with Equation (8-1) we have

$$m = m_s + c_g \rho_b D^2 L_g \left(\frac{H}{D} \right)^{a_g} \left(\frac{v_s \Delta P_g}{\rho_b g^{1.5} D^{1.5}} \right)^{n_g} \quad (8-2)$$

where L_g is the length of the shoe at which the powder is discharging under gravity fill mechanism.

Using dimensional analysis, a model is developed to predict the mass of the powder delivered into the die under suction fill mechanism (m_s). The parameters involved in this process are: shoe velocity (v_s), suction Velocity (v_d), differential pressure developed into the die during suction fill mechanism (ΔP_s), size of the die (D), length of the shoe at which powder is discharging under suction fill mechanism (L_s), bulk density of the powder (ρ_b), acceleration due to gravity (g), viscosity of air (μ), coefficient of friction between particles (μ_p) and between particles and the wall (μ_{pw}), powder permeability (k), shape of the particles, adhesion between the particles and clearances in the system. Therefore, the mass of the powder delivered into the die under suction fill mechanism (m_s) can be written as a function of $v_s, v_d, \Delta P_s, D, L_s, \rho_b, g, \mu, \mu_p, \mu_{pw}, k, shape, adhesion$ and *clearances*.

$$m_s = f(v_s, v_d, \Delta P_s, D, L_s, \rho_b, g, \mu, \mu_p, \mu_{pw}, k, shape, adhesion, clearances) \quad (8-3)$$

Following the Buckingham Π theorem (Gibbings, 2011), by taking ρ_b, g and D as independent parameters (similar to the model developed for gravity fill mechanism) the π groups of $\overline{m}_s, \overline{v}_s, \overline{v}_d$ and $\overline{\Delta P}_s$ are formed as:

$$\overline{m}_s = \frac{m_s}{\rho_b D^2 L_s} \quad (8-4)$$

$$\overline{v}_s = \frac{v_s}{\sqrt{gD}} \quad (8-5)$$

$$\overline{v}_d = \frac{v_d}{\sqrt{gD}} \quad (8-6)$$

$$\overline{\Delta P}_s = \frac{\Delta P_s}{\rho_b g D} \quad (8-7)$$

A dimensional model is proposed to calculate the mass delivered in suction fill as a function of the π groups.

$$\frac{m_s}{\rho_b D^2 L_s} = c_s \left(\frac{v_s}{\sqrt{gD}} \right)^{a_s} \left(\frac{v_d}{\sqrt{gD}} \right)^{b_s} \left(\frac{\Delta P_s}{\rho_b g D} \right)^{n_s} \quad (8-8)$$

In this model, c_s, a_s, b_s and n_s are empirical constants that depending on the material properties and processing parameters that are not included into the model.

The mass of powder delivered into the die under gravity fill mechanism was calculated using the values of the constants c_g, a_g and n_g obtained in Chapter 7 for four grades of MCC (Table 7-5) and Equation (7-8). The length at which the powder is discharging under this mechanism (L_g) was calculated using Equation (8-9) where L is the total length of the shoe.

$$L_g = L - \frac{v_s L_s}{v_d} \quad (8-9)$$

When calculating the mass delivered in gravity fill mechanism (m_g), the differential pressure was taken as the pressure difference between the minimum and maximum pressure in the pressure profile (ΔP_g).

The values of m_g was used in Equation (8-1) to calculate the mass of the powder discharged into the die in suction fill mechanism (m_s).

The values of m_s calculated for different shoe and suction velocities were used in Equation (8-8) and the values of the constants c_s , a_s , b_s and n_s were calculated for four grades of MCC (Table 8-2). The differential pressures used for the suction fill were taken as the minimum pressure reached during the experiment.

Table 8-2. The values of the constant c_s , a_s , b_s and n_s calculated from fitting the experimental results to Equation (8-8).

Material	c_s	a_s	b_s	n_s	R^2
PH101	0.44	-1.25	1.03	0.84	0.98
PH102	0.53	-1.26	0.86	0.63	0.96
PH200	1.33	-0.52	0.98	0.61	0.89
PH302	0.41	-0.65	0.62	1.15	0.86

The coefficients presented in Table 8-2 were used to calculate the theoretical mass of powder delivered into the die during suction fill and the values were compared with the experimental masses in Figure 8-7.

The complete form of the model developed to predict the mass delivered in this process is written in the form of Equation

$$m = c_s \rho_b D^2 L_s \left(\frac{v_s}{\sqrt{gD}} \right)^{a_s} \left(\frac{v_d}{\sqrt{gD}} \right)^{b_s} \left(\frac{\Delta P_s}{\rho_b g D} \right)^{n_s} + c_g \rho_b D^2 L_g \left(\frac{H}{D} \right)^{a_g} \left(\frac{v_s \Delta P_g}{\rho_b g^{1.5} D^{1.5}} \right)^{n_g} \quad (8-10)$$

In order to use this model, the values of the empirical constant should be determined experimentally for the material in use. Also, the differential pressures developed into

the die during suction fill and gravity fill mechanism must be known. In the absence of the necessary data, the differential pressures can be estimated based on the permeability of the powder as well as the clearances in the system. This model (Equation (2-21)) can be modified in the future to include all parameters involved and replace the differential pressure term with a function of powder permeability.

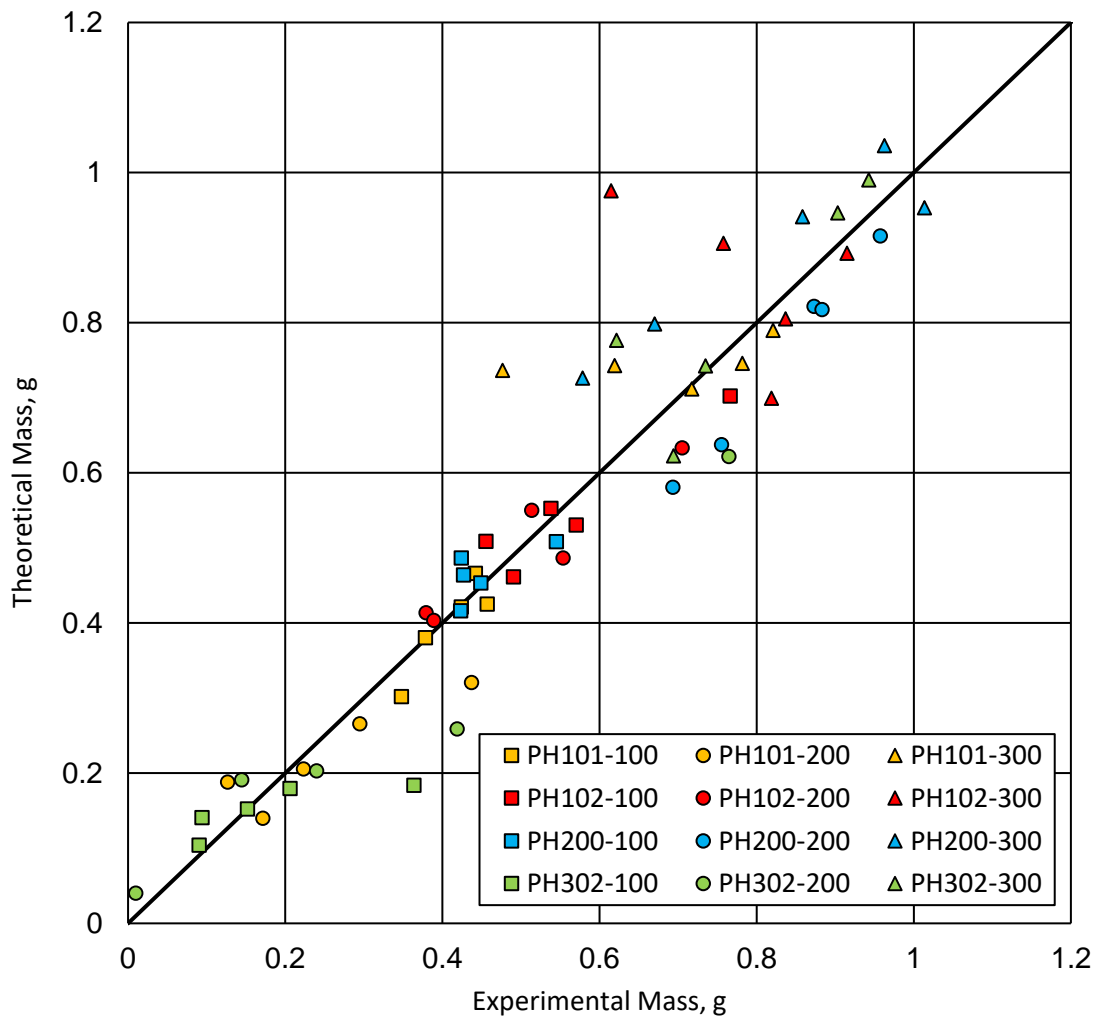


Figure 8-7. The theoretical mass delivered in suction mechanism calculated from Equation (2-21) vs. the experimental values for four grades of MCC.

8.3. Conclusions

The mass of the powder delivered into the die is increased significantly by the suction effect induced by the downward motion of the punch inside the die. For a given shoe velocity there exist an optimum suction velocity at which the mass delivered into the die is the highest. The influence of suction on the mass of the powder delivered is so

significant that the mass delivered into the die using a high shoe velocity can exceed the mass introduced under smaller shoe velocities using the same suction speed. This is due to the fact that at higher shoe velocities more material is available in the vicinity of the die to be sucked-in during the suction period.

In suction fill, the initial acceleration of the punch creates a negative pressure inside the die initiating and facilitating powder flow. The pressure inside the die is then increased as the air inside the die (entered during suction) is compressed between the powder flowing in and the punch. The pressure increase is continued when the suction fill period is over and the powder is discharging under gravity fill mechanism. The increasing pressure opposes the flow of powder

For higher shoe velocities, the differential pressure developed inside the die during suction fill is larger. This effect is limited to powders with small permeability. For powders with high permeability the air can enter the die through the powder bed and the suction effect is reduced.

A dimensional model was developed to predict the mass of powder delivered into the die in suction fill mechanism. The model consists of four empirical constants which should be calibrated for the material. The differential pressures developed in the die should also be determined in order to use this model. In the absence of experimental data, the pressures can be estimated based on powder permeability and clearances in the system.

Chapter 9. Conclusions and future work

9.1. Conclusions

Rankings of powder flowability using different characterisation techniques are not always consistent because the flow behaviour of powders is affected by the processing conditions. For angle of repose and critical orifice diameter measurement, flowability is reduced for powders with smaller particle size while the influence of bulk density on powder flow behaviour is not consistent for these flow measures. In orifice flow the powder with higher bulk density showed improved flow behaviour while the angle of repose experiments lead to opposite trends. A powder flow method is typically designed to characterise a given behaviour, thus the selection of the measurement method should be made with consideration of the actual powder flow process for which flow characterisation is required.

For powder with similar particle morphology (e.g. different MCC grades) the permeability correlates with particle size, smaller particles present lower permeability. Permeability also correlates with bulk density, e.g. the MCC with high bulk density presents lower permeability. In general, better flowing powders (by angle of repose and critical orifice diameter measurement) show higher permeability. The permeability of a powder subject to densification is decreased when the porosity is decreased.

In rotary feeding systems, the mass flow rate of powder discharging from the feeder increases by increasing the paddle's rotational speed and the outlet diameter. For a given exit diameter, there exist a rotational velocity at which the mass flow rate is maximum. This velocity changes for different materials and processing parameters such as the outlet diameter. In rotary feeding systems, the powder flowability ranking changes depending on the rotational velocity. At low paddle speeds, the powders ranked as poor flowing based on the angle of repose and critical orifice diameter measurements have smaller mass flow rate. At higher rotational speed the flowability ranking changes for the materials and a powder which was ranked lowest in terms of flowability out-performed (in terms of the mass flow rate) the other materials with similar bulk density. It is shown that applying a small level of differential pressure at the exit of the feeder, increases the mass flow rate significantly. Examining the pressure

profile inside the feeder showed that every time a paddle covers the exit the pressure inside the feeder increases before decreasing as a result of powder dilation when the flow starts again. This result in an oscillation in the mass flow rate. However, the overall mass flow rate remains constant during the measurement period.

For powders flowing through hoppers or bins, if the exit diameter of the container is smaller than the critical orifice diameter, arching appears above the exit inhibiting further powder discharge. It was discovered that the application of a small level of differential pressure (of the order of 100Pa) reduces the critical orifice diameter significantly: a powder that does not flow through an orifice of 30 mm in open atmosphere can discharge through the exit diameter of 2 mm. A dimensional model was developed to predict the differential pressure required to initiate powder flow as a function of the exit diameter and height of the powder above the die. The two empirical constants in this model are functions of material and processing parameters that are not included in the model and should be calibrated for the system and material in use.

The mass flow rate of powders through orifices is significantly influenced by air pressure conditions at the exit. It was demonstrated that the mass flow rate increases by increasing the differential pressure. Also, the flowability ranking of the powders change depending on the magnitude of the differential pressure applied. At small differential pressure, the mass flow rate of materials ranked as good flowing powder using conventional flow measures is higher than the mass flow rate of relatively poor flowing powders while at larger differential pressure, the poor flowing powders outperform the relatively good flowing materials in terms of the mass flow rate. The existing models to predict the mass flow rate under the effect of differential pressure over-predict the flow rate significantly. A dimensional model was developed to predict the mass flow rate based on the differential pressure applied. This model is reduced to the Beverloo equation when the differential pressure is zero (powder discharge in open atmosphere). The Beverloo constant should be adjusted for fine and cohesive powders to give a correct prediction of powder flow rate in open atmosphere. Due to the complex interplay of material properties and processing parameters development of a mechanistic model is not possible at this stage and the empirical constants should be calibrated experimentally.

In linear shoe-die systems, the powder mass delivered into the die in gravity fill mechanism reduces for higher shoe velocities and powder height inside the shoe. The critical velocity can be used as a measure of flowability and it was found that the critical velocity measured was larger for materials ranked as better flowing powders based on the angle of repose experiments. However, critical velocity is not a material property and changes for different processing parameters. Therefore, the comparison of the flowability based on the critical velocity is specific to a specific set of processing parameters. In gravity fill, the differential pressure between the die and ambient atmosphere increases as more mass enters the die. The increasing pressure inhibits further flow of mass into the die. The dimensional model developed by Schneider (Equation (2-20)) was evaluated and it was shown that the empirical constants included in the model change for different processing parameters and materials. This model was extended by including the influence of powder height in the shoe and the differential pressure developed in the die. A new model was developed and calibrated for each material used.

In suction fill, the mass delivered into the die depend both on the shoe and suction velocities. It is demonstrated that although during gravity fill the mass reduces for larger shoe velocities, under the suction fill the mass delivered using high shoe velocity can exceed the mass introduced using relatively low shoe velocity. For a given shoe velocity, there exists an optimum suction velocity which maximises the mass delivered into the die. The suction fill mechanism is based on the downward motion of the punch inside the die, creating a pressure gradient in the direction of powder flow which facilitates the flow of powder into the die. The magnitude of the negative pressure developed depend on the permeability of powder and clearances in the system. Pressure measurements during the experiment showed that the negative pressure inside the die is developed during the initial acceleration of the punch. As the velocity of the punch reaches the steady state, the powder flowing into the die have higher acceleration and the air that has entered the system is compressed between the powder flowing into the die and the punch. This results in increasing pressure inside the die and although the suction motion is not completed the pressure inside the die starts to rise. The pressure build-up inside the die opposes powder flow. It was shown that the mass delivered for a higher shoe

velocity can exceed the mass delivered under lower shoe velocity for a fixed suction velocity. Therefore, the power law relation (Equation (7-1)) cannot be fitted to the experimental results to determine the critical velocity. A dimensional model is proposed to predict the mass delivered into the die. In this model, the total mass delivered is assumed to be the sum of the mass delivered in suction fill and the mass delivered during the gravity fill period. Similar to the model developed for the gravity fill, in order to use this model the differential pressure should be estimated based on the permeability of the powder and clearances in the system.

9.2. Future Work

Powder flow behaviour is very complex and is influenced by material and processing parameters. It is not practical to examine the effects of these parameters experimentally. In the future, systematic numerical studies can be carried out to examine the influence of parameters such as friction between the particles, friction between particles and wall, and adhesion on the flow behaviour of the powders in processes discussed. These studies can be used to replace the empirical constant present in the dimensional models with the material and processing parameters involved in the process and develop a mechanistic model to predict powder flow behaviour without the need of any experimental measurements

The models developed to predict the mass delivered in linear shoe-die systems under gravity and suction fill mechanisms require the prediction of the differential pressures developed during suction and gravity. In future, these models can be modified by replacing the differential pressure by a function of powder permeability and eliminate the need to predict the pressure developed. This would require numerical simulations of the process and inclusion of the parameters involved in the process that are not currently included.

Using the method described in Chapter 5, a new powder flow testing technique can be developed to characterise the flowability based on the arching of the powders. In this technique, the differential pressure required to break the arch and initiate flow for a good flowing powder is smaller than a poor flowing powder at a given exit diameter. The magnitude of the differential pressure can also be correlated to the strength of the arch formed, which would be a function of material properties and processing parameters.

Additional experimental and numerical studies are required to systematically study the influence of different material properties and processing parameters in rotary feeders, such as paddle shape, paddle cross-section shape, friction and cohesion on the mass flow rate and develop a model to predict the mass flow rate of powders through rotary feeding systems.

References

- ABDULLAH, E. & GELDART, D. 1999. The use of bulk density measurements as flowability indicators. *Powder Technology*, 102, 151-165.
- ALLEN, J. & HAIGH, G. 1954. The permeability method for the measurement of surface areas of fine powders. *Journal of Chemical Education*, 31, 354.
- ASTM STANDARD B213-03: Standard Test Method for Flow Rate of Metal Powders.
- ASTM STANDARD D6773-02: Standard shear test method for bulk solids using the Schulze ring shear tester, ASTM International.
- BARLETTA, D., DONSI, G., FERRARI, G., POLETO, M. & RUSSO, P. 2007. Solid flow rate prediction in silo discharge of aerated cohesive powders. *AIChE Journal*, 53, 2240-2253.
- BASERINIA, R. & SINKA, I. C. 2016. Mass flow rate of fine and cohesive powders under differential air pressure. *Submitted to European Journal of Pharmaceutics and Biopharmaceutics*.
- BASERINIA, R., SINKA, I. C. & RAJNIK, P. 2016. Vacuum assisted flow initiation in arching powders. *Powder Technology*, 301, 493-502.
- BERRY, R., BRADLEY, M. & MCGREGOR, R. 2015. Brookfield powder flow tester—Results of round robin tests with CRM-116 limestone powder. *Proceedings of the Institution of Mechanical Engineers, Part E: Journal of Process Mechanical Engineering*, 229, 215-230.
- BEVERLOO, W. A., LENIGER, H. A. & VAN DE VELDE, J. 1961. The flow of granular solids through orifices. *Chemical Engineering Science*, 15, 260-269.
- BROWN, R. 1961. Minimum energy theorem for flow of dry granules through apertures. *Nature*, 191, 458-461.
- BROWN, R. & RICHARDS, J. 1960. Profile of flow of granules through apertures. *Transactions of the Institution of Chemical Engineers*, 38, 243-256.
- BROWN, R. & RICHARDS, J. C. 1970. Principles of powder mechanics.
- BULSARA, P. U., ZENZ, F. A. & ECKERT, R. A. 1964. Pressure and Additive Effects on Flow of Bulk Solids. *Industrial & Engineering Chemistry Process Design and Development*, 3, 348-355.

- CAI, L., FARBER, L., ZHANG, D., LI, F. & FARABAUGH, J. 2013. A new methodology for high drug loading wet granulation formulation development. *International Journal of Pharmaceutics*, 441, 790-800.
- CARMAN, P. C. 1937. Fluid flow through granular beds. *Transactions of Institution of Chemical Engineeres*, 15, 150-166.
- CARR, J. & WALKER, D. 1968. An annular shear cell for granular materials. *Powder Technology*, 1, 369-373.
- CARR, R. L. 1965a. Classifying flow properties of solids. *Chemical Engineering*, 72, 69-72.
- CARR, R. L. 1965b. Evaluating flow properties of solids. *Chemical Engineering*, 72, 163.
- CARRIGY, M. A. 1970. Experiments on the angles of repose of granular materials. *Sedimentology*, 14, 147-158.
- CORNFORTH, D. 1973. Prediction of drained strength of sands from relative density measurements. *ASTM special technical publication*, 523, 281-303.
- CREWDSON, B., ORMOND, A. L. & NEDDERMAN, R. 1977. Air-impeded discharge of fine particles from a hopper. *Powder Technology*, 16, 197-207.
- DARCY, H. 1856. *Les fontaines publiques de la ville de Dijon: exposition et application*, Victor Dalmont.
- DAVIDSON, J. & NEDDERMAN, R. 1973. The hour-glass theory of hopper flow. *Transactions of Institution of Chemical Engineeres*, 51, 29-35.
- DE JONG, J. & HOELEN, Q. 1975. Cocurrent gas and particle flow during pneumatic discharge from a bunker through an orifice. *Powder Technology*, 12, 201-208.
- DEMING, W. E. & MEHRING, A. L. 1929. The gravitational flow of fertilizers and other comminuted solids. *Industrial & Engineering Chemistry*, 21, 661-665.
- DING, X. J., LIU, L. L. & BRADLEY, M. S. New Instrument PFT for Powder Flow Researching. *Advanced Materials Research*, 2012. Trans Tech Publications, 141-145.
- DONSI, G., FERRARI, G., POLETTI, M. & RUSSO, P. 2004. Gas pressure measurements inside an aerated hopper. *Chemical Engineering Research and Design*, 82, 72-84.

- DRESCHER, A., WATERS, A. J. & RHOADES, C. A. 1995a. Arching in hoppers: I. Arching theories and bulk material flow properties. *Powder Technology*, 84, 165-176.
- DRESCHER, A., WATERS, A. J. & RHOADES, C. A. 1995b. Arching in hoppers: II. Arching theories and critical outlet size. *Powder Technology*, 84, 177-183.
- DUTTA, A. & DULLEA, L. A comparative evaluation of negatively and positively charged submicron particles as flow conditioners for a cohesive powder. AICHE Symposium Series, 1990. 26-40.
- ERGUN, S. 1952. Fluid flow through packed columns. *Chemical Engineering Progress*, 48, 89-94.
- FORMISANI, B., BERNADO, P., GIRIMONTE, R. & MINNICELLI, A. The bed support experiment in the analysis of the fluidization properties of fine solids. Proceedings of the 4th World Congress on Particle Technology, Sydney (Australia), 2002.
- FREEMAN, R. 2007. Measuring the flow properties of consolidated, conditioned and aerated powders — A comparative study using a powder rheometer and a rotational shear cell. *Powder Technology*, 174, 25-33.
- FU, X., HUCK, D., MAKEIN, L., ARMSTRONG, B., WILLEN, U. & FREEMAN, T. 2012. Effect of particle shape and size on flow properties of lactose powders. *Particuology*, 10, 203-208.
- GEBHARD, H. 1982. *Scherversuche an leicht verdichteten Schüttgütern unter besonderer Berücksichtigung des Verformungsverhaltens*, VDI-Verlag.
- GELDART, D., ABDULLAH, E. C., HASSANPOUR, A., NWOKE, L. C. & WOUTERS, I. 2006. Characterization of powder flowability using measurement of angle of repose. *China Particuology*, 4, 104-107.
- GELDART, D., MALLET, M. & ROLFE, N. Assessing the flowability of powders using angle of repose. *Powder Handling & Proc*, 1990. 341-346.
- GIBBINGS, J. C. 2011. *Dimensional analysis*, Springer.
- GOPIREDDY, S. R., HILDEBRANDT, C. & URBANETZ, N. A. 2016. Numerical simulation of powder flow in a pharmaceutical tablet press lab-scale gravity feeder. *Powder Technology*, 302, 309-327.
- GREY, R. & BEDDOW, J. 1969. On the Hausner ratio and its relationship to some properties of metal powders. *Powder Technology*, 2, 323-326.

- GUO, Y., KAFUI, K., WU, C. Y., THORNTON, C. & SEVILLE, J. P. 2009. A coupled DEM/CFD analysis of the effect of air on powder flow during die filling. *AIChE Journal*, 55, 49-62.
- HAGEN, G. 1852. Bericht über die zur Bekanntmachung geeigneten Verhandlungen der Königlich Preussischen. 35, 35-42.
- HASSANPOUR, A. & GHADIRI, M. 2007. Characterisation of Flowability of Loosely Compacted Cohesive Powders by Indentation. *Particle & Particle Systems Characterization*, 24, 117-123.
- HAUSNER, H. H. 1967. Friction conditions in a mass of metal powder. *International Journal of Powder Metallurgy*, 3, 7-13.
- HOU, H. & SUN, C. C. 2008. Quantifying effects of particulate properties on powder flow properties using a ring shear tester. *Journal of pharmaceutical sciences*, 97, 4030-4039.
- INTERNATIONAL ORGANIZATION FOR STANDARDIZATION (ISO) 2014. ISO 4490:2014-Metallic powders - Determination of flow rate by means of a calibrated funnel (Hall flowmeter).
- JACKSON, S., SINKA, I. C. & COCKS, A. C. F. 2007. The effect of suction during die fill on a rotary tablet press. *European Journal of Pharmaceutics and Biopharmaceutics*, 65, 253-256.
- JALLO, L. J., GHOROI, C., GURUMURTHY, L., PATEL, U. & DAVÉ, R. N. 2012. Improvement of flow and bulk density of pharmaceutical powders using surface modification. *International Journal of Pharmaceutics*, 423, 213-225.
- JENIKE, A. W. 1961. *Gravity flow of bulk solids*, Bulletin No. 108, University of Utah.
- JENIKE, A. W. 1964. *Storage and flow of solids*, Bulletin No. 123, University of Utah.
- JENIKE, A. W. 1967. Quantitative design of mass-flow bins. *Powder Technology*, 1, 237-244.
- JOHANSON, J. 1965. A rolling theory for granular solids. *Journal of Applied Mechanics*, 32, 842-848.
- KAMACK, H. 1954. Simple Air-Permeability Method for Measuring Surface Areas of Fine Powders. *Analytical Chemistry*, 26, 1623-1630.
- KATDARE, A. & CHAUBAL, M. 2006. *Excipient development for pharmaceutical, biotechnology, and drug delivery systems*, CRC Press.

- KAYE, B. H. 1967. Permeability techniques for characterizing fine powders. *Powder Technology*, 1, 11-22.
- KETTERHAGEN, W. R. 2015. Simulation of powder flow in a lab-scale tablet press feed frame: Effects of design and operating parameters on measures of tablet quality. *Powder Technology*, 275, 361-374.
- KOZENY, J. 1927. About capillaries conducting water in the earth. *Committee Report of the Viennese Academy*.
- KUMAR, V., DE LA LUZ REUS-MEDINA, M. & YANG, D. 2002. Preparation, characterization, and tableting properties of a new cellulose-based pharmaceutical aid. *International Journal of Pharmaceutics*, 235, 129-140.
- LAVOIE, F., CARTILIER, L. & THIBERT, R. 2002. New Methods Characterizing Avalanche Behavior to Determine Powder Flow. *Pharmaceutical Research*, 19, 887-893.
- LE, V., ROBINS, E. & FLAMENT, M. 2010. Air permeability of powder: A potential tool for Dry Powder Inhaler formulation development. *European Journal of Pharmaceutics and Biopharmaceutics*, 76, 464-469.
- LEE, Y. S., POYNTER, R., PODCZECK, F. & NEWTON, J. M. 2000. Development of a dual approach to assess powder flow from avalanching behavior. *AAPS PharmSciTech*, 1, 44-52.
- LINDBERG, N. O., PÅLSSON, M., PIHL, A. C., FREEMAN, R., FREEMAN, T., ZETZENER, H. & ENSTAD, G. 2004. Flowability measurements of pharmaceutical powder mixtures with poor flow using five different techniques. *Drug Development and Industrial Pharmacy*, 30, 785-791.
- MANUEL VALVERDE, J., CASTELLANOS, A., RAMOS, A., PÉREZ, A. T., MORGAN, M. A. & KEITH WATSON, P. 2000. An automated apparatus for measuring the tensile strength and compressibility of fine cohesive powders. *Review of Scientific Instruments*, 71, 2791-2795.
- MCDUGAL, I. R. & KNOWLES, G. H. 1969. Flow of particles through orifices. *Transactions of the Institution of Chemical Engineers and the Chemical Engineer*, 47, T73-T79.
- MENDEZ, R., MUZZIO, F. & VELAZQUEZ, C. 2010. Study of the effects of feed frames on powder blend properties during the filling of tablet press dies. *Powder Technology*, 200, 105-116.

- MENDEZ, R., VELAZQUEZ, C. & MUZZIO, F. J. 2012. Effect of feed frame design and operating parameters on powder attrition, particle breakage, and powder properties. *Powder Technology*, 229, 253-260.
- MILLS, L. A. & SINKA, I. C. 2013. Effect of particle size and density on the die fill of powders. *European Journal of Pharmaceutics and Biopharmaceutics*, 84, 642-652.
- NEDDERMAN, R., TÜZÜN, U., SAVAGE, S. & HOULSBY, G. 1982. The flow of granular materials—I: Discharge rates from hoppers. *Chemical Engineering Science*, 37, 1597-1609.
- NEDDERMAN, R. M. 1992. *Statics and Kinematics of Granular Materials*, Cambridge, Cambridge University Press.
- PARTY, E. W. 1989. *Standard Shear Testing Techniques for Particulate Solids using Jenike Shear Cell*, Warwickshire, England, Institution of Chemical Engineers.
- PASCALE, C. R. 2014. Comparison of Methods for the Measurement of the Angle of Repose of Granular Materials. *Geotechnical Testing Journal*, 37, 164-168.
- PASHA, M., HARE, C., HASSANPOUR, A. & GHADIRI, M. 2013. Analysis of ball indentation on cohesive powder beds using distinct element modelling. *Powder Technology*, 233, 80-90.
- PASHA, M., HARE, C., HASSANPOUR, A. & GHADIRI, M. 2015. Numerical analysis of strain rate sensitivity in ball indentation on cohesive powder Beds. *Chemical Engineering Science*, 123, 92-98.
- PEETERS, E., DE BEER, T., VERVAET, C. & REMON, J. P. 2015. Reduction of tablet weight variability by optimizing paddle speed in the forced feeder of a high-speed rotary tablet press. *Drug Development and Industrial Pharmacy*, 41, 530-539.
- PODCZECK, F. & JONES, B. E. 2004. *Pharmaceutical Capsules*, Pharmaceutical Press.
- PODCZECK, F. & MIA, Y. 1996. The influence of particle size and shape on the angle of internal friction and the flow factor of unlubricated and lubricated powders. *International Journal of Pharmaceutics*, 144, 187-194.
- RESNICK, W., HELED, Y., KLEIN, A. & PALM, E. 1966. Effect of differential pressure on flow of granular solids through orifices. *Industrial & Engineering Chemistry Fundamentals*, 5, 392-396.

- ROSE, H. & TANAKA, T. 1959. Rate of discharge of granular materials from bins and hoppers. *The Engineer*, 208, 465-469.
- ROWE, R. C., SHESKEY, P. J. & QUINN, M. E. 2009. *Handbook of pharmaceutical excipients*, Pharmaceutical press.
- SANTAMARINA, J. C. & CHO, G. C. 2001. Determination of critical state parameters in sandy soils-simple procedure. *Geotechnical testing journal*, 24, 185-192.
- SCHNEIDER, L. C. R., SINKA, I. C. & COCKS, A. C. F. 2007. Characterisation of the flow behaviour of pharmaceutical powders using a model die–shoe filling system. *Powder Technology*, 173, 59-71.
- SCHULZE, D. 1994a. Development and application of a novel ring shear tester. *Aufbereitungs Technik*, 35, 524-535.
- SCHULZE, D. A new ring shear tester for flowability and time consolidation measurements. Proceedings of 1st International Particle Technology Forum, 1994b. 11-16.
- SCHULZE, D. 2006. Flow properties of powders and bulk solids. *Braunschweig/Wolfenbu ttel, Germany: University of Applied Sciences*.
- SCHULZE, D. 2008. *Powders and Bulk Solids: Behavior, Characterization, Storage and Flow*, Springer.
- SCHWEDES, J. & SCHULZE, D. 1990. Measurement of flow properties of bulk solids. *Powder technology*, 61, 59-68.
- SEVILLE, J. P., TÜZÜN, U. & CLIFT, R. 1997. *Processing of Particulate Solids*, Springer.
- SHINOHARA, K., SUZUKI, E. & TANAKA, T. 1973. Effect of air pressure on flow criterion of cohesive powders from a hopper. *Journal of Chemical Engineering of Japan*, 6, 84-91.
- SINKA, I. & COCKS, A. 2009. Evaluating the flow behaviour of powders for die fill performance. *Powder Metallurgy*, 52, 8-11.
- SINKA, I. C., MOTAZEDIAN, F., COCKS, A. C. F. & PITT, K. G. 2009. The effect of processing parameters on pharmaceutical tablet properties. *Powder Technology*, 189, 276-284.

- SINKA, I. C., SCHNEIDER, L. C. R. & COCKS, A. C. F. 2004. Measurement of the flow properties of powders with special reference to die fill. *International Journal of Pharmaceutics*, 280, 27-38.
- STANDARD, A. 2000. C1444-00: Standard Test Method for Measuring the Angle of Repose of Free-Flowing Mold Powders (Withdrawn 2005). *Annual Book of ASTM Standards*. ASTM International, West Conshocken, PA.
- USP29-NF24 2006. *United States Pharmacopeia [and] National Formulary*, United States Pharmacopeial Convention.
- VEMAVARAPU, C., SURAPANENI, M., HUSSAIN, M. & BADAWY, S. 2009. Role of drug substance material properties in the processibility and performance of a wet granulated product. *International Journal of Pharmaceutics*, 374, 96-105.
- VERGHESE, T. M. 1991. *The discharge of fine powders from conical hoppers*. University of Cambridge.
- WALKER, D. M. 1966. An approximate theory for pressures and arching in hoppers. *Chemical Engineering Science*, 21, 975-997.
- WANG, C., HASSANPOUR, A. & GHADIRI, M. 2008. Characterisation of flowability of cohesive powders by testing small quantities of weak compacts. *Particuology*, 6, 282-285.
- WASAN, D., KAYE, B., WNEK, W., DAVIES, R. & JACKSON, M. 1976a. Analysis and evaluation of permeability techniques for characterizing fine particles Part I. Diffusion and flow through porous media. *Powder Technology*, 14, 209-228.
- WASAN, D. T., RANADE, M., SOOD, S. K., DAVIES, R., JACKSON, M., KAYE, B. & WNEK, W. 1976b. Analysis and evaluation of permeability techniques for characterizing fine particles Part II. Measurement of specific surface area. *Powder Technology*, 14, 229-244.
- WEIGHARDT, K. 1952. Some experiments on the flow of sand. *Ingenieur-Archiv*, 20, 109.
- WELLS, J. I. 1988. *Pharmaceutical preformulation: the physicochemical properties of drug substances*, E. Horwood.
- WU, C.-Y. & COCKS, A. 2004. Flow behaviour of powders during die filling. *Powder Metallurgy*, 47, 127-136.

WU, C.-Y. & COCKS, A. C. 2006. Numerical and experimental investigations of the flow of powder into a confined space. *Mechanics of Materials*, 38, 304-324.

WU, C.-Y., DIHORU, L. & COCKS, A. C. F. 2003. The flow of powder into simple and stepped dies. *Powder Technology*, 134, 24-39.

WU, C.-Y. & GUO, Y. 2012. Numerical modelling of suction filling using DEM/CFD. *Chemical Engineering Science*, 73, 231-238.

ZAFAR, U., HARE, C., CALVERT, G., GHADIRI, M., GIRIMONTE, R., FORMISANI, B., QUINTANILLA, M. A. S. & VALVERDE, J. M. 2015. Comparison of cohesive powder flowability measured by Schulze Shear Cell, Raining Bed Method, Sevilla Powder Tester and new Ball Indentation Method. *Powder Technology*, 286, 807-816.

Appendix

Table A - 1. Averaged differential pressures required to break the arch measured for each exit diameter

orifice diameter, mm	Material											
	PH101			PH102			PH200			PH302		
	50mm	75mm	100mm	50mm	75mm	100mm	50mm	75mm	100mm	50mm	75mm	100mm
2	144	219	289	110	162	179	65	117	123	148	188	186
3	121	161	215	88	123	129	55	86	93	126	150	155
4	109	119	123	79	107	110	48	71	75	119	135	134
5	111	109	111	71	108	101	41	65	71	112	135	126
6	104	104	117	69	92	107	39	58	60	106	133	125
7	93	104	103	67	94	96	31	51	61	100	123	115
8	78	78	104	64	81	92	32	52	59	95	118	107
9	73	84	96	53	79	81	26	46	52	83	101	101
10	65	74	89	53	72	79	-	35	45	80	99	101
11	63	77	83	42	66	69	-	-	45	70	90	98
12	59	68	80	45	56	69	-	-	-	68	87	88
13	54	66	81	37	58	60	-	-	-	63	82	83
14	51	60	72	34	48	58	-	-	-	52	71	77
15	55	55	68	30	49	52	-	-	-	49	67	64
16	44	52	63	28	42	47	-	-	-	49	57	64
18	33	45	48	25	41	32	-	-	-	39	46	54
20	32	49	40	21	38	40	-	-	-	36	44	-
22	32	43	54	-	32	-	-	-	-	-	47	-
24	28	43	53	-	30	-	-	-	-	-	-	-
25	28	43	52	-	28	-	-	-	-	-	-	-
26	26	41	49	-	-	-	-	-	-	-	-	-
28	30	37	-	-	-	-	-	-	-	-	-	-
30	24	-	-	-	-	-	-	-	-	-	-	-